Università degli
Studi di Padova

FACULTY OF ENGINEERING
DEPARTMENT OF INDUSTRIAL ENGINEERING
DIPARTIMENTO DI INGEGNERIA INDUSTRIALE

MASTER THESIS

TESI DI LAUREA MAGISTRALE

Materials Engineering – Ingegneria dei Materiali

ENERGY STORAGE WITH HYDRIDES:

SOLID HYDROGEN STORAGE AND NI-MH BATTERIES

Supervisor – Relatore:
Prof. Amedeo MADDALENA (Università di Padova, IT)
Co-Supervisors-Correlatori:
Dr. Marek BIELEWSKI (European Commission JRC-IET, NL)
Prof. Fokko MULDER (Technische Universiteit Delft, NL)
Prof. Giovanni PRINCIPI (Università di Padova, IT)

Author - Laureando: Nicolò Campagnol

Academic year – anno accademico 2011-2012

To all the people who,
when I asked for help or for suggestions,
answered and helped
with the smile on their faces

A tutte le persone che,
quando ho chiesto loro aiuto o suggerimenti,
mi hanno risposto e aiutato
e lo han fatto col sorriso sul volto

Abstract

This thesis is the sum up of one year of experimental work that has been done between three locations in Italy and the Netherlands:

- ✓ Padua University – Università degli Studi di Padova (Padova, Veneto, IT) labs (industrial engineering department, gruppo idrogeno), where the author has been enrolled as master student from September 2009 till March 2012,
- ✓ The Joint Research Center of the European Commission, Institute for Energy and Transport (Petten, Noord Holland, NL), SYSAF (SYstemS for Alternative Fuels) group, where the author has been trainee researcher from March till August 2011.
- ✓ Delft Institute of Technology – Technische Universiteit Delft (Delft, Zuid Holland, NL) (TU Delft, Reactor Institute, Fundamental Aspects of Materials for Energy research group), where the author worked as visiting researcher from September till December 2011.

The main argument is a hot topic in today science: energy storage. More precisely this thesis talks about solid hydrogen storage, done with materials called metal hydrides.

Through two experimental campaigns on candidate materials it gives an overview, without any claim of final resolution, of the two technologies which are seen as of key role in the future oil-free economy: batteries and hydrogen.
The thesis can therefore be divided in these two main arguments with the work on "direct" hydrogen storage done in Padua and Petten and the work on batteries done in Delft.

The aim of the work on hydrogen storage was the study of a new mixed material for solid hydrogen storage, in line with the present trend of compounds with very high hydrogen gravimetric density but with problematic high desorption temperatures.
In order to decrease the desorption temperature, the materials, different mix of lithium borohydride and magnesium borohydride, have been synthesized at Padua University labs with three different syntheses techniques: Ball Milling (BM), Drying From Solution (DFS) and Impregnating in graphite (IMP).
The samples received in Petten have been studied with different techniques: Thermal Desorption Spectroscopy (TDS), X-Ray Diffraction (XRD), Fourier Transformation Infra Red (FTIR) and Scanning Electron Microscopy (SEM) with Energy Dispersion Spectroscopy (EDS).
The results show that the best compromise of quantity of hydrogen desorbed and desorption temperature has been obtained with mixed borohydrides synthesized with the DFS technique. The temperature of the first desorption main peak has been lowered from 480^{o}C and 298^{o}C of the as received borohydrides to ~263^{o}C in the case of the mix. Dried From Solution and Impregnated samples desorb all the hydrogen below 300°C, in comparison to 400-500^{o}C of the pure borohydrides. Another good result of DFS is that an important desorption takes place at 170^{o}C, working temperature of High Temperature Polymer Electrolyte Fuel Cells (HTPEFC).

The aim of the work on batteries was the study of the electrochemical hydrogen storage properties of an electrode made by magnesium hydride (MgH_2) doped with titanium fluoride (TiF_3).

Electrochemically stored energy with hydrides is the principle behind the commonly used rechargeable Nickel-Metal Hydrides batteries (Ni-MH). The hydride used today for this application is a Lanthanum based mix of rare earths. Magnesium is cheaper and can store several time the hydrogen (and so the energy) that can be stored in those alloys. Nevertheless it suffers of slow kinetics and of corrosion issues connected with the strong alkaline environment of the electrolyte used in the commercial Ni-MH batteries.

Therefore, in this thesis, different approaches for protection have been explored and a catalyst has been used to improve the kinetics.

The chosen catalyst, TiF_3, shows an excellent improvement in hydrogen absorption and desorption kinetics of MgH_2, keeping a huge amount of the high gravimetric capacity of the pure material.

To overcome the corrosion issue it was decided to assemble a sandwich composite pellet made of MgH_2-TiF_3 with a thin layer of Pd or Ni, to join the corrosion resistance properties of the layer with the energy storage properties of the magnesium-based material. The thin layers were applied in two ways: with a bulk foil on top or the active material pellet and with sputtering of the pellets in a magnetron sputtering.

In order to analyse the samples different electrochemical techniques have been used: a classic three electrodes setup at the TU Eindhoven (NL) labs and an assembled battery-like setup at TU Delft (NL) labs.

The experiments with the sandwich material showed that it is possible to use MgH_2 for electrochemical hydrogen storage even if the obtained capacity is still low in comparison to the expected one. The result opens possible new paths for the application of better performing and/or cheaper materials in the field of batteries

Riassunto

Questa tesi è la sintesi di un anno di lavoro sperimentale che è stato svolto in tre luoghi geografici in Italia e nei Paesi Bassi:

- ✓ Università di Padova – Università degli Studi di Padova (Padova, Veneto, IT) nei laboratori del Gruppo Idrogeno del Dipartimento di Ingegneria Industriale. L'autore è stato iscritto alla laurea magistrale presso il suddetto ateneo da Settembre 2009 a Marzo 2012.
- ✓ Il Joint Research Center della Commissione Europea, Istituto per l'Energia e i Trasporti (Petten, Regione del Nord Olanda, NL) gruppo SYSAF (SYstemS for Alternative Fuels, Sistemi per Carburanti Alternativi), dove l'autore ha lavorato come ricercatore tironante da Marzo ad Agosto 2011.
- ✓ L'Università Tecnica di Delft - Technische Universiteit Delft (Delft, Regione del Sud Olanda, NL), laboratori del gruppo FAME (Aspetti Fondamentali dei Materiali per l'Energia) nell'Istituto del Reattore Nucleare, dove l'autore ha lavorato come ospite ricercatore da Settembre a Dicembre 2011.

L'argomento principale della tesi, molto dibattuto nella scienza di oggi, è lo stoccaggio di energia. Più precisamente questo lavoro affronta lo stoccaggio tramite idrogeno usando materiali chiamati idruri.

Grazie a due campagne sperimentali su materiali potenzialmente utilizzabili allo scopo, la tesi fornisce una visione d'insieme, senza alcuna pretesa di risoluzione finale, delle due tecnologie che sembra siano destinate ad avere un ruolo chiave nella futura economia verde: le batterie e l'idrogeno.
La tesi può quindi essere divisa in questi due argomenti principali con il lavoro fatto sullo stoccaggio "diretto" in fase solida dell'idrogeno svoto a Padova e Petten ed il lavoro svolto sulle batterie a Delft.

Lo scopo del lavoro sullo stoccaggio "diretto" di idrogeno è stato lo studio di un nuovo materiale misto per lo stoccaggio dell'idrogeno solido, in linea con l'attuale tendenza di cercare composti con densità gravimetrica di idrogeno molto alta, ma che generalmente hanno anche problematiche alte temperature di desorbimento.
Al fine di diminuire la temperatura di desorbimento, i materiali, diversi mix di boroidruro di litio e boroidruro di magnesio, sono stati sintetizzati presso l'Università di Padova con tre tecniche diverse: macinazione (BM), essiccamento da soluzione (DFS) ed impregnazione di grafite (IMP).
I campioni ricevuti a Petten sono stati studiati con diverse tecniche: spettroscopia di desorbimento termico (TDS), diffrazione di raggi X (XRD), infrarossi con trasformata di Fourier (FTIR) e microscopia elettronica a scansione (SEM) con spettroscopia a dispersione di energia (EDS).
I risultati mostrano che il miglior compromesso di quantità di idrogeno desorbito e temperatura di desorbimento è stato ottenuto con boroidruri misti sintetizzati con la tecnica dell'essiccamento. La temperatura del primo picco di desorbimento è stata abbassata dai 480°C e 298°C dei boroidruri come ricevuti, a ~263°C nel caso della miscela. I campioni

essiccati e quelli impregnati desorbono tutto l'idrogeno al di sotto dei 300 °C, in confronto ai 400-500°C dei boroidruri puri. Un'altro buon risultato con i campioni essiccati, è che un primo desorbimento importante avviene a 170°C, temperatura di funzionamento delle Fuel Cell ad alta temperatura con elettrolita polimerico (HTPEFC).

Lo scopo del lavoro sulle batterie era lo studio delle proprietà di immagazzinamento di idrogeno per via elettrochimica di un elettrodo costituito da idruro di magnesio (MgH_2) drogato con titanio fluoruro (TiF_3).
L'energia elettrochimica immagazzinata con idruri è il principio base delle batterie ricaricabili al nichel-metallo idruro comunemente utilizzate (Ni-MH). L'idruro ad oggi utilizzato per questa applicazione è un mix a base di lantanio e altre terre rare e nikel. Il magnesio è più economico e può stoccare diverse volte più idrogeno (e quindi energia) di quello immagazzinabile con tali leghe.
Tuttavia soffre di cinetica lenta e di problemi di corrosione connessi con l'ambiente fortemente alcalino dell'elettrolita utilizzato nelle commerciali Ni-MH.
Pertanto, in questa tesi, sono stati esplorati diversi approcci per la protezione e un catalizzatore è stato utilizzato per migliorare la cinetica.
Il catalizzatore scelto, TiF_3, mostra un eccellente miglioramento della cinetica di desorbimento di idrogeno da parte del MgH_2, mantenendo gran parte dell'elevata capacità gravimetrica del materiale puro.
Per superare il problema di corrosione si è deciso di assemblare un composito di tipo sandwich realizzato con MgH_2-TiF_3 ed uno strato sottile di Pd o di Ni, per unire le proprietà di resistenza alla corrosione del film con proprietà di immagazzinamento di energia del materiale a base di magnesio. I film sottili sono stati applicati in due modi: con un foglio sottile posto sopra alla pastiglia di materiale attivo o utilizzando un magnetron sputtering.
Al fine di analizzare i campioni sono state utilizzate diverse tecniche elettrochimiche: un classico setup a tre elettrodi presso l'Univerisità di Eindhoven (NL), e un setup per test di batterie presso i laboratori del TU Delft (NL).

Gli esperimenti con il materiale a sandwich dimostrato che è possibile utilizzare MgH_2 per lo stoccaggio elettrochimico di idrogeno, anche se la capacità ottenuta è ancora bassa rispetto a quella attesa. Il risultato apre nuove possibili vie per l'applicazione di materiali con capacità più alte e/o più economici nel campo delle batterie.

INDEX

General introduction

I Overview……1
I.1 An old end and a new beginning……..1
I.2 Towards the renewable energy based society……...4
I.3 Hydrogen fuel history…….……..……7
I.4 Hydrogen society... now……...…...…….……8
II Hydrogen storage ……9
II.1 Hydrogen storage: a showstopper? ……9
II.2 Solid Storage……12
II.3 Ni-MH Batteries……...……15
III Aim of the thesis……...17

Experimental Techniques

I Synthesis Techniques ……20
I.1 Ball milling……20
I.2 Magnetron sputtering……..20
II Sample characterization……21
II.1 X-Ray diffraction (XRD)……..21
II.2 Scanning Electron Microscopy with EDS (SEM-EDS)……23
II.3 Fourier Transformation Infra Red (FTIR)……24
III Hydrogen desorption analysis……25
III.1 TPD with quadrupole Mass Spectroscopy (TPD-MS)……25
III.2 Volumetric Sivert's technique ……27
III.3 Differential Scanning Calorimetry (DSC)……...29
IV Electrochemical characterization……30
IV.1 Three electrodes setup……30
IV.2 Maccor battery test apparatus……..…….……...32

Experimental work

I Complex Hydrides: borohydrides……..35
I.1 Introduction on the materials……..35
$LiBH_4$……....35
$Mg(BH_4)_2$…….……36
Destabilization…….……37
Catalysts…….……40
Nano-sizing…….……42
Infiltration: Nano-confining and Supporting ……..……43
Reversibility……45
I.2 Experiments……48
I.3 Results and Discussion……..……51

I.3.1 TDS Analysis……...51
Ball milled samples……52
Dried From Solution samples……53
Impregnated Samples……55
Secondary Masses Desorption……56
Comparison between preparation techniques……59
Quantitative Data……..61
I.3.2 Reversibility……...62
I.3.3 XRD Analysis……..63
I.3.4 FTIR analysis……..68
I.3.5 SEM analysis……..70
Ball milled samples……..70
Dried From Solution……..71
Comparison between preparation techniques……72
Impregnated Samples……..75
I.3.6 A new $Mg(BH_4)_2$ phase?.. ……..76
XRD, TDS-MS, IR and EDAX analysis……..76
Conclusions……..81
I.4 Conclusions……..82

II MgH_2 and magnesium based electrodes.……84
II.1 Introduction on the materials……84
Catalyzed MgH_2……...84
Mg based electrodes……85
II.2 Experiments……...88
II.3 Results and Discussion……..90
Characterization of the material……..90
Characterization of sputtered layers……..91
Hydrogen desorption properties - DSC……..95
Three electrodes setup tests at TU Eindhoven……96
Swagelok tests- The New Procedure Setup……..98
Swagelok tests-Results with Mg based electrodes……101
II.4 Conclusions.....……...105

Conclusions.……..107

Acknowledgements……..…...108

References…….……109

General Introduction

I believe that water will one day be employed as fuel,
that hydrogen and oxygen which constitute it, used singly or together, will
furnish an inexhaustible source of heat and light, of an intensity of which
coal is not capable. Some day the coalrooms of steamers and the tenders of
locomotives will, instead of coal, be stored with these two condensed
gases, which will burn in the furnaces with enormous calorific power

Jules Verne, The Mysterious Island, Chapter 33

I Overview

1.1 An old end and a new beginning

It is well known that the world as it is now, and the industrialized countries in particular, relies heavily on fossil fuels. In fact 87% of the world energy consumption in year 2010, see figure 1.I.1, was addressed with oil, natural gas and coal. The rest came mainly from nuclear power and hydro power [@1].

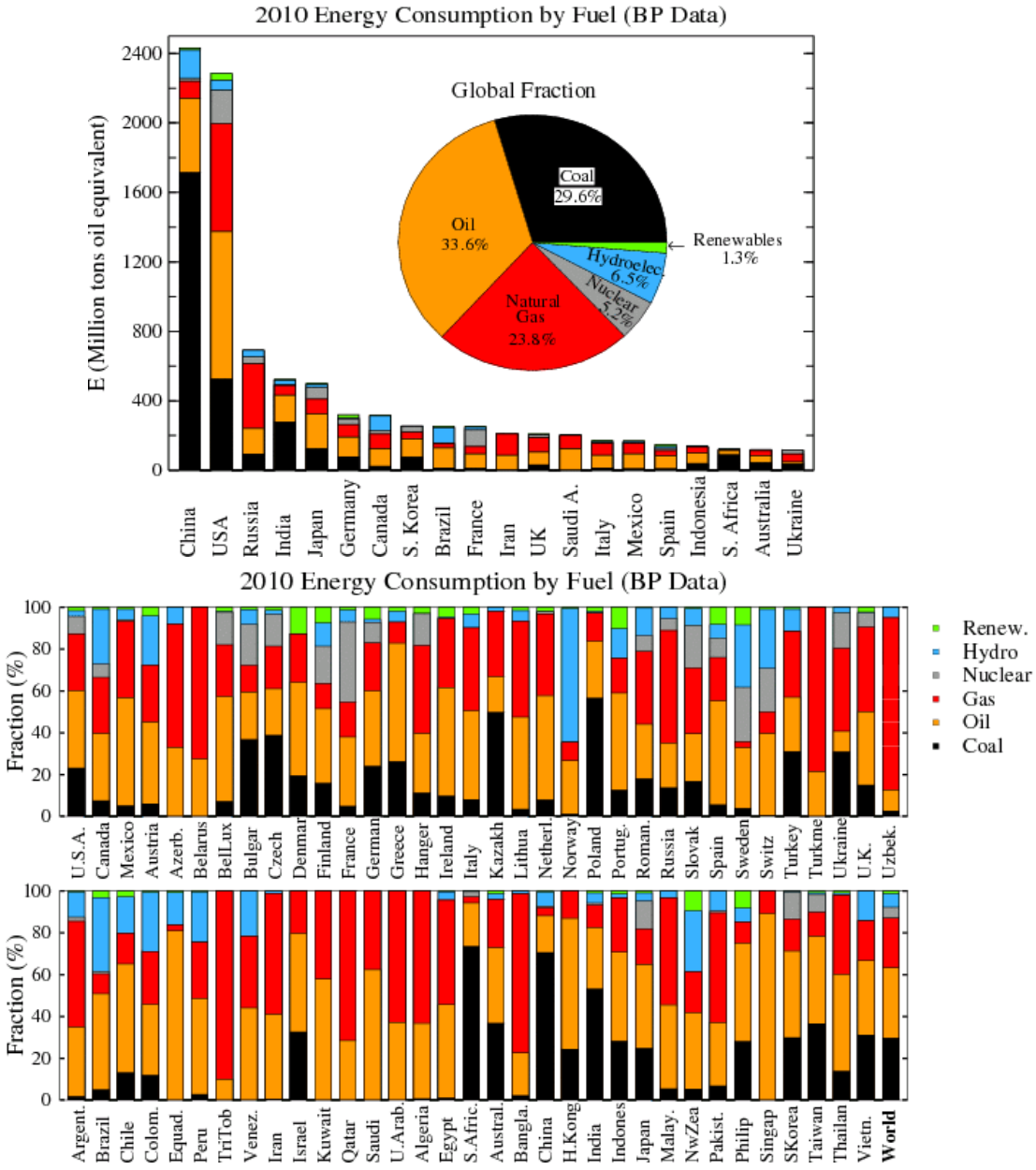

Figure 1.I.1 and 1.I.2: World energy consumption by source and by country in 2010 [@1]

Although energy consumption from sustainable energy sources such as wind and solar is rapidly increasing the overall world contribution is still low, around 1.3 %. In Europe renewable energy in power generation grew by 15.5% in 2010 [@2].
The overall growth remains concentrated in the leading consuming centres: Europe and Eurasia, Asia Pacific, and North America. Renewable forms of energy account for 3.3% of global power generation, with the highest share (5.8%) in Europe and Eurasia [@2].
The consume of fossil fuels is due to a wide variety of reasons: houses heating, food cooking, transport and manufacturing of consumer goods.
Population growth and a general increase in living standards lead to a ever increasing energy consumption. According to one of the UN possible scenario, the world population has been projected to increase from approx. 7 billion today to approx. 9 billion by year 2050 [1] and especially the explosive development in Asia, in particular in China, requires a massive amount of energy.

The main issues coming from the future share of energy resources are related with: environment and geo-political power.

One of the things that developed countries want to reduce is the oil dependence, due to the vulnerability of the supplies to conflict and politic disturbance in oil-exporting nations [2]. The oil production is a problem that is hunting modern society since the 70s, with the oil crisis in the US. Since than the production of oil has been foreseen to peak in the near future [3][@3], at least till the last report of the IEA (International Energy Agency) where it is stated that the oil peak, now seen as an undulating plateau, is not to come but has already been passed in the 2006.
Below a piece of a recent article published in the New York Times [4]:

"That's the conclusion of the International Energy Agency, the Paris-based organization that provides energy analysis to 28 industrialized nations. According to a projection in the agency's latest annual report, *released last week, production of conventional crude oil — the black liquid stuff that rigs pump out of the ground — probably topped out for good in 2006, at about 70 million barrels a day. Production from currently producing oil fields will drop sharply in coming decades, the report suggests."*

According to figures from BP (British Petroleum) the total proven oil reserves of the world are approx. 1258 (1409 including the tar oil sands of Canada) billion barrels of oil, gas condensate and natural gas liquids as well as crude oil [5]. With the current oil consumption rate, which is approximately 30 billion barrels a year, the proven reserves would last for only 41 years from 2010.
The increasing demand and the shortage in the offer of oil will lead to an increase of the price of oil and then of energy that will make the dependence from oil-producer foreign countries even harder to bear from the western world and for Europe in particular.
To keep our living standard energy is needed and since oil will not last forever and nuclear power after Fukushima disaster [@4] seems to be no more an option for some of the European countries, among them Germany and Italy, other options must be explored.

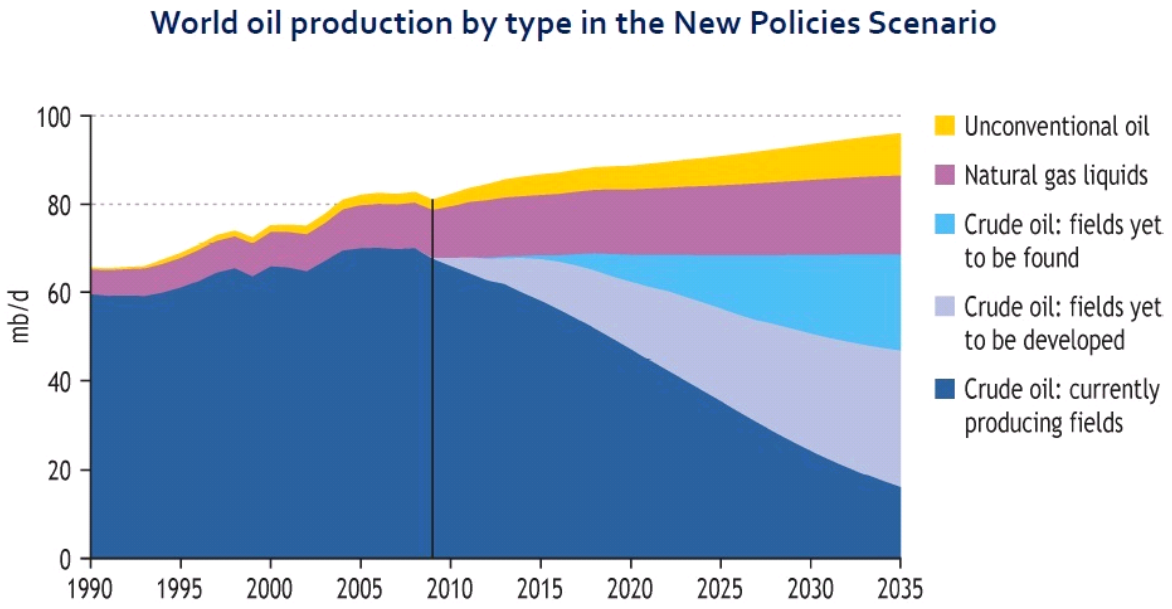

Figure 1.I.3: World oil production in the new policies scenario. From the World Energy Outlook 2010 of IEA [4]

Another issue which might become critical even before we run out of fossil fuels is connected to the global environment.
The global warming might potentially threaten the life of many people due to rising sea levels and increasingly harsh weather conditions that lead to food shortage. One of the main causes of the global warming is, according to many authors, the increased emission of CO_2 [6].
Having in mind this problem the European Parliament proposed the action plan "Europe 2020" that aim to cut the emissions of CO_2 of the 20% and improve the share of renewables to 20% of the energy source share, in comparison to the levels of 1990 [7][@5].
But global warming is not the only problem connected with the oil economy. The last years demonstrate that the exploitation of oil fields can bring to natural disasters that move deeply the public opinion and in the same time cause lost of millions of Euro [8].

1.2 Towards the renewable energy based society

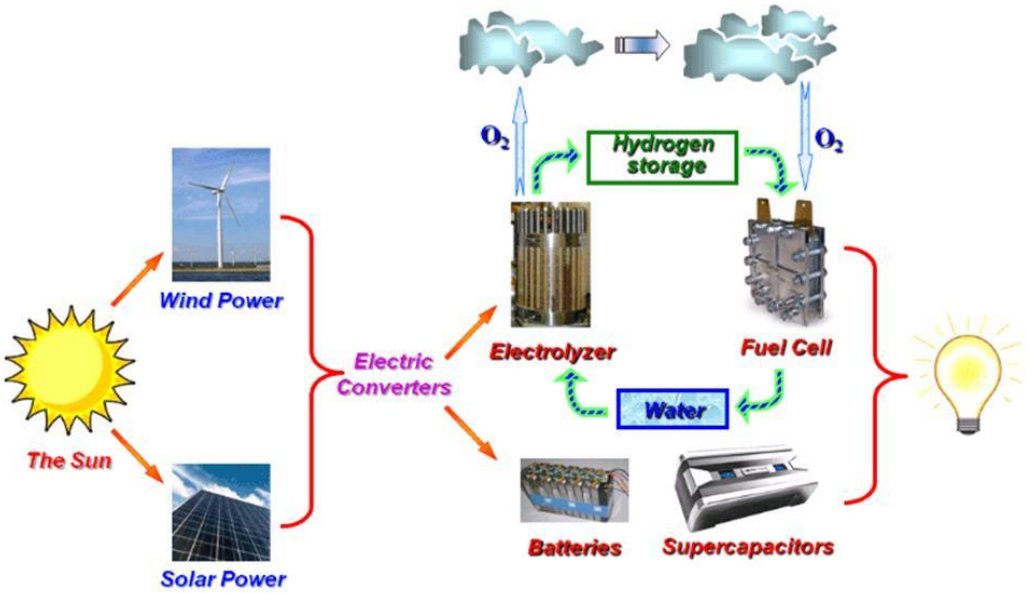

Figure 1.I.4: Hydrogen economy is based on renewable energies (such as wind, solar and hydroelectric). The "clean" energy is converted into electricity by means of converters and than into hydrogen with an electrolyzer, or directly into hydrogen bypassing the electricity stage. Oxygen is released to the atmosphere and hydrogen is intermediately stored, transported and distributed before being electrochemically combusted with oxygen (from the atmosphere) in a fuel cell whereby electricity is produced leaving clean water or steam into the atmosphere. For some uses electricity will be directly used from the grid or stored with batteries or supercapacitors. Figure from UNIPD-CheMaMSE website [@6]

A possible way of addressing both the global warming issue and to keep a sustainable energy supply, also after the fossil fuels have been depleted, is a gradual transformation of our present fossil fuel based society to one where renewable energies (renewables) are the most important energy sources.

Since the production of energy by renewables is often intermittent, due to the weather conditions, and with a low energy density in comparison to fossil fuels based technologies, the energy has to be produced and stored during the moments of low demand to be released afterwards in the moments of need and low production.
In these years electricity storage has basically been done with batteries (lead-acid, Li-ion or Ni-MH) but in the future their low energy density might become a problem to fulfill all the needs of a society used to the high energy density, both gravimetric and volumetric (see figure 1.I.5), of oil and gasoline. Another problem of batteries is the long recharging time. While for city cars used everyday by commuters this should not be a problem, for trucks and sedans used in long trips the idea of stopping every 4-5 hours and wait at the "gas" station for tens of minutes in order to recharge the batteries is not seen as practicable, see table 1.I.1.
The example of energy storage for vehicular applications is normally used when talking about hydrogen economy since it is one of the most close to the public in comparison to forklifts or stationary electricity generators. Even if it is only one aspect of the problem of energy and hydrogen storage, it alone accounts for the 23% of the CO_2 global emissions [9].

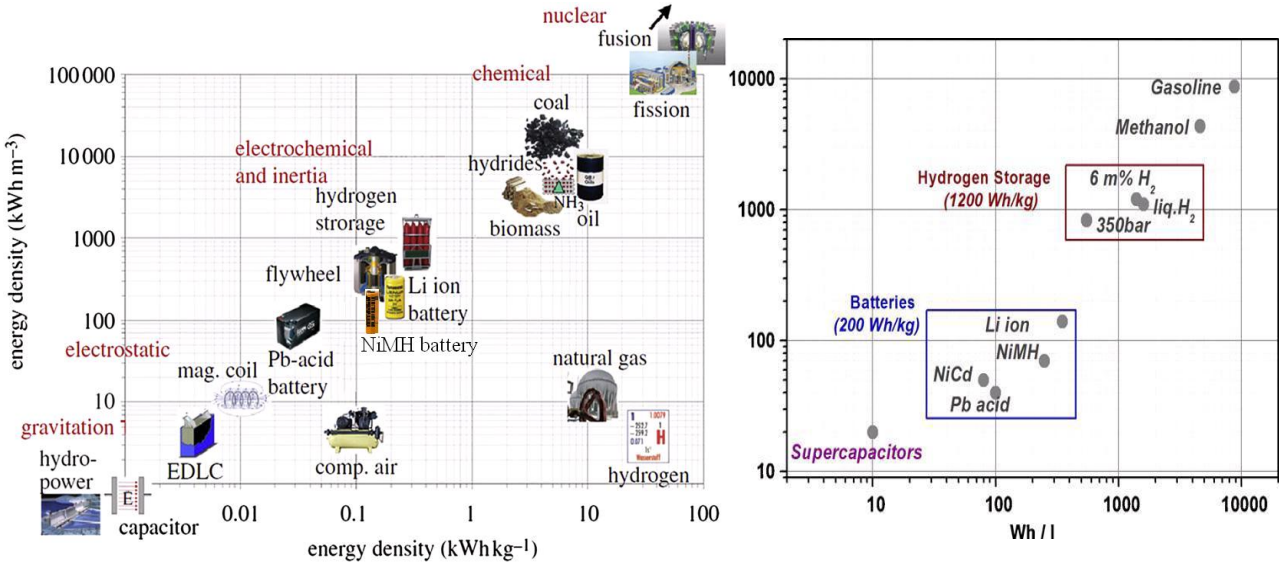

Figure 1.I.5 and 1.I.6: indicative comparison between different energy storage techniques and zoom (right) on the range under investigation (inverse axes). Batteries are so far too low in capacities (in gravimetric and volumetric terms) to substitute oil based technologies, especially for automotive application. Images modified from [9] and [10]

Therefore also in this work it will be kept as the main example of a field where clean fuels have to be introduced and where energy storage is an important issue.

Gaseous hydrogen is a clean synthetic fuel, also called energy carrier, which after being produced has to be transported and stored till the users need it. Since hydrogen is not naturally abundant on earth as H_2 it must be synthesized starting from other compounds like water (H_2O).
Today most of the gaseous hydrogen is produced from steam reforming of natural gas or higher hydrocarbons [7], but in the future hydrogen, to be considered a clean fuel, has to be produced only from water, using electrolysis with electricity produced from sustainable energy sources e.g. solar, wind, hydro power or directly from photolysis biological [11] or synthetic [12][13].
Fuel cells (FC) (or Fuel cell stacks) convert hydrogen into a usable form of energy, combusting it electrochemically with oxygen coming from the air, of from a dedicate supply, and the only outputs of the system are electricity and water. Nowadays the efficiency of a FC is already more than 50%, almost twice as much of a commercial internal combustion engine (ICE). Moreover, see figure 1.I.5 and 1.I.6, the energy density achievable with hydrogen storage is already higher than the other green possibilities available for vehicular applications (batteries and supercapacitors). Still, a mix of the three looks like the best solution for different reasons.
This aspect of the technology mix has been recently analyzed and a possible market division between FC vehicles and electric vehicles has been published [10] and is here reported in table 1.I.1.

	Micro-Compact	Compact	Middle	Luxury- & Family	City-Bus	Interurban Bus	Light duty truck	Medium duty	Heavy duty
Fuel Cell vehicle	(✓)	✓	(✓)	(✓)	✓	SOFC	✓	✓	SOFC
Battery vehicle	✓	(✓)	-	-	-	-	(✓)	-	-

Table 1.I.1: Expected applicability of future battery cars and fuel cell cars [10]
√ possible (√) possible with limitation, SOFC Solid Oxides FC

As can be seen from the table, for light duty and for compact cars battery vehicles are a possible option, while it is foreseen that for all other applications FC cars will be the most probable solution.

In conclusion, as it can be seen in the scheme of figure 1.I.4, and is reported by many scholars [14], the model of the hydrogen based society is sustainable, does not produce any emission but water vapor and might be a solution to environmental problems.

1.3 Hydrogen fuel application history

The first hydrogen car, figure 1.I.7, was built in 1807 by the Swiss Francois Isaac de Rivaz [15]. This first experimental prototype was powered by a ICE working with hydrogen and oxygen. The Rivaz car stored compressed hydrogen gas in a balloon and it had an electrical Volta cell ignition.

Figure 1.I.7 (left): The first hydrogen car in the history, from de Rivaz
Figure 1.I.8 (right): The modified car of Professor Kordesch

The first fuel cells vehicle, a farm tractor, was developed by Harry Karl Ihrig in 1959. The tractor contained 1008 small alkaline fuel cells that provided 15 kW of power, enough to allow the tractor to pull 1350 kg in demonstrations.
With the exploitation of hydrogen technology (especially for the space race) and the first oil crisis, the attention grew step by step and new prototypes appeared [16][17][@7].
One of the most important pioneers of the hydrogen technology is Karl Kordesch, an Austrian scientist who moved to the United States after the recruitment as a member of Operation Paperclip. During his brilliant carrier he filed 120 patents and among them the one of the alkaline battery [@8]. In 1970 he modified his own car, an Austin A 40, as a fuel cell hybrid car using seven lead acid batteries and a 6 kW Union Carbide alkaline fuel cell powered by hydrogen gas. Compressed hydrogen gas was contained in six tanks strapped to the top of the car, see figure 1.I.8. Professor Kordesch ran on public roads for three years with this prototype [@7][@8].
Among all the projects from different authors in the following years, one in particular should be outlined in this thesis: the Provo-Orem bus of Roger Billings that had the peculiarity of store the hydrogen with metal hydrides. Thanks to the larger dimensions, the vehicle could easily accommodate the added weight of the hydrogen stored in metal hydride form. Moreover is reported that the bus in stop and go driving conditions was 80% more efficient than gasoline-powered vehicles [@7].
Hydrogen has not only been studied for cars. Different vehicles, from bicycles to forklifts have already been tested and are in the way to be soon on the market. Also airplanes, submarines and ships have been built and the possibility to substitute the old and noisy vaporettos in Venice with FC boats has been taken in consideration before the 2008 crisis stroke.

1.4 Hydrogen society... now.

Figure 1.I.9: Honda FCX. The 350 bar tank in the back occupies four time the volume of a gasoline one.

"Ten years ago […] car manufacturers didn't even dare to expose their experimental fuel cells vehicles to cold weather: they worried that when the cells shut down, residual water could freeze and wreak havoc in the delicate insides. Instead the companies would shuttle the vehicles around in heated trailers." J. Tollefson 2010 [18].

Time has passed and nowadays in Europe, Japan and US it is possible to come in sight of one not-anymore-futuristic vehicle.
With the CUTE project [@9] some important cities, like Amsterdam, London and Berlin, have been provided with hydrogen propelled busses to be used in daily traffic. Among those cities even Reykjavik, capital of Iceland, a city not famous for its temperate weather. According to some authors Iceland was, at least before the Icelandic financial crisis, the most probable country where the hydrogen economy could start up, due to the peculiar energetic situation: Iceland produces more energy than its necessity thanks to the little demographic density and the huge availability of geothermal energy, but on the same time it has to import thousands of barrels of oil every year to feed the car and fishing boats fleets.

In 2005, Honda leased the first commercial hydrogen car to a family in Redondo Beach, California. In 2008 the Honda FCX Clarity, see figure 1.I.8, became the first hydrogen fuel cell car ever produced in line and the first lease vehicle went to the same family of Redondo plus to dozens other people.
In an article of 2008 [19] is described a test drive with the car. The Honda FCX is depicted not as a futuristic prototype but as a completely modern 134 horse power car, with a "surprisingly roomy interior".

II Hydrogen storage

II.1 Hydrogen storage: a showstopper?

As seen from figure 1.I.4 the hydrogen society is ultimately completely CO_2 release free as well as independent from fossil fuels. Although all the steps of the cycle reported in the figure can actually be performed with present available technology, there are sizable barriers preventing the transition to a hydrogen based society:

1) Hydrogen production is very expensive compared to present fuels, for example gasoline, both if it is synthesized by reforming of from renewable energies. The actual price of H_2 in California's gas stations, even if it's quite close to the target of the DOE for the diffusion of hydrogen cars [20], does not reflect the real price that it could or should be if a non-experimental distribution grid was opened.
   The production of hydrogen by reforming is now the easiest way to bust the take off of hydrogen economy, but the price of the hydrogen sold with this technique is not the price of the production with renewable energies, which, at least in this moment, would be much higher.
2) The infrastructure has to be modified to accommodate the new gaseous fuel instead of the most common liquid ones, but no one would ever invest in this change if there is no demand of hydrogen gas. Obviously if no infrastructure is available no car manufacturer will invest on hydrogen cars [14].
3) Fuel cells are already commercially available for the transport sector, but the production cost is high due to the use of expensive membrane and electrode materials: Nafion for the first and Pt/Ru for the second. Being a relatively new technology on the market, it still shows also some problems when exploited in high requiring environments like in Norway [16].
4) But the previous are just minor problems in comparison to what is considered the main bottleneck of the hydrogen economy: the hydrogen storage [20][21].

The infrastructure chicken-and-egg problem can be solved, and some countries are doing it, by government interventions and by agreements between car manufacturers and oil and gas distribution companies. Projects like NOW in Germany and the California Hydrogen Highway in the US are examples (post 2008 crisis) of these collaborations [18][@10].
Still it is not clear yet the answer to the question if it is more convenient to build a hydrogen gas pipeline infrastructure or if hydrogen will be eventually generated on site with energy transported with electricity via cables.

The price of FC components is expected to fall when the production volumes will reach values in the order of millions of pieces [17] and the liability of the products should follow the same trend as already happened with other technologies.

The issue connected with hydrogen storage is not as easy to be solved. Although hydrogen has a high gravimetric energy density of approx. 3 times that of gasoline [22], at room temperature and pressure it is a gas with very low volumetric energy density in comparison to liquids or solids, see figure 1.I.5. Hydrogen occupies an enormous volume in normal

conditions: 1 kg takes at room temperature and pressure 11 cubic meters [23], more than the boot of a touristic bus [@11].
Therefore it is necessary to store this gas either compressing it or changing its state i.e. solidifying of liquefying it.

In order to introduce hydrogen as a fuel the Department of Energy (DOE) of the United States published a series of goals for 2010, after reviewed in 2009, and 2015 [9]. Even if some experts in the field disagree with the high demanding targets of the department, they are seen by the scientific community as the ultimate objectives for their researches.

"Concentrating efforts on the mass of the fuel tank alone is like asking an obese patient to lose weight from his left arm to control his total weight" Schlapbach [21]

The main US DOE 2015 targets for hydrogen storage materials reviewed by Satyapal [24] and summarized and reported by Lan [9] are:

- ✓ High gravimetric storage capacity: minimum 9 wt% abundance of hydrogen and at least 81 g/L of hydrogen available from the material;
- ✓ Low cost, less than US$67/kg H_2;
- ✓ Operating temperature from -40°C to 60°C; minimum/maximum delivery temperature from -40°C to 80°C; maximum delivery pressure 100 bar;
- ✓ System filling time for 5 kg, less than 2.5 min; start time to full flow rate at 20°C, less than 5 min;
- ✓ Loss of useable hydrogen 0.05 g/h/kg H_2 storage or 0.12% per day;
- ✓ Low-toxicity of a non-explosive and possibly inert (to water and oxygen) storage medium;
- ✓ Cycle life (from ¼ to full) 1500 cycles, and cycle variation 99 % of the original capacity

According to the best of the author's knowledge no technique today fulfill all the requirements of DOE for 2015 [25] but also the modified ones for the 2010.

The unsatisfactory results coming so far from solid hydrogen storage, explained afterwards, brought to the adoption of compressed hydrogen tanks for car prototypes and first commercially available models. The choice is mainly due to the relative simplicity of the technique and the experience already present in the field thanks to compressed natural gas (CNG normally commercialized as methane) and liquid petrol gas (LPG) fuelled cars.
There are four types of high pressure tanks in the market, made of carbon composite, aluminum or steel [25]. High pressures are unavoidable if the required energy densities are to be achieved and the most common used are 350 bar and 700 bar; in comparison the commonly used methane pressure tanks work at maximum 220 bar while LPG tanks do not exceed few tens of bar. For pressures higher than 70 MPa the deviation from ideal gas behavior is too large and the energy content cannot be significantly increased by increasing the pressure [26].
Part of the energy stored as hydrogen (10% for 700 bar and 5% for 350 bar) is used for the compression and has to be considered in the total account [25]. Hydrogen can be compressed with a traditional compressor or using a single step or a double step hydride compressor

which, increasing the temperature automatically increases the pressure of the gas following the pressure-composition-temperature diagram characteristic of the hydride [27][28].

Liquid hydrogen has been considered an option for automotive due to its good volumetric and gravimetric densities. Unfortunately the operating temperatures are between -253 and -243°C leading to an unavoidable heat flow to the environment. Nowadays 40 or more metallic and vacuum layers are used to insulate the content of the tank making the system quite complex [25]. To lower the surface to volume ratio the geometry is very important and the bigger and close to spherical is the tank the lower are the losses in terms of heat and energy as hydrogen due to the boil-off [17]. In fact when the pressure inside the tank reaches a limit value a valve vents the system. These problems are no issue if a truck or a similar vehicle is considered, but, if the vehicle has to be small and if it might remain unused for a certain amount of time as can happened with a car, the boil-off and the dimension of the tank lead to consider liquid hydrogen storage not as a good choice [18]. Another drawback similar to high pressure storage is that 30% of the energy stored in liquid hydrogen is already consumed for the liquefaction [26].
Nevertheless some big car manufacturers like BMW are still working on the subject with hybrid gasoline-hydrogen cars that are soon expected to be for sale if a sufficient hydrogen distribution grid is available [@12][@13].

The third option are hydrides i.e. the solid phase hydrogen storage. Compounds containing nucleophilic hydrogen (and no oxygen) are named in chemistry hydrides. Metals and intermetallic compounds react with hydrogen forming: ionic, covalent, interstitial and metallic hydrides [27].

Many groups are working on the possibility of putting together two of the previously said technologies and prototypes of cryo-compressed hydrogen tanks [25][30] as well as high-pressure metal hydride tanks [29][10] are already being built with promising results.

In conclusion, according to the researchers of the Argonne National Laboratory (Argonne, IL, USA) none of the today available options has the potential to meet all the ultimate targets simultaneously. Some options can meet several of the intermediate targets but not all the targets simultaneously [30].

II.3 Solid storage

Before start talking about solid hydrogen storage a special and important unit of measurement has to be introduced: Hwt% (Hydrogen Weight Percent). All scientific articles on the subject and all the goals for this technology are normally expressed in these terms. This storage capacity can be easily calculated knowing the stoichiometry of the compound and dividing the number of hydrogen (with atomic mass ca 1) by the molar mass of the hydride.

The advantages of using a solid phase are mainly due to safety reasons. Energy is required to release hydrogen from the compound and this was thought to be a better alternative to a very high-pressure vessel [31] keeping in mind the unforgotten disaster of the Hindenburg of 1937 [@8]. The separation between hydride categories is not easy to determine [27]. A commonly used subdivision is between classic or metal hydrides and complex hydrides, but others are also adopted.

Electropositive elements react with hydrogen and form hydrides with a predominant metallic character [27]. They normally are good conductors of electricity and can show large deviations from ideal stoichiometry. Only few transition metals do not have stable hydrides and the gap in the periodic table called "hydride gap" begins at group 6 and ends at group 11 with the main exception of Pd hydride [27].
Hydrogen absorption (and desorption in the reverse order) can be divided in four phases:

- ✓ First, molecular hydrogen dissociates at the surface before absorption;
- ✓ Then the metal starts hosting atomic hydrogen in the lattice as solid solution in interstitial sites.
- ✓ As the hydrogen pressure and the concentration of hydrogen in the lattice increases, interactions between hydrogen atoms become locally important, and nucleation and growth of the hydride phase takes place. Till all the metal phase is transformed in hydride phase, the hydrogen pressure remains constant following the Gibb's law. This stage is visible as a plateau in PCT (pressure-composition-temperature) diagrams explained in chapter III.2 of the experimental part. Some compounds show multiple hydride phases and so multiple plateau in PCT curves.
- ✓ When all the metal phase is transformed in the last hydride phase the plateau ends and the pressure raises again.

The PCT curves plateau pressure depends on the working temperature and is similar in absorption and desorption, given a certain amount of hysteresis, making the storage with metal hydrides reversible [32]. PCT curves are the key to understand why classical hydrides have not being introduced so far in the starting hydrogen economy. No single element hydride absorbs a satisfactory amount of hydrogen at room temperature and pressure; therefore a series of alloys has been invented. Promising metal hydrides alloys are grouped in AB5, AB2 and A2B groups [23] where A is a stable-hydride forming material and B is an element with low affinity with hydrogen [27].
Among AB5 group, $LaNi_5$ based alloys are the most promising and exploited for electrochemical hydrogen storage as will be explained in the relative chapter. At the beginning of the century the production of secondary batteries based on the compound was over a billion pieces per year [22] and the production has only slightly decreased since the extraction rate and the price of the ores has increased even during the years of 2008 crisis [@14], it might be said therefore that batteries are nowadays the most important field of

application of metal hydrides and $LaNi_5$ based alloys the most commonly used. These alloys have fast and reversible sorption with a small hysteresis, plateau pressure of few bars at room temperature and good cycling life (or "cyclability") [22].
AB2 alloys have lower capacities and less interesting properties but, being often composed by relatively cheap elements such as Zr [22][27] they are kept in consideration for applications where the low price is determinant and high gravimetric storage is not required, but they have also been considered for automotive [33].
MgH_2 has very interesting property: 7,6 Hwt% storage capacity; but unfortunately it has also many drawbacks: high thermodynamic stability and bad corrosion resistance in basic environments [31]. To overcome these issues a possibility is alloying it with Ni; the results is a AB2 type alloy with relatively high capacity (3,6 Hwt%), low cost, light weight and low-toxicity [31].

Complex hydrides are systems formed by a cation and one or more hydrogen containing anodic groups, namely: alanates $[AlH4]^-$, amides $[NH2]^-$, imides $[NH]^{3/2-}$ and borohydrides $[BH3]^-$. They are interesting because of their light weight and high number of hydrogen atoms [31].
Borohydrides will be further explained in a dedicated chapter. $LiBH_4$, one of the compounds analyzed in this thesis, has a nominal capacity of 18 Hwt% and the hydrogen can be extracted both thermally and making it to react with water. $NaBH_4$ can also produce hydrogen via hydrolysis and has been considered as an excellent choice for one-time applications as the reaction is not reversible [34].
Ammonia Borane (AB), one of the most studied compounds in this moment, has 19,6 Hwt%. However AB still has many problems of reversibility and catalysts are needed in order to decrease the desorption temperature [32][33]. Moreover, developing an AB regeneration scheme that is practical, economical and efficient still remains a significant challenge [30].
Other chemical hydrides (non reversible on board) have and are still considered as valid option as hydrogen carriers. Among them: AlH_3 [35] (10 Hwt%), N_2H_4 (12,6 Hwt%) and NH_3 [34] (17,7 Hwt%).

Although some complex hydrides have promising capacities and other show good reversibility, like sodium alanate which has been brought to the tank prototype phase [36][37]; often these materials are too thermodynamically stable and irreversible, at least for on-board standards.

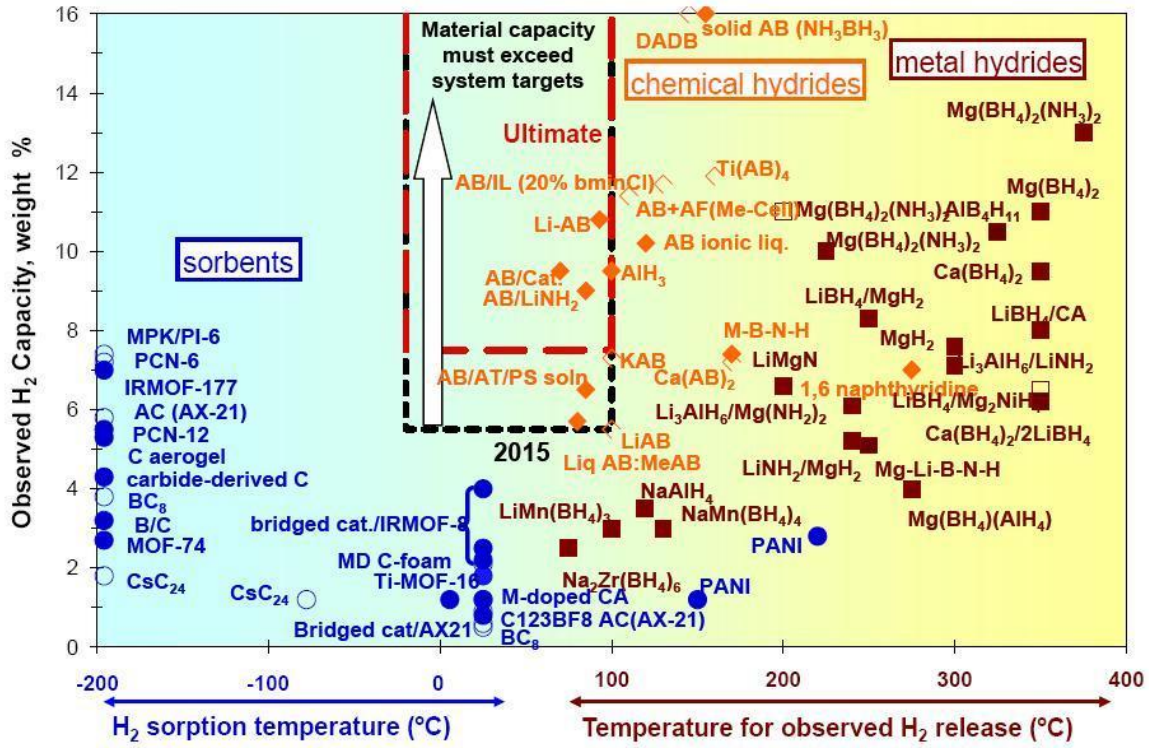

Figure 1.II.1: 2010 updated situation of hydrogen storage materials performances in relation to available gravimetric hydrogen density and working temperature with the frame of the 2015 DOE target. Chemical hydrides such as Ammonia Borane (AB) still have to overcome problems on cycling and desorption of impurities of ammonia and borane during the dehydrogenation. No material up to date fulfills the requirements of DOE [38]

To complete the picture of solid phase hydrogen storage also sorbent materials, where hydrogen is only weakly bonded, should be introduced. The storage capacities of these materials, including the recently developed MOFs (Metal-Organic Frameworks) are less than 2 Hwt% at room temperatures. Lowering the temperature can enhance the physisorption and some materials can reach at -196°C (liquid nitrogen boiling point) capacities of 7,5 Hwt% of excess H_2 and 11,2-wt% of absolute H_2 at 70 bar [30].

Reported in figure 1.II.1 is the situation of hydrogen storage in solid phase in 2010 [38]. On the left side, at low temperature lay the sorbent materials, on the right the metal hydrides with part of the complex hydrides and on the top right the chemical hydrides.

Unfortunately although a huge effort has been made by the scientific community in these years and hundreds of compound have been synthesized and tested, none of them show to have at room temperature and pressure the storage capacity required by the DOE targets [30][26] and the few within the DOE target frame of figure 1.II.1 like the AB based materials are either non reversible on board or have other shortcomings.

II.4 Ni-MH Batteries

The best way to store hydrogen is still a topic of serious discussion, and even if the solid state was chosen to address it, the way of loading and unloading the hydrides is not unique.
Nickel-Metal Hydride (Ni-MH) batteries are a mature technology already on the market and are used to power hybrid vehicles and cheaper electronics, whereas competitor lithium-ion batteries have conquered high-end electronics and are now being used in power tools. Lithium-ion batteries are also entering the hybrid/electric-vehicle market and are a serious contender to power the hybrid or electric cars of the future [39] if new anode materials for Ni-MH batteries are not found.
Ni-MH batteries in comparison to Lithium-ions are safer and relatively cheap. They have good resistance to overcharge and over-discharge and this makes them most suitable for applications where multiple cells need to be used in parallel or in series when higher voltages and currents are needed, as in the case of hybrid/electric-vehicles. However, the aqueous electrolyte limits the voltage of an individual cell to 1,2-1,5 V.
The electrolyte used for commercial Lithium-ion batteries on the other hand, is organic and gives the possibility to have a much higher average discharge voltages of ~3.7 V. As a result, the energy density in Wh/kg or Wh/l is higher for Lithium-ion than for Ni-MH, see figure 1.5, even if the storage capacity in mAh/g is lower, which is the reason why portable electronics almost exclusively use Li-ion batteries nowadays.
The research on Ni-MH batteries is currently focusing on improving the power density and/or reducing costs using cheaper electrodes [40].
Commercially used MH negative electrodes have capacities of about 300 mAh/g, corresponding to ~1,1 Hwt% [41] and are made of intermetallic alloys where the use of "Mischmetal" (Mm, rare earth mixtures with composition similar to the ores) is preferred to $LaNi_5$ in commercial cells for cost reasons [42].
The positive electrode is made of Nickel oxy-hydroxide ($Ni(OH)_2$)and the electrolyte is a basic aqueous solution. The reactions of charge and discharge can be summarized as follow [60]:

Positive	$Ni(OH)_2 + OH^- \leftrightarrow NiOOH + H_2O + e^-$ (E_o = 0,490V vs Hg/HgO)	(1.1)
Negative	$Mm + H_2O + e^- \leftrightarrow MmH + OH^-$ (E_o = -0,828V vs Hg/HgO)	(1.2)
Total	$Ni(OH)_2 + Mm \leftrightarrow NiOOH + MmH$ (E_o = 1,318V)	(1.3)

$Ni(OH)_2$ has lower hydrogen density than $LaNi_5H_x$ (the hydride from which the commercial anode composition in derived): 1,1 versus 1,3 Hwt%, but the energy density, 390 Wh/kg in comparison to ~80 Wh/g, is much higher due to the lighter weight of the second compound.

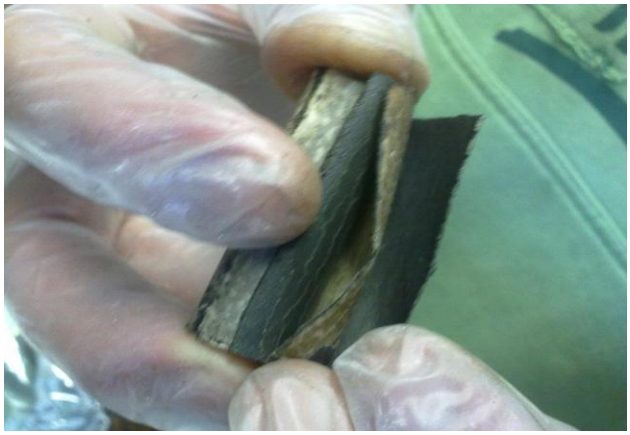

Figure 1.II.2: commercial Ni-MH battery. The anode is plated on a Ni foil and rolled with a separator impregnated of basic solution and two Ni hydroxide layers,

Commercial AA Ni-MH batteries are normally built with a Ni grid plated with the anodic material, a separator (sulphonated polypropylene [40]) impregnated of the basic solution and two Ni oxy-hydroxide layers.

To date commercial solution to the problem of hydrogen evolution during discharge (and also oxygen evolution during overcharges) is the over-sizing of the Ni oxy-hydroxide electrode and a release valve on the cap of the battery.

When an overcharge is applied to the cell, at the positive electrode ($Ni(OH)_2$) oxygen is formed, reaction 1.4, and it migrates to the negative electrode.

At the negative electrode the reduction of metal to the hydride stage, 1.5, is then coupled with another reaction: the reduction of oxygen which consumes the metal hydride, as can be seen in formula 1.6:

Positive:	$4OH^- \leftrightarrow O_2 + 2H_2O + 4e^-$	(1.4)
Negative:	$2Mm + 2H_2O + 2e^- \leftrightarrow 2MmH + 2OH^-$	(1.5)
	$2MmH + O_2 + 2e^- \leftrightarrow 2Mm + 2OH^-$	(1.6)
Total at M/MH:	$2H_2O + O_2 + 4e^- \leftrightarrow 4OH^-$	(1.7)

The total reaction, 1.7, does not consume any reagent or produce any gas, and works similarly for hydrogen in deep discharges.

III Aim of the thesis

The aim of this thesis is the investigation of the possibility to store energy using hydrides not yet commercially exploited for this purpose.
Analyses of different properties with several techniques have been carried out in order to gain confidence with them and to study different aspects of energy with the use of hydrides.

In particular the thesis follows a division corresponding to the two main energy storage techniques with hydrides already described before: storage of hydrogen to be desorbed with temperature and pressure changes: classical or "direct" solid hydrogen storage; and electrochemical hydrogen storage commonly used in commercial Ni-MH batteries.

- ✓ In the first part, hydrogen desorption properties of complex borohydrides with high gravimetric hydrogen storage capacities will be analyzed. The data come from the JRC Institute for Energy of Petten (NL). The samples used are a mix of Mg and Li borohydrides synthesized with three different techniques and five different compositions, all of them synthesized at Padua University (IT) with materials either purchased or coming from Padua's CNR labs (IT).
  The results will be discussed both looking at the composition and at the technique used for the synthesis. Aim of the work is to find the best way to lower the desorption temperature of the compounds.

- ✓ The desorption properties of an innovative Mg based compound have been studied and the material, sensitive to the alkaline solution used in commercial Ni-MH batteries, have been used to assemble high capacity electrodes. Different shielding techniques have been explored to prevent the corrosion, and the electrodes tested with different devices at the TU Delft (NL) and TU Eindhoven (NL). In order to do so, a new procedure to use the already present devices has been invented and will be described.
  Aim of the experiments is to verify if the protection methods proposed are effective and if it is possible to assemble a MgH_2 based electrode for Ni-MH batteries.

Experimental Techniques

There is a powerful agent, obedient, rapid, facile, which can be put to any use and reigns supreme on board my ship. It does everything. It illuminates our ship, it warms us, it is the soul of our mechanical apparatus. This agent is – electricity.
Mixed with mercury, sodium forms an amalgam that takes the place of zinc in Bunsen batteries, [..]Moreover, I can tell you, sodium batteries are more powerful. Their electric motive [sic] force is twice that of zinc batteries

Jules Verne, 20'000 Leagues Under the Sea, chapter 11

Various equipments have been used for the syntheses and analyses reported in this thesis. In this chapter all the devices will be schematically summed up and explained.
The equipments used have four main goals: synthesis, morphology and chemical characterization, hydrogen desorption properties analysis and electrochemical properties analysis of the samples.
In order:
- Almost all the handling has been done in Ar filled gloveboxes and the syntheses have been done with high energy Ball Milling (BM) and with wet chemistry in Padua and also with BM in Delft. The deposition of Pd layers for the battery samples has been done with an in house magnetron sputtering.
- Analyses of powders or samples morphology and chemical characterization have been done with a Scanning Electron Microscope (SEM), LEO Supra 50 in Petten and Phillips FEI XL 30S in Delft; X-Ray Diffractometer (XRD), different models all by Panalytical; and infrared spectroscopy with a Bruker Vertex 70V. All the experimental settings are reported further in the thesis.
- To study the hydrogen storage properties of the materials the following machines have been used: Thermal Programmed Desorption (TPD) by Hiden, Sivert's apparatus by AMC in Petten and Differential Scanning Calorimetry (DSC) by TA instruments, in Delft.
- Electrochemical characterization have been carried out in two ways: with an in house three electrodes setup (Pd counter electrode and Hg/HgO as reference) for the study of single electrodes and with a Maccor battery tester apparatus coupling the material under investigation with a commercial $Ni(OH)_2$ cathode and a separator, simulating a real battery.

I Synthesis techniques

I.1 Ball Milling

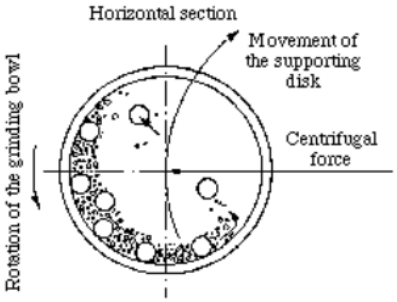

Figure 2.I.1 and 2.I.2: Scheme and picture of a planetary ball mill

Balls and powder are made to collide with high energy in a stainless steel jar.
The rotation movement of the jar and the one of the supporting plate are in opposite direction. These movements impress high centrifugal forces to balls and powder, as shown in figure 2.I.1.
High energies are involved in the process and consent to both crush and reduce to micrometric size the particles and to alloy compounds.
The particle size and/or the alloying rate depend on the balls to powder ratio, on the quantity of material involved, on the milling time and on the speed measured in rounds per minute.
The atmosphere in the jar plays a role as well. For the samples analyzed in this work all the millings have been carried on in Ar atmosphere closing and opening the jar inside a glovebox. It is possible however fill the jar with hydrogen, ammonia or other materials, obtaining different reactions inside the jar during the milling.

I.2 Magnetron Sputtering

Plasma sputtering, or magnetron sputtering, is a deposition technique which uses accelerated noble gas ions to eject material from a target in order to deposit it on a substrate.
The chamber is filled with Ar at a pressure of 10^{-6} bar. Two tungsten filaments ionize the gas via emission of electrons. The Ar ions are directed with a high electric field (500 – 1000 V) to the target (Pd in this case). Clusters of material are ejected from the target and directed to the substrate which is than plated with the target material.
The deposition rate depends on the Ar pressure, the current, the voltages applied and the substrate material. To have a sure measure of the deposited layer thickness a quartz flat piece was attached with adhesive tape on the sample holder and sputtered with the samples of each batch. Afterwards the tape has been removed and the step left between the coated and uncoated part measured with Atomic Force Microscopy (AFM).

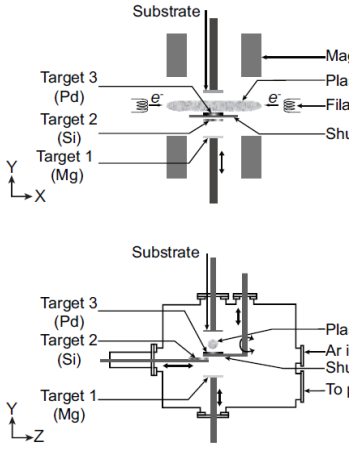

Figure 2.I.3: Working scheme of the magnetron sputtering used in Delft

II Sample characterization

II.1 X-Ray diffraction (XRD)

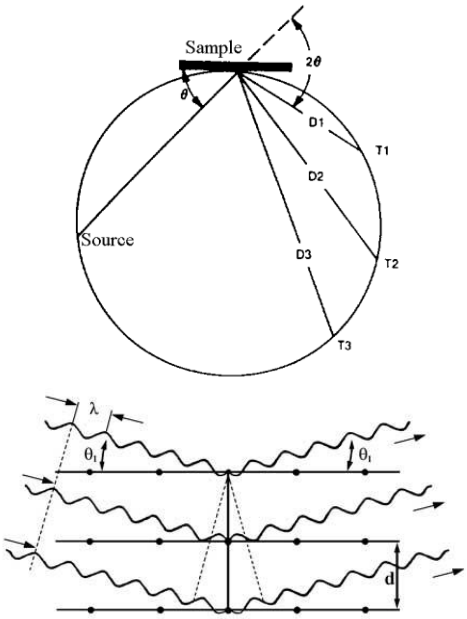

Figure 2.II.1 (left): Picture of an X ray diffractometer from Panalytical
Figure 2.II.2 and 2.II.3 (right): Bragg's law and XRD Bragg-Brentano geometry schematic diagrams

X-Ray Diffraction (XRD) is a technique which employs collimated monochromatic x-rays for characterization and identification of crystalline structure.
In figure 2.II.1 is reported a scheme of Bragg Brentano configuration. The cathode (Source) emits the electrons that are accelerated into the vacuum towards the anode by a high voltage. The electrons impact the anodic material, which for the uses reported in this thesis normally is made of copper, and produce X-rays. The produced radiation is filtered and collimated on the sample.
The detector is able to move in circle to reach different angles, see figure 2.II.2 and at each angle it stops to collect the X-rays diffracted by the sample in that direction.
According to Bragg's Law, see figure 2.II.3, when X-rays are scattered from a crystal lattice constructively, signals are detected by the detector. The observed peaks positions follow the Bragg's equation:

$$n\lambda = 2d\sin(\theta) \qquad (2.1)$$

Where θ is the angular position between the incident and diffracted rays, d is the spacing between the planes of atoms lattice, n is an integer, and λ is the wavelength of x-rays, as schematically plotted in figure 2.II.3.
The basic principle of Bragg-Brentano geometry is used for a large range of materials, from bulk to powders and is one of the most common configurations in commercial diffractometer.

Elaboration of the patterns is done to have different information: a first, easiest, approach is to detect the phases present in the sample (indexing), then, a more refined approach, named Rietveld analysis, is able to give information on: dimension of the crystals, or particles

assuming the particles to be monocrystalline, stresses present in bulk materials, distortion of lattice parameters in case of alloys and distribution of the phases in the sample in term of percentage.
Crystallite sizes can be approximately determined using the Scherrer equation:

$$L = \frac{k\lambda}{B_r \cos\theta} \quad (2.2)$$

Where λ is the wavelength of the x-rays used, θ is the Bragg angle, L is the average crystallite size measured in a direction perpendicular to the surface of the specimen, and k is a constant, with the assumption that k = 1.0, B_r is the line broadening at half the maximum intensity (FWHM) in radians.
Deviation or movements of only part of the peaks of a phase are generally due to changes in term of distance of some particular planes. The change might be due, depending on the sample, to stresses in the structure (bulk samples) and/or to hosted elements in the lattice (alloys).
Quantitative information on the phase composition, in terms of percentage of each phase in the total, can be estimated from the intensity of the peaks of each phase in comparison to the others.

A major drawback of this technique is that only crystalline fraction of the samples can be detected and analyzed, even if advanced software are now able at least to estimate the quantity of amorphous phase present. In facts, all the amorphous phases are seen only as noise or huge bumps.
Another issue connected with XRD is that a good analysis of the patterns is possible only when all the phases are known and when the peaks are well defined.

II.2 Scanning Electron Microscopy with EDS (SEM-EDS)

Scanning Electron Microscopy (SEM) gives morphological and topographical information of solid surfaces. In SEMs the sample is bombarded with an electron beam that scans its surface. The shorter wave length of electrons creates a better resolution than in optical microscopy, therefore pictures of samples with higher magnifications can be obtained.
In order to have no charging effects on the samples due to the bombardment of electrons, a good sample conductivity is required.
In case of a poor- or non-conductive samples there are different techniques to operate: for bulk samples or in the case where only morphology is under investigation, a layer of gold or carbon is sputtered on the surface, for fine powders a copper grid is usually enough to drag the majority of the electrons that were not able to come out from the samples after the penetration. The vacuum needed in the sample chamber used to limit strongly the technique in the past to materials that have no problem with it, nowadays different technologies have been developed and it is now possible to see biological and or oil-bearing rock that formerly, with the normal SEM, needed to be either dried or cryogenically frozen.

The electron beam, emitted from the filament in the electron gun, is accelerated towards the sample and focused by several condenser magnetic lenses, see figure 2.II.4. When the focused beam hits a point on the sample, numerous collisions between the electrons from the beam and atoms in the sample occur. As a result of these collisions some of electrons will be scattered outside of the sample either coming from the original beam (back scattered electrons, BSE), still with high energy, or from the atoms of the sample. These electrons, called secondary electrons (SE), have relatively low kinetic energy and can easily be attracted by a side detector, while the high energy back scattered are usually detected by a ring detector placed parallel to the sample, around the in coming electron beam, see figure 2.II.4.
The detectors count the electrons emitted from each point of the scanned area where the beam is focused and the result are displayed as points of different brightness on a computer screen. A magnified image of the sample is created by scanning the electron beam over a smaller area, detecting and displaying the number of electrons originating from each smaller point. Both the topography of the sample and the atom numbers (Z) affect the number of electrons emitted and these factors are therefore represented in the picture. The resulting image has shadows and perspective, much like ordinary photographs, and is consequently rather easy to interpret.
The influence of the topography and atomic number is not the same for the different kind of electrons: the backscattered (BSE) are more influenced by Z because the lower the atom number the higher is the possibility for the electrons to pass trough the sample while for

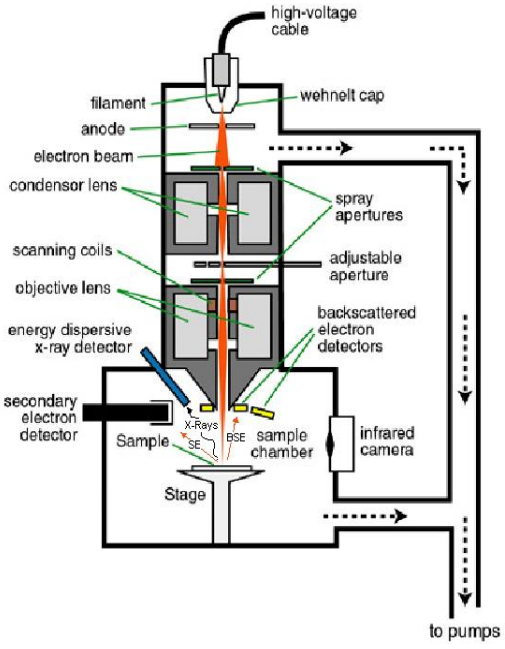

Figure 2.II.4 scheme of a SEM (Scanning Electron Microscope)

higher Z the electrons are more easily back scattered to the detector, resulting in a brighter spot in the BSE image. On the other hand secondary emitted (SE) have low energy and the smaller the path trough the sample the higher is the probability for them to reach the surface and then the detector. This in the reason why the morphology is more detailed for SE pictures and the edges result as brighter spots in comparison to the valleys.

An important apparatus that gives more information on the sample is the EDS (Energy Dispersive Spectroscopy) or EDX (Energy Dispersive X ray spectroscopy). One of the events connected with the impact of an electron with the sample lattice is the possibility of excite and then have the relaxation of an orbital electron. The relaxation takes place with the emission of the characteristic X-ray photon connected with the difference of the orbital energy of the excited and relaxed state.
The EDS detector collects the photons coming from the samples and, based on the quantity and the energy distribution, is able to give spectra or maps for elemental analysis.
The upper resolution limit of the EDS is the electron beam energy, the lower is the energy absorbed by the lenses. Unfortunately many light elements have low characteristic X-ray energy and elements like Lithium and Hydrogen are thus not detectable with this technique.

II.3 Fourier Transformation Infra Red (FTIR)

Infrared spectroscopy is used in a wide variety of fields, since the analyzed sample can be used for further analyses after IR, it is considered a non-destructive technique.
The FTIR spectrum is obtained by passing electromagnetic radiation through the sample. The electromagnetic waves used for this technique are in the rage between 2500 to 16000 nm (InfraRed), with a corresponding frequency range from $1.9*10^{13}$ to $1.2*10^{14}$ Hz [@15]. When the frequency of the radiation is the same of the vibrational frequency of a band of a sample, absorbance occurs.
Transmittance or absorbance is plotted against wave number obtaining peaks which position and intensity reveal details about the molecular structure of the sample.
At each wavelength corresponds a frequency and the frequency to a characteristic vibration of a bond of the molecules present in the sample [43].
An FTIR spectrometer uses the mathematic Fourier transform to elaborate the data coming from the detector. Thanks to that it can simultaneously collect spectral data in a wide spectral range. This confers a significant advantage over an old dispersive spectrometer which measures intensity over a narrow range of wavelengths at a time.

III Hydrogen desorption analysis

III.1 TPD with quadrupole Mass Spectroscopy (TPD-MS)

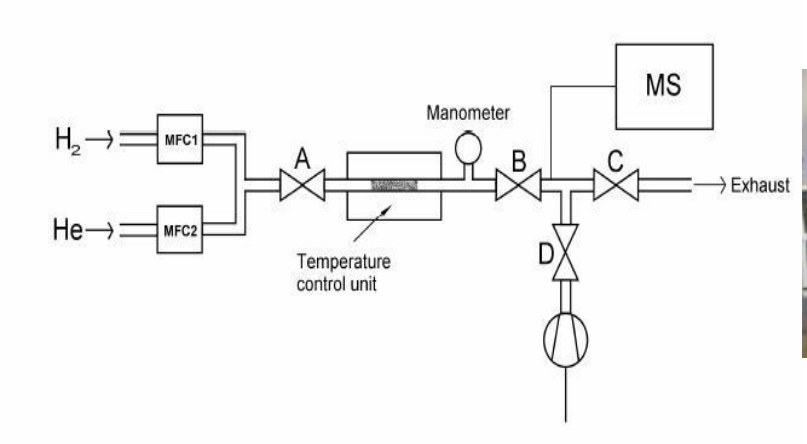

Figure 2.III.1 (left): Schematic diagram of thermal desorption spectroscopy apparatus from [44]
Figure 2.III.2 (right): picture of the Hiden apparatus in Petten

Temperature-Programmed Desorption (TPD), also known as Thermal Desorption Spectroscopy (TDS), is a well known technique in hydrogen storage but it is also used in surface science and to study the desorption of adsorbates from porous materials and adsorbents, for applications such as catalysis [44].
The technique can be summarized as follow: the sample is heated with a controlled ramp to a desired temperature, in general for experiments with complex hydrides is 500^{o}C, under inert gas flow, generally is He because of the low mass that gives less problem for the Mass Spectrometer (MS).
The input of helium flow is monitored and part of the gas output goes to the MS for the selective detection of the evolved species, not only hydrogen, and their partial pressures. From the partial pressure of each gas and the quantity of He that went in, if the calibration is good, it can be calculated the absolute amount of each gas that have been released by the sample during the experiment. Knowing the mass of the sample and the M/H ratio in case of metal hydrides the result can be converted in Hwt% or average hydrogen atoms release from each atom of metal.

To illustrate the principle in figure 1.1.1 is reported a schematic diagram of a TPD apparatus. The system can operate in three modes: flowing mode to determine the gas release of the sample, static mode using either the MS or the manometer to monitor the desorbed quantity of gas.
With the setting normally used for the experiments reported in this thesis, pure helium passes first trough Mass Flow Controllers (MFC2) then to valve A that controls the gas inlet, and arrive to the sample in the temperature control unit. There are two temperature controllers: one in the chamber and one inside the sample holder, in contact with the sample itself. The evolved gasses mixed with the helium carrier pass trough valve B and can go, depending on

the experiment setting, to the vacuum pump or to an exhaust outlet, using valve C and D. In all the cases a small amount of the gas can pass trough a capillary to reach the MS quadrupole that can selectively detect the gasses present in the gas mix coming from the sample chamber. To re-hydrogenate the sample, if possible, the normal procedure is to close valve B and let in a certain pressure of hydrogen keeping it for a suitable time depending on the material. For some materials is required also to increase the temperature and for some others the harshest setting possible of the machine is not enough to obtain re-hydrogenation, this is the case for example of AlH_3 [35].

The load and unload of the sample, if it is air sensitive as the majority of the materials studied for hydrogen storage, has to be done under inert gas atmosphere. In the apparatus used in Petten a portable mini glovebox, provided by Hiden, is mounted and dismounted every time a sample has to be loaded or unloaded. 40 minutes of nitrogen gas flow have been seen to be enough to clean the atmosphere from all the oxygen present, leaving only traces as can be found in a normal glovebox. The sample is transported from the apparatus to the glovebox and back with a sealed sample holder.

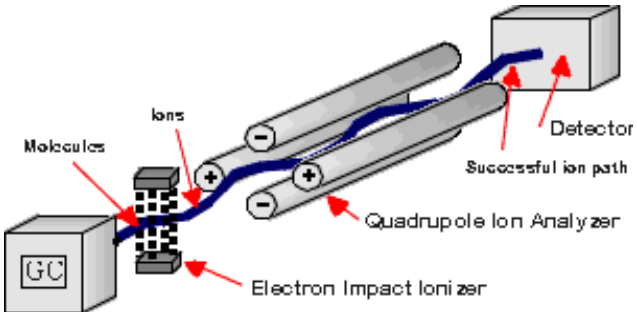

Figure 2.III.3: basic scheme of a Mass Spectrometer with the main components.

Temperature ramps have to be chosen carefully. It can be said that the slower they are the better because the effects of the kinetics are lower, but some information can be acquired from different ramps with the same material. This is the case of the Kissinger plots with which the activation energy can be derived from TPD or DTA (differential thermal analysis) peaks taken at different heating rate [45][46]. This is an interesting approach in the case of materials with oxidized shells and has been already applied for possible hydrogen storage materials [47].

A quadrupole mass spectrometer consists of an ionizer (bombardment by electrons from a hot filament), an ion accelerator, and a mass filter consisting of four parallel metal rods arranged as in the figure 2.III.3. Two opposite rods have an applied potential of $(U+V\cos(\omega t))$ and the other two rods have a potential of $-(U+V\cos(\omega t))$, where U is a dc voltage and $V\cos(\omega t)$ is an ac voltage. The applied voltages affect the trajectory of ions traveling down the flight path centered between the four rods. For given dc and ac voltages, only ions of a certain mass-to-charge ratio pass through the quadrupole filter and all other ions are thrown out of their original path. A mass spectrum is obtained by monitoring the ions passing through the quadrupole filter as the voltages on the rods are varied [@16].
To know the mass over charge ratios to check, given a certain compound, one option is to use databases, as NIST's one [@17]. If this is not possible or several compounds might be present an alternative it is to use a screening mode to detect all the charged fragments coming from the samples and then compare the results with standards or literature.

With the machine provided by Hiden, in the case of few known M/Z ratio, the used set is MID mode, the most precise; while for screening it is used the BAR mode that is less precise but is able to detect all the signals of a given M/Z range.
The hydrogen signal (i.e. its partial pressure over the flow) against time data produced from a TPD experiment can be used in one of two general ways: Firstly, the spectrum produced can be analyzed in terms of peak positions or, secondly, an integration under the spectrum will give a total desorbed quantity of the selected gas [44]. In order to do this a good calibration of the flow must be carried on after each experiment.

III.2 Volumetric Sivert's technique

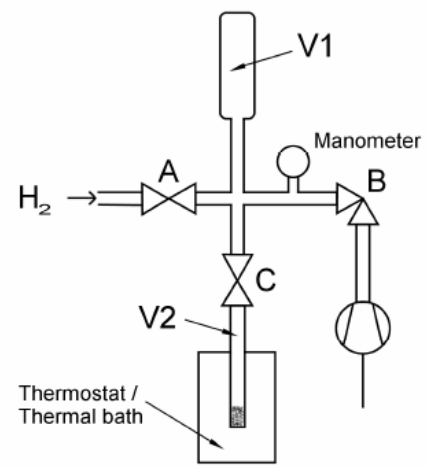

Figure 2.III.4 (left): Schematic diagram of volumetric Sivert's apparatus from [44]
Figure 2.III.5 (right): Picture of the machine used both in Padua and in Petten, by AMC

The volumetric technique is used to determine the amount of hydrogen ad- or absorbed by a sample by monitoring the drop in hydrogen pressure in a fixed calibrated volume in direct contact with the sample. During the desorption process, the quantity of hydrogen released is determined by the increase in the hydrogen pressure, following evacuation of some or all of the hydrogen in the gas phase. To illustrate the principle, Figure 1 shows a schematic diagram of a basic volumetric set-up. V1 and V2 have known volumes and valves A and B control the hydrogen gas inlet and vacuum outlet, respectively, allowing the control of the hydrogen pressure in V1.
Valve C allows the introduction or removal of gas to or from V2, and the pressure in V1 is measured using the manometer. The sample is placed at the bottom of V2, with a temperature sensor (not indicated in the diagram) either near or in contact with it. As in all of the measurements described in this report, the sample should be secured appropriately to avoid to be sucked from the vacuum pump. This is usually done with a stopper, quartz wool in the case of powders.
The thermostat or thermal bath can be any temperature-controlling system, including a liquid N_2 Dewar flask, a cryostat, a low temperature fluid bath or a furnace. The temperature of the system has to be carefully controlled and monitored, with temperature sensors in more than

one position, preferably including the measurement of the gas temperature away from the sample.
The manometer represents one or more pressure measuring devices, depending on the hydrogen pressure ranges required. In a system designed for both low and high pressures, this is likely to include separate gauges for different ranges. The generic vacuum pump can be of any type, although an oil-free system with a ultra-high vacuum (UHV) compatible pump, for example a turbomolecular.
To perform a simple, single step absorption experiment on an activated sample in the apparatus shown in Figure 2.III.4, valves B and C are first opened to evacuate V1 and V2. After sufficient time, valves B and C are then closed. Valve A is opened, allowing V1 to fill with hydrogen to an initial pressure *Pi*. Valve C is then opened thus filling V2. Any drop in pressure beyond that which is expected from the volume difference between *V1* and (*V1* + *V2*) is then assumed to have resulted from the absorption of hydrogen.
From the pressure change, knowing the volumes of the sample, stopper and chamber V2, the type of gas and the temperature, it can be calculated the amount of gas released or adsorbed by the sample. This is usually performed using complex mathematical equations implemented for the non-ideal behavior of hydrogen at high and moderate pressure. As in the case of TPD measurements knowing the mass or the number of atoms of the sample, the quantity of hydrogen can be converted into Hwt% or H/M.

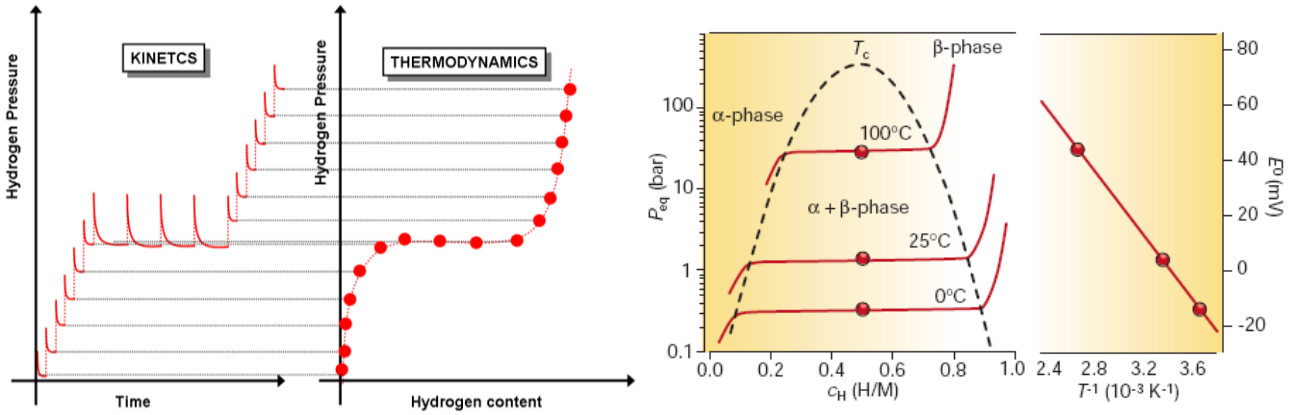

Figure 2.III.6 (left): Volumetric measurement: at a fixed temperature the sample chamber is refilled by steps with hydrogen. At each kinetic step corresponds a point in the PCT diagram on the right (thermodynamics) when the equilibrium is reached.
2.III.7 (right): If the procedure is done at different temperatures the "bell diagram" can be obtained and from the values of temperature and plateau pressure, the Van't Hoff Diagram can be draw in function of pressure or potential.

Two common approaches are used with this apparatus: kinetics and isotherms.
The first approach is used to study, at a set temperature, the speed of absorption or desorption of the sample, in terms of quantity of hydrogen (absolute, Hwt% of H/M) in the time unit (seconds, minutes or hours depending on the material). The speed is calculated monitoring the pressure drop in the V2 chamber and converting the result as described above.
A second approach is normally used with cyclable materials:
At a set pressure and temperature a material can absorb only a limited amount of hydrogen. As described in figure 2.III.6, several kinetics can be performed monitoring the pressure drop

for different pressure steps. Plotting the obtained equilibrium pressures versus the hydrogen adsorbed (or desorbed) at each step, an isotherm curve can be obtained.
Isotherms at different temperatures correspond to different plateau pressures. The plateau pressure P_{eq} as a function of temperature is related to the changes ΔH and ΔS of enthalpy and entropy, respectively, by the Van't Hoff equation:

$$\ln\left(\frac{P_{eq}}{P^{\circ}_{eq}}\right)=\left(\frac{-\Delta H}{R}\right)\left(\frac{1}{T}\right)+\frac{\Delta S}{R} \quad (2.3)$$

From the slope of the van't Hoff plot, figure 2.II.6, obtained with the previous formula, experimental values of the enthalpy of hydride formation ΔH can be evaluated [22].

Figure 2.III.8: The DSC apparatus by TA instruments used at the TU delft.

III.3 Differential Scanning Calorimetry (DSC)

DSC is a very versatile and relatively old technique, introduced during the 60s. It mainly consists in increasing (or decreasing) the sample temperature following a set ramp and collect the data of heat emission or absorption to reach each temperature step.
The sample is coupled with a known standard to obtain the results by comparison.
In many cases the peaks correspond to endothermic or exothermic reactions but also other properties like phase changes can be detected and linked with heat absorptions or desorptions.
With the machine used for this thesis (Q2000 TA instruments USA) it is possible to load many samples and an automatic arm will take them one after another when each experiment is finished.
The temperature range possible is quite broad since it makes use of liquid nitrogen to cool down, but only a range of 450°C (from room temperature to 475°C) have been considered for the experiments ran with the machine.

IV Electrochemical characterization

There are two main ways to prepare a sample for electrochemical measurements, both with positive and negative aspects. Thin films have well defined areas but generally small weights, pressed powders are harder to handle because it is normally hard to have a mechanically stable pellet, but are more massive, can be checked with X rays diffraction techniques and generally have larger areas.
Two approaches are used in battery electrochemistry: Galvanostatic or Galvanostatic Intermittent Titration Technique (GITT) and Cyclic Voltammetry.
In this work only galvanostatic measurements have been carried on.

IV.1 Three electrodes setup

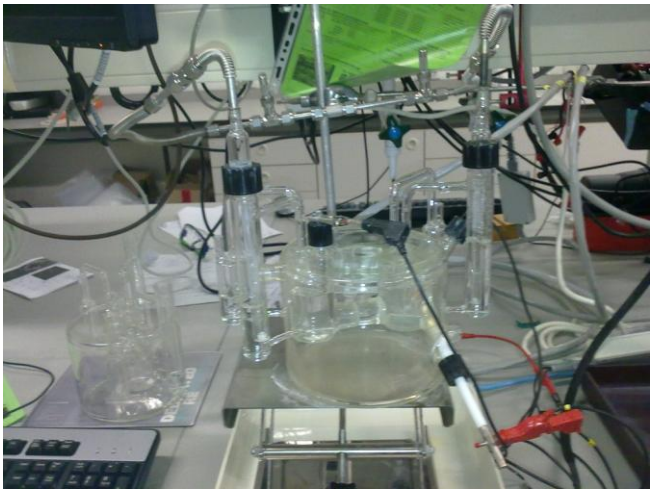

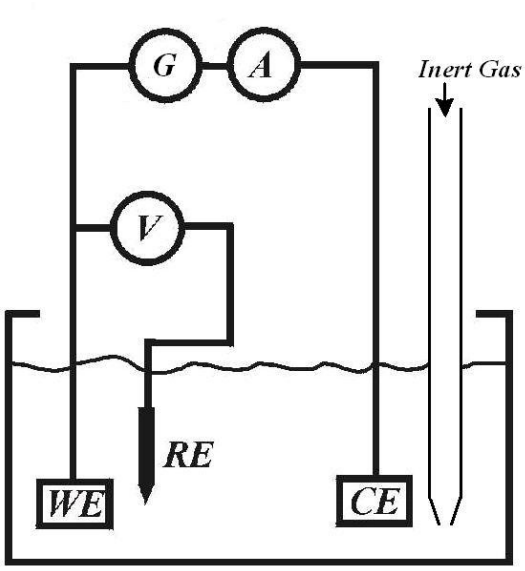

Figure 2.IV.1 (left): three electrodes setup used at the TU Eindhoven
Figure 2.IV.2 (right): Scheme of a basic three electrode setup made by Working Electrode (WE), Counter Electrode (CE), Reference (RE) and Inert gas inlet.

Two Three Electrodes Setups have been used for this thesis work: an already well tested setup at the Technische Universiteit (TU) Eindhoven and a new home made setup developed during the researching period at the Delft Institute of Technology (TU Delft).Both of them consist in three electrodes immersed in a basic solution (6 M KOH).
In galvanostatic measurements a set constant current is passed through the system between the working electrode (WE), made of the material under investigation placed over a silver rod used as holder and current collector, and a counter electrode (CE) a palladium foil or wire. The voltage needed to let this current pass is registered at each time step. The potential of the WE is monitored versus a reference electrode (RE) placed near the surface of the WE in order to minimize the Ohmic drop due to the electrolyte. The RE was for all the experiments Hg/HgO (by Kolsow Scientific Company) assembled in Pb free container. The RE must have, under normal experimental conditions, an invariant potential stable in time. The device used to measure the potential difference between the WE and RE has a high impedance, thus the current that passes through the RE is much lower of the WE one and does not affect the measurement.

The constant current applied to the electrode causes reactants at the electrode surface to react. The potential of the working electrode changes to values characteristic of the electrochemical reaction that is occurring. At each reaction corresponds a plateau in the V-t diagram.
The plateau of the electrochemical techniques gives the same information of the one in the PCT measurements. The relation between the two is [48][49]:

$$E(V\ vs\ Hg/HgO) = -0.932 - 0.0296 \log(p(H_2)) \qquad (2.4)$$

Galvanostatic experiments give information about the charge and discharge capacities of electrode materials.
For instance, as the discharge current is constant in time, the applied current multiplied by the charging time will give the exact amount of charge transferred during a particular potential response of the working electrode, i.e. the capacity at that discharge rate in mAh.
Dividing the capacity by the sample weight gives the capacity of the material in mAh/g.
The quantity of hydrogen stored in the material can then be easily calculated with the Faraday law:

$$H_x = \frac{|I|tM}{AdρF} \qquad (2.5)$$

Where I is the current, t the time, M the weight of the metal, A the surface area, d the thickness of the sample, ρ the density of the material and F is the Faraday constant [50].
From the previous formula it can be calculated that 1 mAh/g of charge corresponds to 0.00376 Hwt% and 1 Hwt% to 263 mAh/g.

From the classical galvanostatic technique the GITT has been derived in order to have data closer to the equilibrium. The technique is based on galvanostatic pulses and relaxation periods, continuously alternated.
Firstly, a (short) current pulse is applied to the system during which a small amount of charge is transferred, thereby slightly changing the oxidation state of the material under investigation. Afterwards the electrode is allowed to relax to its new equilibrium under open-circuit conditions. This procedure is repeated until the compound has reached, dependent on the current applied, its fully oxidized or reduced state.
It's reported to be important to have reliable results (on potential and capacities) to work in an oxygen free environment for two reasons: the materials under investigation are air sensitive and the oxygen present in the solution changes the response of the system, giving lower potentials and capacities [51].
Therefore all the handling of the materials has been done in the glove-box and the exposure has been minimized in the transport to the three electrodes setup. Before inserting the electrode

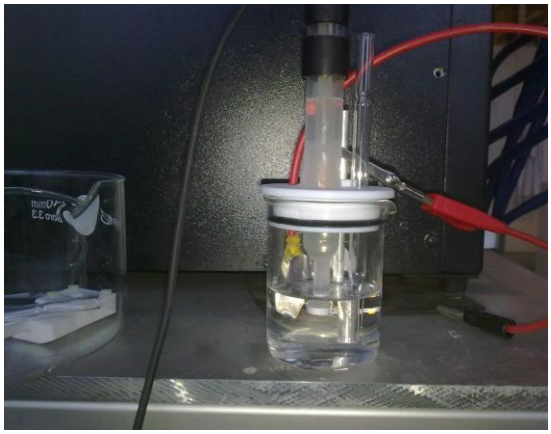

Figure 2.IV.3: The Three electrodes setup assembled and preliminary tested at the TU Delft

in the solution, the electrolyte has been purged with vigorous bubbling of highly pure inert gas (being nitrogen or argon depending on the setup) and the gas flow has been kept for the whole time of the experiment leaving also a small overpressure of gas in the sealed cell.

IV.2 Maccor battery test apparatus

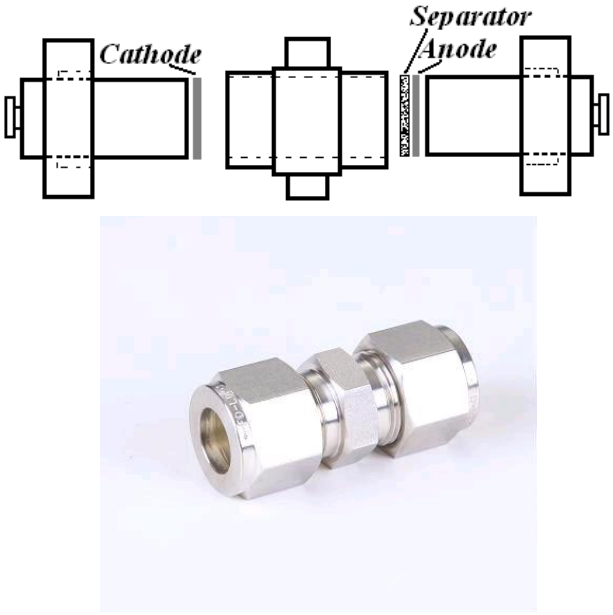

Figure 2.IV.4 (left): The 8 channels Maccor apparatus in the TU Delft labs.
Figure 2.IV.5 and 2.IV.6 (right): Scheme and picture of a Swagelok battery tester. The cathode, anode and separator are put in the main body and the two nuts are screwed tight to prevent leaking and further open air exposition.

Another way to test batteries is assembling the anodic material under investigation with a glass wool separator and an appropriate cathodic material, wet them with the electrolyte, seal the system and test with charge discharge cycles.
The cycles are normally carried on in a similar way of the ones with three electrodes setup. A fixed current density is applied and the voltage is measured every time step (usually one second). The cut off voltage limits the charge and the discharge.
Unfortunately this experimental layout is optimized, at least in the lab of FAME research group, for Li-ion batteries and not for Ni-MH.
The main problem is the use of an aqueous solution and of air sensitive materials. The solution cannot enter the glovebox because the water vapour level has to remain low, but the active materials have to be exposed as less as possible to air.
To overcome the oxidation issue of the cathodic material which had to be kept, with the solution, outside the glovebox, a bigger amount of it has been used every time.
Unfortunately doing so it is lost the overcharging protection described in the introduction. The anodic material on the other hand has been protected with the metallic holder and the

quartz wool separator (previously dried in a vacuum oven and stored in the glovebox) trying to limit the exposure as much as possible.
The solution used is not oxygen-free but the use of a pipette to pour some drops in the separator would anyway introduce new oxygen in the liquid.
Part of the work has also been the set-up an "ad hoc" procedure to characterize the Ni-MH batteries with the Maccor Battery Tester system.
As explained in chapter III of the 3rd part, the method is not optimized yet but, thanks to the comparison with the tests on commercial materials and commercial assembled batteries, it is possible to have a feeling of how the samples should behave if used in place of the current used materials in commercial batteries.

Experimental Work

“I return then to my large-grained powder, which removes those difficulties. In his Columbiad charges Rodman employed a powder as large as chestnuts, made of willow charcoal, simply dried in cast- iron pans. This powder was hard and glittering, left no trace upon the hand, contained hydrogen and oxygen in large proportion, took fire instantaneously, and, though very destructive, did not sensibly injure the mouth-piece”

Jules Verne, From the Earth to the Moon, chapter 9

I Complex hydrides

I.1 Introduction on the materials

$LiBH_4$

$LiBH_4$ is a potential candidate for hydrogen storage materials because of its very high gravimetric and volumetric hydrogen densities: respectively 18.5 Hwt% and 121 kgH_2/m^3 [52]. The first report of a pure alkali metal borohydrides appeared in 1940 by Schlesinger and Brown [53] who synthesized some $LiBH_4$ by the reaction of ethyl lithium with diborane (B_2H_6). By Fedneva et al [54] is the first Differential Thermal Analysis (DTA). The "thermogram" of $LiBH_4$ showed three endothermic effects: at 108–112, 268–286, and 483–492 °C. The endothermic effect at 108–112 °C is reversible and corresponds to polymorphic transformation of $LiBH_4$. The second peak at 268–286 °C corresponds to the melting of $LiBH_4$. The melting is accompanied by a slight decomposition, which liberates approximately 2% of the hydrogen in the compound. The main evolution of gas starts at 380 °C and liberates 80% of the hydrogen in $LiBH_4$. The reason for the small effect at 483–492 °C is according to the authors uncertain. However, it coincides with the liberation of 50% of the hydrogen [54]. Those results have been confirmed by more recent works [52][53].

In the 70s the attention went back to the borohydrides and the possibility of storing hydrogen in this form. A patent from La Compagnie Francaise de Raffinage [56] not only claims the method of using lithium borohydride for the storage and generation of hydrogen, but even the use of catalysts such as Al to decrease the temperature of desorption. In the patent the reversibility is claimed to be achieved but the kinetic was very slow.

Different paths have been proposed [52] even with not-yet-well-identified compounds such as $Li_2B_{12}H_{12}$ [55][57]. The most accepted reaction seems to be the simple:

$$LiBH_4 \rightarrow LiH + B + \frac{3}{2}H_2 \qquad (3.1)$$

That desorbs 13.8 wt% of hydrogen.
Two important steps have been made in order to use $LiBH_4$ as hydrogen storage material, dated 2002 and 2004, some years after the expiration of the patent on the compound. The first, by Zuttel [55], has been the decreasing of the desorption temperature thanks to the mix with SiO_2 working as catalyst. The second main goal with this compound has been the achievement of re-hydrogenation at 35 MPa and 600°C [52] and afterwards at 350 °C and 10 MPa. The second achievement, by Vajo et al [58], has been possible after the addition of MgH_2 in 1:2 proportion and the system proved to be cyclable even by other scholars [59].
To date researches are mainly focusing on further decreasing the desorption temperature by adding different catalysts or destabilizing elements or infiltrating the borohydride in scaffolds, generally made of carbon because the compound is reactive with silicon, as showed by Zuttel [53].

$Mg(BH_4)_2$

According to a complete review on the material by Chlopek [61], the first researches on $Mg(BH_4)_2$ are from the 50s, but still in the 70s only few data were available [62]. Moreover till the raising interest on complex hydride of the last years no more important researches have been done. Magnesium borohydride has a lower gravimetric hydrogen desorption capacity in comparison to $LiBH_4$, 14,9 Hwt%, due to the heavier cation, but Mg has a Pauling electronegativity of 1.31, which is greater than that of Lithium (0,98), therefore the relative borohydride is less stable than $LiBH_4$[63]. The low stability is important to have a low desorption temperature, due to the thermodynamic.
Being a newer material in comparison to $LiBH_4$, less works are available in literature and the first dehydrogenation studies are from 2007-2008 [61][63][64] when not the decomposition reaction or the crystalline structure were well known.
From XRD in situ analysis Chlopek et al derived that the dehydrogenation path depends on the condition under which the reaction takes place. In general, anyway, it follows this path [61]:

$$Mg(BH_4)_2 \rightarrow MgH_2 + 2B + 3H_2 \rightarrow Mg + 2B + 4H_2 \rightarrow MgB_2 + 4H_2 \quad (3.2)$$

It is important to note that the dehydrogenated product is a single phase material, MgB_2, while other borohydrides, as $LiBH_4$ or $CaBH_4$ [65], decompose to a binary system.
Other authors propose an amorphous intermediate $Mg(B_xH_y)_n$ detected with Raman and IR [61] that could be important for the reversibility.

According to the complete data of a group of Japanese authors [66], the desorption takes place in three steps: a first weight loss (3.33 wt%) is at 293°C without compromising the crystal structure and the second (2.6 wt%) at 320°C with the disappearance of the crystalline order. At 365°C MgH_2 is formed and the desorption is 5.1wt%. In the end, at temperatures above 460°C, Mg and amorphous Boron combine to form MgB_2 and the final desorption is 3.4wt%, for a total of 14.4wt%, close to the theoretical 14.9 Hwt%.

To improve the properties linked with hydrogen storage, similar approaches of the one for $LiBH_4$ have been followed: Destabilization, impregnation and use of catalysts. To prove the reversibility Severa et al studied the direct hydrogenation of the products, magnesium boride and hydrogen, obtaining a yield of 11 Hwt% [67] and apparently bypassing the complex compound reported by Li [66].

Destabilization

Destabilization is different to simply creating new alloys which can reversibly store hydrogen because the decomposition products of a destabilized system will reversibly react with hydrogen to reform the starting materials used. This technique was first demonstrated in 1967 when Mg_2Cu was reversibly hydrogenated to MgH_2 + $MgCu_2$ [68] following the reaction:

$$MgCu_2 + 3MgH_2 \leftrightarrow 2Mg_2Cu + 3H_2 \quad (3.3)$$

Vajo et al. have investigated several systems including the destabilization of LiH by MgH_2 with silicon (Si) and also of $LiBH_4$ with MgH_2 [58].
These types of system could prove to be very useful in the search for a more viable H_2 storage medium because when destabilizing species are present within a material they can offer lower energy pathways for the dehydrogenation reaction. The alternative reaction pathways for the dehydrogenation of the sample may be both kinetically and/or more thermodynamically favorable than when using the starting materials alone.

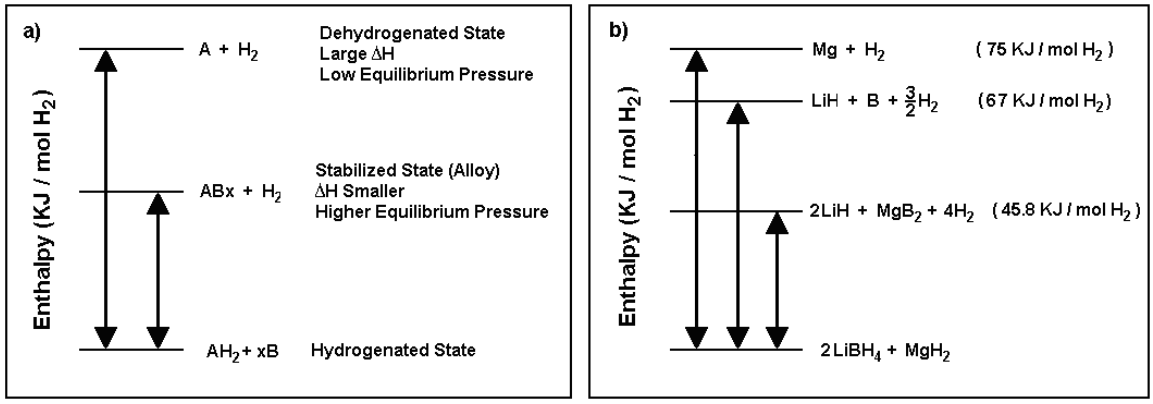

Figure 3.I.1 a) General Destabilization case b) Comparison of the decomposition enthalpy for pure Mg, pure $LiBH_4$ and a mixed $LiBH_4$ + MgH_2 system [69].

The most promising destabilized system for $LiBH_4$, the one with MgH_2, has a different desorption pathway in comparison to the one by which the two materials individually desorb. The result is that less energy is required to remove their hydrogen, therefore it can be defined as a thermodynamic destabilization.
Studies on the decomposition of the system have been made, leading to slightly different conclusions.
According to Yu et al [70] the reversibility of the system does not depend on the formation of MgB_2. They propose a path, supported by ex situ XRD patterns, that leads to the formation of amorphous B during the decomposition of $LiBH_4$ catalyzed by the Mg, at 400°C, and than from 420°C the products react again to form a three phases composition: $Li_{0.184}Mg_{0.816}$, MgB_2 and $Li_{0.3}Mg_{0.7}$.

$$MgH_2 \xrightarrow{\sim 360\ ^\circ C} Mg + H_2 \tag{3.4}$$

$$0.30\ LiBH_4 \xrightarrow{\sim 405\ ^\circ C,\ Mg} 0.30\ LiH + 0.30\ B + 0.45\ H_2 \tag{3.5}$$

$$Mg - 0.30\ LiH + 0.30\ B \xrightarrow{> 420\ ^\circ C} 0.37\ Li_{0.184}Mg_{0.816} + 0.15\ MgB_2 + 0.78\ Li_{0.30}Mg_{0.70} + 0.15\ H_2 \tag{3.6}$$

On the other hand, according to Vajo et al [58][69][71] and other authors [72][73] the system evolves, especially in the presence of catalysts, directly to MgB_2 in two steps:

$$LiBH_4 + {}^1/_2MgH_2 \rightarrow LiBH_4 + {}^1/_2Mg + {}^1/_2H_2 \rightarrow LiH + {}^1/_2MgB_2 + 2H_2 \tag{3.7}$$

Another important possibility to destabilize borohydrides is with another borohydride. A systematic study by Nakamori et al.[74] has shown that stability of metal borohydrides can be roughly estimated by the electronegativity of the cation (see in set figure 3.I.2); a less electronegative metal can form a more stable metal borohydride.

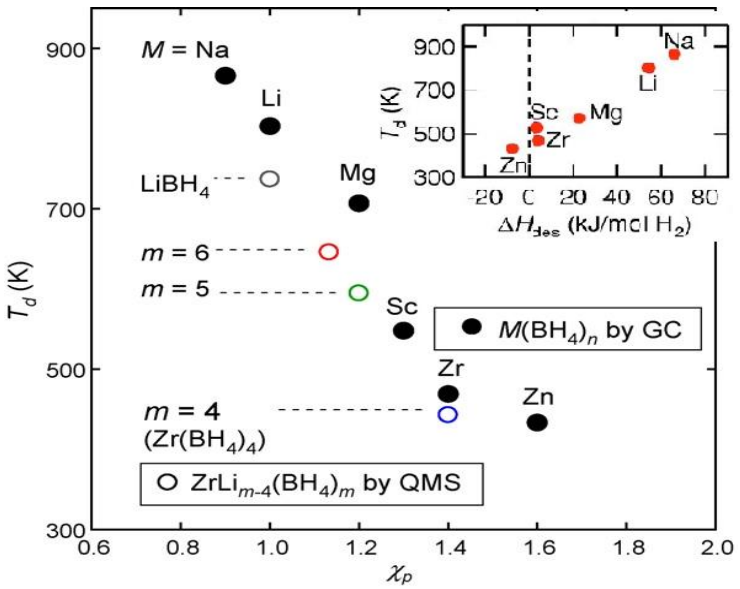

Figure 3.I.2: The first peak desorption temperature T_d as a function of the Pauling electronegativity χ_P. Inset shows the correlation between Td and estimated ΔH_{des} for the desorption reaction [74][75]

According to a second work [75] of the previous said Japanese group, the electronegativity of the mixed cations in $MM'_{m-n}(BH_4)_m$ borohydrides can be calculated with the following formula:

$$\chi_{mix} = \frac{\chi_1 + \chi_2(m-n)}{1+(m-n)} \qquad (3.8)$$

Where χ_1 and χ_2 are the electronegativity of the two cations, χ_{1mix} is the resulting electronegativity of the mixed one, *n* is the coordination of the first cation and *m* is a ratio factor. The T_d, defined as the temperature of first main desorption peak, in the experiments made by the group, is closely related to the electronegativity and this is valid also for mixed borohydrides. See figure 3.I.2.

Considering Mg (χ_1 = 1.3) and Li (χ_2 = 1.0) in the mixed borohydride $MgLi_{m-2}(BH_4)_m$, it can be calculated the χ_{mix} and than have an idea of the theoretical desorption temperature that should stay between of the two T_d of the pure borohydrides.

m	2	2.5	3	3.5	LiBH4
χ_{mix}	1.3	1.2	1.15	1.12	1

Table 3.I.1: calculated value of χ_{1mix} in $MgLi_{m-2}(BH_4)_m$ for different ratios of $Mg(BH_4)_2$ and $LiBH_4$.

To knowledge of the author the same Japanese group was the first to prepare $ZrLi(BH_4)_5$ and $ZrLi_2(BH_4)_6$ by mechanically milling $LiBH_4/ZrCl_4$ mixtures in appropriate molar ratios [75], and they observed a dehydrogenation temperature decrease of the dual-cation (Li, Zr) borohydrides relative to $LiBH_4$.

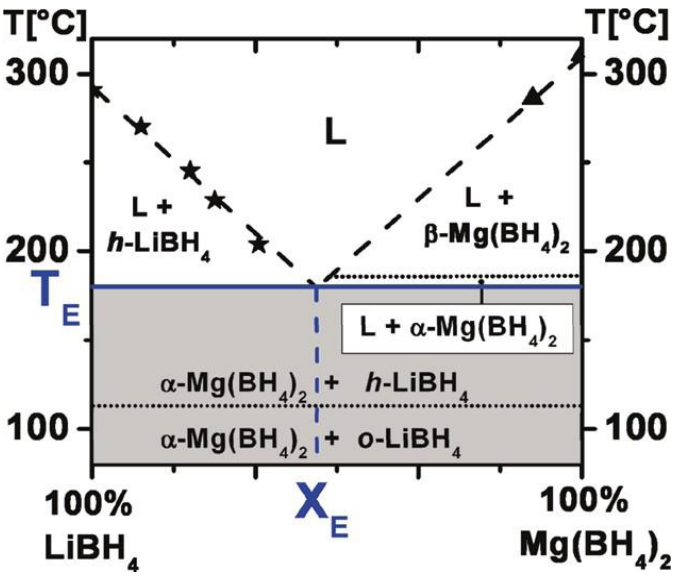

Figure 3.I.3: $LiBH_4$ - $Mg(BH_4)_2$ phase diagram from Bardaji et al. [76]. The best composition is reported to be the eutectic at 1:1 ratio.

Their result suggests that "the hydrogen desorption temperature of metal borohydrides can be precisely adjusted by the appropriate combination of cations" [75]. So not exactly a destabilization of the two borohydrides to have a lower desorption temperature but an adjustment to have characteristics that are in between of the ones of the starting materials. A similar approach of the one normally used with A – B metal hydrides: tailoring the properties varying the composition [27].

By then other works have been carried on with Li and: Ca [77], K, Mg [78] and Zn [79], but also $NaZn_2(BH_4)_5$ and $NaZn(BH_4)_3$ [79].

Only two very recent works are reported in literature on the destabilization of $Mg(BH_4)_2$ with $LiBH_4$, and one is in press [80].
The first, by Fang et al [78], focuses on the improved dehydrogenation properties of the BM mix that seems to be slightly better than the pure $Mg(BH_4)_2$ for the kinetics and the H_2 wt% desorbed. From the XRD analysis they conclude that a new complex dual-cation hydride phase has been obtained with its well characterized melting point. The second work, by Bardaji et al [76], focuses more on the tentative of producing a phase diagram for the physical mixture.
The hypothetic diagram is reported in figure 1.3 and is the results of several ex situ XRD analyses with different compositions. It is suggested that the best mixture for hydrogen storage is the eutectic, around 1:1 composition, the one already tested by Fang.
The preparation of the 1:1 mixture of the two borohydride was different for the two groups. The first used ball-powder ratio of 40:1 and the second of 100:1; also the milling time was different: 10h for the Chinese and 4 h for the Germans. This difference might be the reason of the very different behavior in desorption: with similar condition, Ar or He flow and 5°C/min ramp, the group of Bardaji obtained an onset at around 170°C for the mixed compounds while Fang had the onset at ca 220°C and the gap with the pure compounds is even higher due to the higher desorption temperature of the $Mg(BH_4)_2$ used by Bardaji, onset at ca 280°C in comparison to 250°C of Fang's one.

Catalysts

Catalysts are one of the most common approach to enhance the properties of materials for hydrogen storage. Carbon derivates, transition metals, halides and oxides are the most common categories of catalysts used with almost all the materials studied so far [81].

The first catalyst to be found as effective for decreasing the dehydrogenation temperature of a borohydride is reported to be, as already said, aluminum.

After that many others have been proved to be even more efficient not only with the pure $LiBH_4$ but also with complex systems. Even Vajo in his first work on destabilized $LiBH_4$ used $TiCl_3$ as a catalyst [58].
The most studied catalyst are chlorides and oxides, but also some work on pure elements and hydrides can be found.
Researches over oxides as catalysts demonstrated interesting behavior of even not exotic compounds such as Fe_2O_3 in comparison to more expensive Nb_2O_5 or V_2O_5 [82].
A good overview over some oxides and chlorides catalysts for $LiBH_4$ has been made by Au and Jurgensen [83] where they reported the effects of: V_2O_3, SnO_2, ZrO_2, $TiCl_3$ and TiO_2.
From their study all the previous catalysts have shown a decreasing in the desorption onset of around 200°C and a better kinetic in desorption as well as in absorption in comparison both to the pure $LiBH_4$ and to the pure material catalyzed with Al.
A report on the catalytic effect of SiO_2 [84] highlights that quartz reacts with molten $LiBH_4$ in a irreversible way and forms Li_2SiO_3, therefore, hydrogen release at lower temperature from samples of $LiBH_4$ containing SiO_2 is likely to be consider more a chemical reaction and not a catalytic process.

$TiCl_3$, LiCl and Au have been analyzed in the same work with in situ synchrotron X ray diffraction. According to the same Scandinavian group [84] $TiCl_3$ reacts at room temperature with $LiBH_4$ to form LiCl, and they claim that the chloride, above 120°C, partially dissolves in the borohydride high temperature hexagonal β-phase. This should be due to the increased structural flexibility and reactivity of the borohydride phase at that temperature.
An other interesting feature is due to the low density of $LiBH_4$ that make necessary a mass ratio of 1:1 of some catalyst to obtain a full dehydrogenation at lower temperature. The use of 1:1 weight ratio leads anyway to the same wt% of H_2 desorbed of the pure $LiBH_4$ below 600°C, around 9% [82].

Being a relatively new material only few catalysts have been tested on $Mg(BH_4)_2$. To the knowledge of the author only few works focused on the effect of catalysts on the hydrogen desorption properties of the compound. Ti-based additives demonstrate to be all ineffective except for $TiCl_3$ [85], TiF_3 and $ScCl_3$ enhance the desorption kinetics significantly.

In a recent paper [86] some authors argue against the current notion that only metal cations and/or their derivatives contribute to the property improvements and suggest that combined cation/anion doping may provide a new promising approach for simultaneously improving the kinetic and thermodynamic properties of $LiBH_4$. They demonstrated that TiF_3 is more effective as a catalyst in comparison to $TiCl_3$ because of F^- partially substitution with H, both in the borohydride and hydride stage, while Cl^- can replace only the $[BH_3]^-$ anion.

Catalysts for the destabilized system $LiBH_4/MgH_2$ have been studied. Chlorides have shown good results in lowering the first desorption peak and among them $TiCl_3$ seems to be the best and 5 mol% the optimum quantity [87].
Other authors focused on Ce based catalysts [73]. It has been observed that the catalysts are more effective in dehydrogenation in comparison to hydrogenation. Moreover the cyclic stability has been improved in comparison to the not catalyzed system without a starting back pressure.
Studies on titanium isopropoxide as a catalyst proposed that the desorption process of the $LiBH_4$-MgH_2 system is limited by the heterogeneous nucleation of the hexagonal MgB_2 phase. The additive, in the form of TiB_2, works at the interfaces acting as a nucleation site for MgB_2 when the $LiBH_4$ is in the liquid phase, thanks to the similar lattice structure [88].
Later works [73] based on the SEM observations explained the superior cyclic stability of Ce-added composites was related to their stable nanostructures upon hydriding-dehydriding cycling, in contrast to the rapid microstructural deterioration in the pure $LiBH_4$+1/2MgH_2 composite. In this case the structure does not match but CeB_6 appear to be effective in the same way of TiB_2. The authors than suggest that a larger number of metal borides may act as nucleating agent even if the structure is not the same of the MgB_2 phase.

Nano-sizing

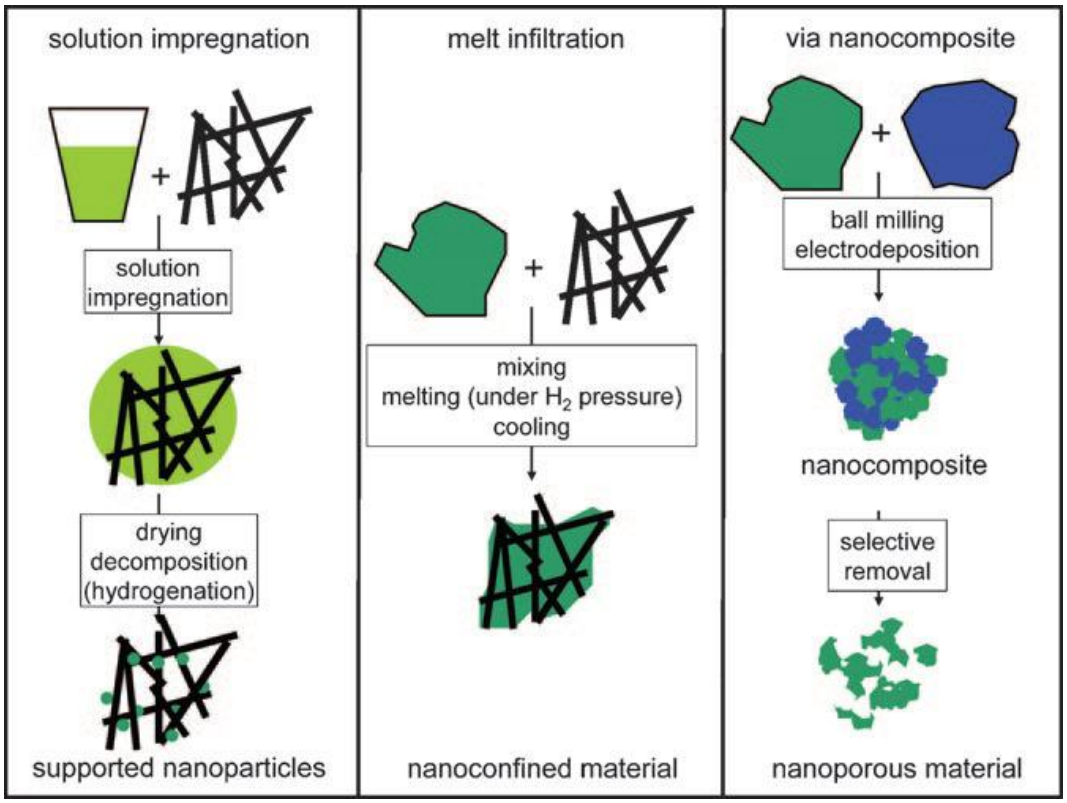

Figure 3.I.4: Illustration of the different methods to prepare nanostructured light metals or metal hydrides by using a matrix or support.[89]

It is not the aim of this work to explain why is so interesting the new branch of Material Science called Nanotechnology, still the properties coming from having more material in the surface than in the bulk have been explored and exploited also in the research of hydrogen storage materials.
Two principal approaches are commonly used to prepare nanoparticles: bottom-up and top-down. A bottom-up approach is, for example, preparing nanoparticles by growth in solution. Typically, a precursor is dissolved in a liquid solution, and by evaporation of the solvent, a change in temperature or pH, or simply waiting for nucleation and growth, nanoparticles of the target phase can be prepared either as a suspension of colloidal particles, or, in the presence of a support, as supported nanoparticles [89].
A top-down approach on the other hand starts from a bulk material to reach nanometric dimensions at least of the crystalline dominions. This is the case of ball milling (BM) that in the late 90s was the most promising technique to obtain better kinetics from MgH_2 and other hydrides [22]. Other approaches used for hydrogen storage materials are for examples: spark discharge, used on Mg and Pd [47] and nanowires [90].
An example of BM with borohydrides is the already quoted work of Li et al [85] where they investigate the best milling time to have the lower dehydrogenation temperature and found that 2 h are enough for their $Mg(BH_4)_2$ samples. The decreasing in the desorption temperature anyway was not very big.

Infiltration: Nano-confining and Supporting

After the first work in 2005 on nanoconfining ammonia borane in mesoporous silica to decrease the hydrogen desorption temperature [91], a big effort has been devoted to study infiltration and supporting of materials for hydrogen storage.
Up to date the attention of the big journals, regarding hydrogen storage, focuses on complex amino-borohydride, with very high Hwt%, and on new kinds of supports [92][93].
The difference is mainly in the efficiency with which the active material is loaded in the scaffold and the porosity of the scaffold itself.
Supporting the nanoparticles prevents the sinterization and may induce heterogeneous nucleation of the decomposition products on the surface, lowering the desorption temperature [94]. Nano-confining holds even more promises and expectation: improved thermodynamics [89], kinetics [95], cyclability [72][96], no release of unwanted and toxic compounds [96][97] and protection from oxidation [92]. All those qualities, unfortunately, on the expense of a partially compromised gravimetric hydrogen content of the system.

Works on $LiBH_4$ demonstrate the possibility to lower the desorption onset by milling [98] or dispersing [94] the material in different carbonaceous supports.
During the dehydrogenation process, pure liquid $LiBH_4$ needs to be superheated in order to promote nucleation of the dehydrogenated products. The scaffold with a high specific surface area (SSA) may serve as nucleating point for the borohydrides avoiding the necessity of superheating [98].

In many works on nanoconfinement is shown the comparison between the pure active material, the material and the scaffold physically mixed and the impregnated compound [97][99] to demonstrate the superiority of infiltration technique in comparison to supporting and the improvement from the pure starting material.
It has been shown that not only the dimension of the pores but also the loading of the scaffold drive to different results [57][96].
Comparing carbon aerogels, nano-porous carbon and graphite, some authors concluded that the smaller the pore size the lower the desorption temperature and the better is the reversibility [57][95][96]. Unfortunately the loading decrease as well and the active material is rarely higher than 50 wt%. Exceeding the limit load part of the active material is no more inside the pores and so not anymore nano-confined, losing part of the aimed properties.
Another issue connected with the use of carbon scaffolds is their degradation. It has been found from some groups that the emission of borane are lowered, increasing the cyclability of the active material, but as a drawback the signal of methane during the desorption and the peaks of Li-C compounds in the XRD patterns [95] suggest that the scaffold deteriorates with time.

$Mg(BH_4)_2$ infiltrated in nano-porous carbon has been studied in 2009 by two different groups. One focused more on the morphology and phase characterization [100], the other on the desorption properties. The decomposition temperature of the composite (43wt% of active material) was reduced by 50°C and the obtained H_2 was calculated as 6% in weight, below 450°C [99].

Up to date nanoconfinement is applied even with catalysts and/or destabilized compounds. Nanoconfinement of $LiBH_4$-MgH_2 demonstrates an enhanced kinetic [72] while the synergetic effect of nano-confinement and Ni catalyst addition with $LiBH_4$, lowered the desorption temperature of more than 100°C and doubled the hydrogen desorption of the rehydrided sample in comparison to the one without the catalyst [57]. The destabilized system ball milled with Multi Walled Carbon NanoTubes (MWCNT) catalyzed by platinum nano-particles has shown good results too: the kinetic and the cyclability have been improved [59]

The state of the art, that worth the group from Berkeley a publication on Nature Materials in 2011, is a nano-composite of MgH_2 and Poly Methyl MethAcrylate (PMMA) that desorbs 4 wt% of H_2 at 200°C in 30 min and is not even strongly air sensitive [93].

Reversibility

It has been observed that $LiBH_4$ and $Mg(BH_4)_2$ show a partial reversibility under certain conditions, see table 3.I.2.

Sample	**Dehydrog. wt%**	**Rehydrog. wt%**	**Dehydrog. Backpressure**	**Rehydrog. conditions**	**Ref.**
JRC-IE's Setting			He flow 480 ^oC	5 MPa 4h 480 ^oC	
$LiBH_4$	?	?	1 MPa H_2 600 ^oC	35 MPa 600 ^oC	[52]
75%$LiBH_4$ 25%TiO_2	8.5	8.25 (I), 5.6 (II), 4.2 (III)	500 Pa H_2	7 MPa 600 ^oC	[83]
67%$LiBH_4$ 33%MgH_2 Carbon Aerogel (D ~21nm)	3.9	2.8	0.2 MPa H_2 390 ^oC	7 MPa 370 ^oC	[72]
67%$LiBH_4$ 33%MgH_2 Carbon Aerogel (D ~21nm)	3.9	>3.6 (I) >3.0 (II)	0.2 MPa H_2 390 ^oC	9.8 MPa 390 ^oC	[72]
20% $LiBH_4$ 80% MgH_2	9.2	8.5	Vacuum 400 ^oC	10 MPa 400 ^oC	[70]
67%$LiBH_4$ 33% MgH_2 + $TiCl_3$ 3mol%	8.5 (?)	Mg and not MgB_2, no rev.	Dynamic vacuum 450 ^oC	10 MPa 350 oC	[58]
67%$LiBH_4$ 33% MgH_2 + $TiCl_3$ 3mol%	8.5	8.5 (I), 8.5 (II)	0.6 MPa H_2 450 ^oC	10 MPa 8.5h 350 ^oC	[58]
67% LiBH4 33%MgH_2	5.8	5.8 (I) 5.6 (II) 5.4 (III)	4 MPa 500 ^oC	4MPa 500 ^oC	[59]
67% $LiBH_4$ 33% MgH_2 in MWNT+PtRu NP	~ 7	~ 7 (I)(II)(III)	4MPa 500 ^oC	4MPa 500 ^oC	[59]
$LiBH_4$ in NC (2-3 nm) + Ni	3.5	2.3	Ar flow 450 ^oC	4MPa 2h 320 ^oC	[57]
$LiBH_4$ + $Mg(BH_4)_2$	~ 15	2.5	Ar flow 500 ^oC	10MPa 12 h 400 ^oC	[78]
$Mg(BH_4)_2$	>14	6.1	10 to 2 MPa 300 ^oC	40 MPa 48h 270 ^oC	[66]

Table 3.I.2: Dehydrogenation and re-hydrogenation achievements with Li and Mg borohydrides of different authors in Hwt% with experimental settings used.

From the works of many authors can be seen that destabilization of $LiBH_4$ leads not only to lower desorption temperature, but in some cases also to an improved reversibility. Researches on the promising $LiBH_4$-MgH_2 system demonstrate that a backpressure is indispensable to obtain MgB_2 which is the key for reversibility according to some authors [58][88].
Although MgB_2 formation is thermodynamically favored at elevated temperature, it is kinetically more favorable for MgH_2 and $LiBH_4$ to decompose independently in a two-step dehydrogenation starting with $MgH_2 \leftrightarrow Mg + H_2$ [71].
Applying an H_2 gas overpressure of at least 3 bar (0,3 MPa) during dehydrogenation suppress direct decomposition of $LiBH_4$ favoring the reaction of Mg with $LiBH_4$ to produce LiH and MgB_2, which appears to be fully reversible [71].

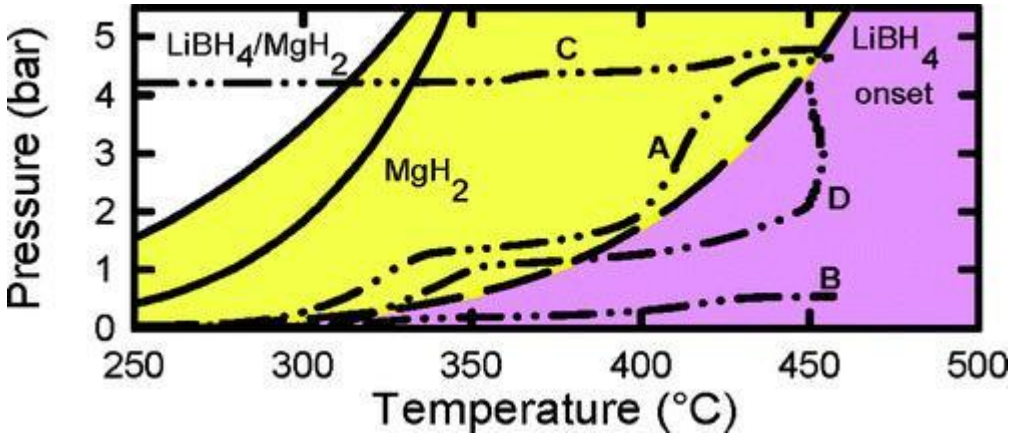

Figure 3.I.5: Temperature-pressure phase diagram for the Li-Mg-B-H system. Solid lines represent thermodynamic stability boundaries for $LiBH_4 + 1/2MgH_2$ f $LiH + 1/2MgB_2 + 2H_2$ (left) and MgH_2 f $Mg + H_2$ (right). [71].

$LiBH_4$ nano-confined in nano-porous carbons shows a small release of borane and a cyclability of 6 cycles losing around half of the initial capacity [96]. According to some authors the scaffold or support introduces additional effects. It allows preparing and stabilizing particles of a certain size and it might also influence diffusion, provide additional nucleation sites at the interface, induce mechanical strain in the active phase. If conductive, the support might also play an important role in heat transfer and management [89]. The loading of the support with the hydride plays also an important role eliminating the long range order of the active material that is nanoconfined while have different effect on the reaction if the active material is only mixed [95][101].
The intermediate $Li_2B_{12}H_{12}$ reported for bulk $LiBH_4$, reported by some authors, might limit the reversibility of the system, while for the nanoconfined system there is no trace of its formation in a two-step decomposition. Hence, nano-sizing and -confinement might change the reaction pathway, as was also observed for $NaAlH_4$ [101].

To the knowledge of this thesis author only one group [66] claim the re-hydrogenation of $Mg(BH_4)_2$. It is only a partial rehydrogenation, due to the fact that only 6.1 wt% was absorbed by the compound after the first dehydrogenation. This, according to the authors should correspond to the second and third reactions of the proposed decomposition path:

$$\begin{aligned} Mg(BH_4)_2 &\rightarrow \frac{1}{6}MgB_{12} + \frac{5}{6}MgH_2 + \frac{13}{6}H_2 \\ &\leftrightarrow MgH_2 + 2B + 3H_2 \\ &\leftrightarrow Mg + 2B + 4H_2 \end{aligned} \qquad (3.9)$$

As said in the introduction, to prove the reversibility Severa et al studied the direct hydrogenation of the products, magnesium boride and hydrogen, obtaining a yield of 11 Hwt% [67] and bypassing the complex compound reported by Li [66].

The only report on the reversibility of $LiBH_4$-$Mg(BH_4)_2$ system is from Fang and it is demonstrated that with their conditions (10 MPa, 400 ºC) the compound can not the recovered to the borohydride stage [78].

I.2 Experiments

Several mixtures of $LiBH_4$ and $Mg(BH_4)_2$ in different ratios have been synthesized with three approaches and then analyzed with five different techniques, see table 3.I.3.

Lithium borohydride powder was purchased from Sigma-Aldrich (>95% purity) and the magnesium borohydride was synthesized at Padua's CNR labs from $MgBut_2$ and BH_3SMe_2 following the method described in [102]. Some more $Mg(BH_4)_2$ have been purchased by Sigma Aldrich and is labeled as Mg(BH4)2ALD.

Microporous graphite, starting from commercial graphite purchased from Carlo Erba Reagenti was obtained by milling it in the conditions reported in the introduction for the borohydride, but with different milling times: 15, 90 and 600 minutes (in this last case 660 min adding 10 min pause every hour). Its porosity characterization was done with N_2 adsorption measurements at 77 K using a Quantachrome Nova 1200e Surface Area and Pore Analyzer.

Sample	**$LiBH_4$ (mol-wt %)**	**$Mg(BH_4)_2$ (mol-wt%)**	**Treatment**	**TDS**	**TDS II cycle**	**XRD pre**	**XRD post**	**SEM EDS**	**IR**	**# Exp**
A011	100 -100	0	As received	X					X	1
A021	100 - 100	0	BM	X						2
A031	100 - 100	0	DFS	X						2
B021	66 - 44.9	33 – 55.1	BM	X		X				1
B031	66 - 44.9	33 – 55.1	DFS	X		X	X			1
B041	66 - 44.9	33 – 55.1	IMP	X	X	X	X			1
C021	50 - 28.9	50 – 71.1	BM	X		X		X	X	1
C031	50 - 28.9	50 – 71.1	DFS	X		X	X	X		1
C032	50 - 28.9	50 – 71.1	DFS	X				X	X	2
C041	50 - 28.9	50 – 71.1	IMP	X	X	X	X	X		2
D021	33 – 16.9	66 – 83.1	BM	X		X		X		1
D031	33 – 16.9	66 – 83.1	DFS	X		X	X			1
D041	33 – 16.9	66 – 83.1	IMP	X X	X X		X X			1
E011	0	100 - 100	As received	X X	X	X	X		X	1
E012	0	100 - 100	As received	XX		X	X			2
E021	0	100 - 100	BM	X			X			2
E031	0	100 - 100	DFS	X X						2
$Mg(BH_4)_2$ ALD	0	100 - 100	As received	X			X		X	2

Table 3.I.3: name, composition, treatment and analyses of each sample. With some samples it was tried a re-hydrogenation and a second TDS has been carried on after(TDS II cycle). XRD have been collected before (pre) and after (post) TDS. In total more than 50 experiments have been carried on with 5 techniques on the samples received in two expeditions (#1 and #2)

Specific surface areas (SSA) of the different supports were calculated by means of multi-point Brunauer-Emmet-Teller (BET) method (in the range 0.02-0.3 p/p_o), while the micropore area was derived with de Boer statistical thickness method in the range from 0.2 to 0.5 p/p_o.

The milled graphite was degassed at 300 °C in rotary vacuum and then poured into the solution of borohydride mixtures in methyl tert-butyl ether (MTBE) and stirred for further 24 h. Afterwards it was dried using a Schlenk flask connected to rotary pump vacuum and, finally, heated to 100 °C for 3 h.

The mixtures, summarized in table 3.I.3, have been synthesized in three different ways: via ball milling (BM, labelled 02), dispersed in MTBE and dried (DFS, 03), and dispersed in the same solution and then infiltrated in porous graphite (IMP, 04).
Different molar mixtures have been analyzed: 100% $LiBH_4$ (labelled with letter A), 66 % $LiBH_4$ and 33 % of $Mg(BH_4)_2$ (B), 50 % and 50 % (C), 33 % and 66 % (D) and 100 % $Mg(BH_4)_2$ (E).
The last number of the sample code is an ordinal number for the synthesis. The first number after the letter is 0 if the sample is hydrogenated and 1 if the analysis is carried on with a sample after desorption.
In summary:

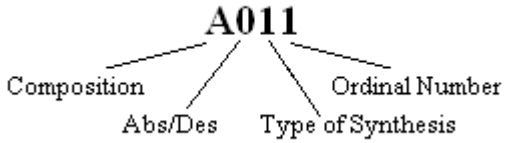

All the synthesis of the mixtures and the characterization of graphite have been done at University of Padua labs, while the used $Mg(BH_4)_2$ have been synthesized at Padua CNR (the Italian National Research Council) facility.
The TDS experiments were performed with a TPD apparatus coupled with a quadrupole mass spectrometer (MS, Catlab Hiden). The MS identifies gaseous species with a set helium flow of 100 mL/min. For all the experiments the temperature was raised at 2.5°C/min rate till 480°C and then kept for around 2 hours. The samples where loaded and unloaded in inert atmosphere, under N_2 gas flow.
The second cycle has been carried on with the same parameters after rehydrogenation of the dehydrogenated sample. The re-hydrogenation procedure was performed as follows: The hydrogen pressure was set at 5 MPa and the temperature, after a ramp of 10°C/min, was kept for more than 4 hours at 480ºC, than the temperature was let to drop till room temperature.

Structural analysis was performed using X-ray diffraction (XRD; Panalytical X'PERT PRO diffractometer) with Cu Kα radiation. Also in this case the samples were loaded and transported in a chamber with inert gas.

Scanning Electron Microscope (SEM) investigations were performed in a high resolution LEO Supra 50 scanning electron microscope equipped with an in-lens detector and an energy dispersion detector (EDS). The specimens were prepared by dispersing the powder material on a copper grid or on a carbon tape depending on the conductivity of the sample. In the case

of borohydrides the conductivity is too low and that can result in charging of the particles preventing a good vision. For the impregnated material the carbon tape gave enough conductivity to have a good vision. The setting for each picture is normally reported on the bottom of images.
The loading of all the samples has been done under N_2 flow.

Infrared technique has been exploited for the study of the materials after synthesis. This technique is not commonly used for hydrogen storage material but the use of not common materials with light metals that are not well visible with the EDS and might have phases unknown or amorphous led to the idea of using also this technique.
The pellets for the analyses have been produced with a pelleter in the glovebox using KBr and the sample in a weight ratio of 100:1. The inclusion in the KBr gives a certain confidence for the exposure to air. Even if the pellet should prevent the oxidation of the material the handling has been done under inert atmosphere as much as possible.
The apparatus is a Bruker Vertex 70V, equipped with a globar MediumIR source (U-shaped silicon carbide piece [@18]) and Modified Triglycine Sulphate (TGS) detector with resolution 4 cm^{-1}. The spectra have been taken with an average of 50 scans in a vacuum at 0.7 mbar.

I.3 Results and Discussion

I.3.1 TDS Analysis

As reported also in the in introduction, several studies have been done already on the dehydrogenation process of $Mg(BH_4)_2$ and $LiBH_4$ both as synthesized or treated with different techniques: ball milling, supporting or infiltrating in scaffolds.

$Mg(BH_4)_2$ shows a complex shape in the MS spectrum due to the multi-step desorption reaction [64]. The main desorption is reported to start from 250°C [64] - 200°C [99] for bulk and 150°C in case of nano-confined material [99].

For $LiBH_4$ the literature is more abundant. After the melting, approximately at 300 °C, the dehydriding reaction accompanied by the phase decomposition proceeds mainly above 480°C: ball milling slightly decrease this temperature [52][70][83] while nano-confinement do the same with apparently better results [94][96][97]

There are not many works on the destabilization of borohydrides via multication combination and only two up to date are on $Mg(BH_4)_2$ and $LiBH_4$ by Fang [78] and Bardaji [76]. The experimental setting used is similar to the one used by the two groups therefore the results are easy to compare. According to both the articles the desorption temperature of the mixed borohydride is lower than the two of the starting materials and the desorption takes place in two steps: one around 180-220°C and the other around 250-300°C depending on the author [78][76]. The shape of the MS signal of hydrogen during the thermo-gravimetric analysis is reported to be with two well defined hills corresponding to the two decomposition steps [76].

Big efforts have been made to lower the temperature of dehydrogenation of borohydrides using catalytic agents [83][84][88] or making composites with scaffolds to nano-confine the material [89]. Dispersed in multi walled carbon nanotubes (MWCNT) $LiBH_4$ has a dehydriding temperature 60°C lower than the bulk material [94], similar result have been obtained with nanoporous carbons with different pore sizes [96][97]. $Mg(BH_4)_2$ infiltrated in activated carbon doesn't seem to show great improvements [99].

The results of the samples (ball milling, dried from solution and infiltration) are first analysed grouped by techniques and then by composition.

Ball milled samples

In figure 3.I.6 are reported the MS spectra of signal M/Z 2 (hydrogen) observed during the TDS of the ball milled samples. The mechanically alloyed samples (violet, green and cyan in figure 3.I.6) show lower desorption temperature of around 40 ºC in comparison to the pure ball milled samples (blue and red).
From the data collected it can be derived that the best composition might be 1:2 (D021), because is the one with more $Mg(BH_4)_2$ and shows more the behaviour of this component.
All desorption spectra look different from the one of ball milled samples prepared by Bardaji [76], while they look more like the ones obtained by Fang.
The quantitative data, how much hydrogen in wt% is desorbed by each sample, are not possible to be given due to a not reliable calibration of the instrument concerning this aspect of the analysis. It can be stated anyway that more than half of the hydrogen of the D021 sample is desorbed below 320ºC, like the pure $Mg(BH_4)_2$ but the on-set temperature is much lower (around 60ºC).

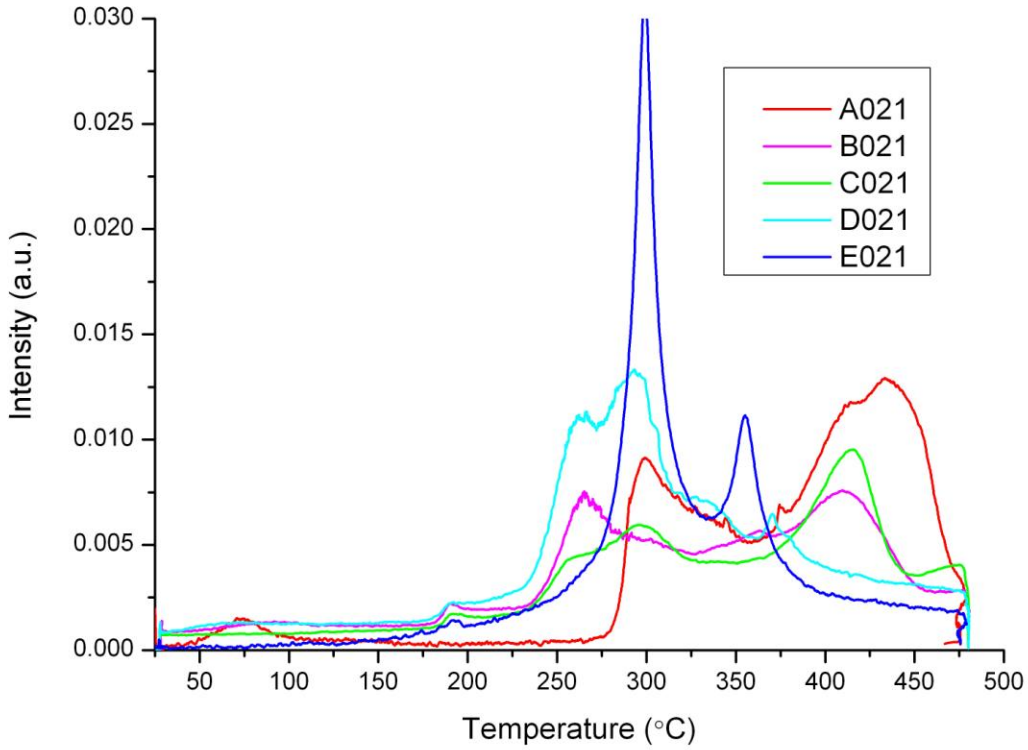

Figure 3.I.6: TDS spectra of hydrogen desorption of BM samples. From the top $LiBH_4$, composition 2:1,1:1,1:2 and $Mg(BH_4)_2$. The desorption onsets of mixed borohydrides are at lower temperature in comparison to the pure ones

Dried From Solution samples

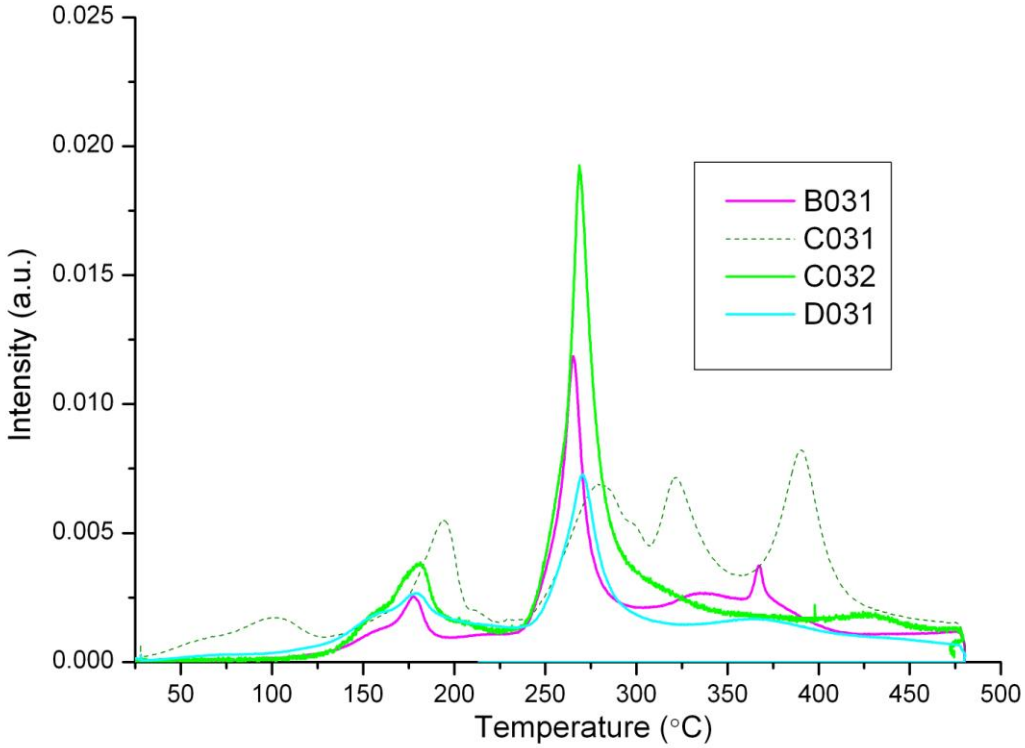

Figure 3.I.7: TDS spectra of hydrogen desorption for DFS samples. From the top composition 2:1,1:1 (two samples),1:2. The desorption of these samples is mainly in two steps at ca 180°C and 270°C. Sample C031 shows a different but interesting behaviour, maybe due to a wrong synthesis or to some pollutant

As shown in figure 3.I.7 the 3-4 peaks of hydrogen desorption, observed with the TG data reported in literature [76], are detected only in the case of dried from solution samples. In the samples treated by ball milling, see figure3.I.6, the shape is much smoother and it is hard to define which event takes place and the respective desorption temperature.
The on-set temperature is lower than the pure compounds but in this case the difference between the compositions is not appreciable. The spectra are characterized by two main desorption peaks, one at low temperature (ca 160°C) and one at high temperature (ca 240°C), very similar to the results of Bardaji [76] with ball milled samples.

Only one sample, C031, probably mixed or synthesized slightly differently showed a much different, if not better, desorption behaviour with multiple peaks starting from 110°C, see figure 3.I.7 green dotted line.
This difference needs more investigation but seems to suggest that the presence of impurities, which may act as catalysts, could leads to a different reaction path.

Having all the TDS patterns of all BM compositions it is possible to add the results to the graph of Li et al. of the mixed borohydrides [75], and also the DFS results have been added for comparison.
In the original graph, see figure 3.I.2, it is shown a direct relationship between the cation electronegativity of the borohydrides and the temperature of the first hydrogen desorption T_d. In the case of mixed borohydrides, for example $ZrLi_{m-4}(BH_4)_m$, the desorption temperature has been found to lay between the pure borohydrides ones.
It can be seen from figure 3.I.8, that the hydrogen desorption temperatures of the samples are not in line with the theory of the Japanese group. The mixed borohydrides do not show an intermediate behaviour but a generally lower desorption temperature T_d, both in the case of BM or DFS synthesis.

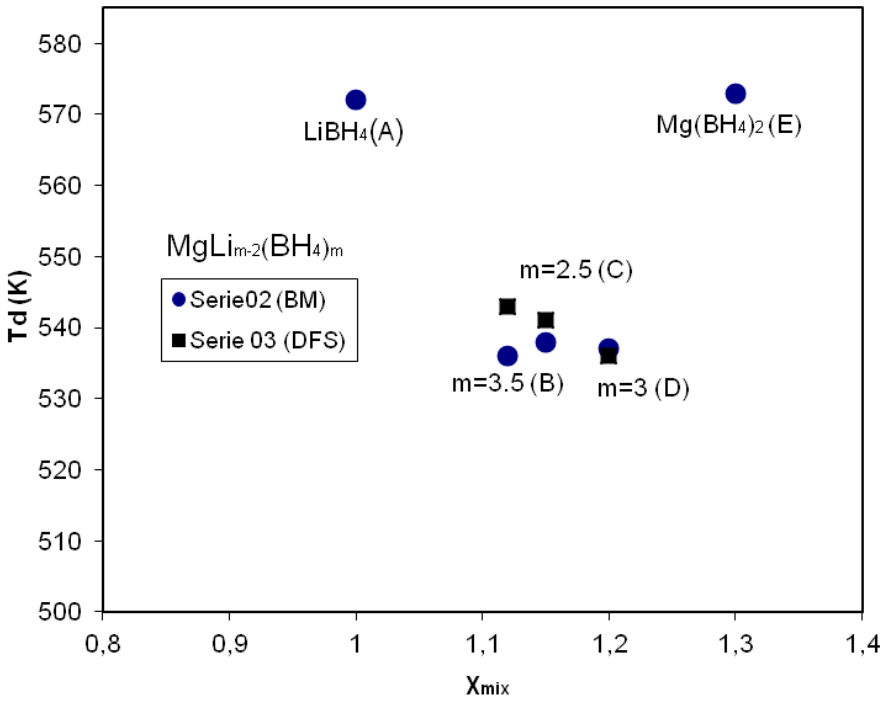

Figure 3.I.8. The first desorption peak temperature T_d as a function of the Pauling electronegativity χ_P. Mixed borohydrides, both from DFS or from BM synthesis show a lower T_d in comparison to the pure materials, in contrast to a previous work found in literature [75], see figure 3.I.2.

Impregnated Samples

Two of the three impregnated samples studied, C041 and B041, show a common behavior with a single main peak at 275 ºC and all the hydrogen desorbed below 400ºC instead of 400-450 ºC.

On the other hand D041 seems to desorb at much lower temperature and the hydrogen peak is below 200 ºC, unfortunately the quantity of gas released is very low even if the weight of the sample was the same of all the other experiments. A new analysis, with more material, is needed to have a better signal and draw conclusions.

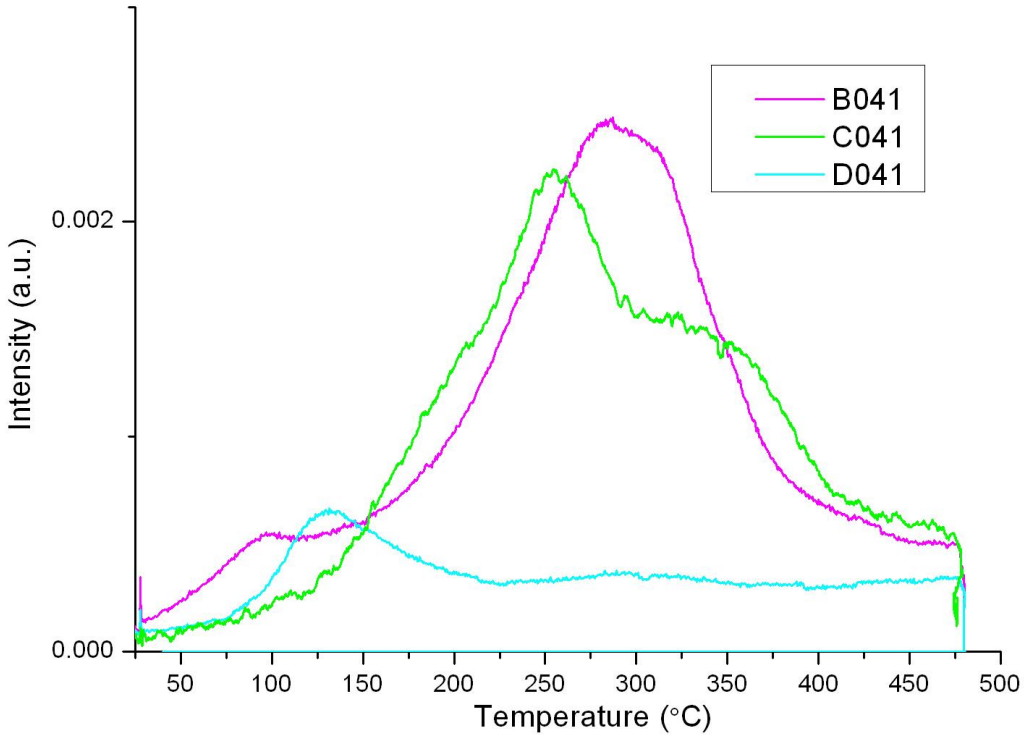

Figure 3.I.9: TDS spectra of hydrogen desorption of impregnated samples. From the top composition 2:1,1:1 and 1:2. Samples B041 and C041 look similar while D041 has a desorption peak at lower temperature but desorbs much less hydrogen.

Secondary Masses Detected During Desorption

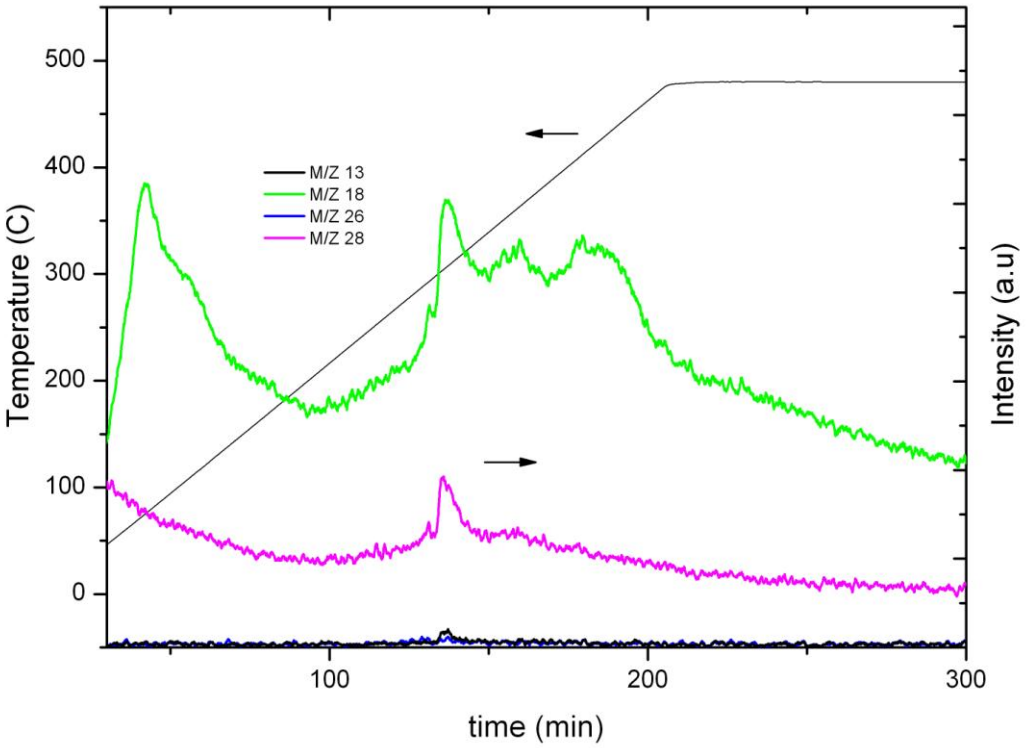

Figure 3.I.10: MS spectrum of secondary masses desorbed by sample A011 during TDS with the most intense and representative signals.

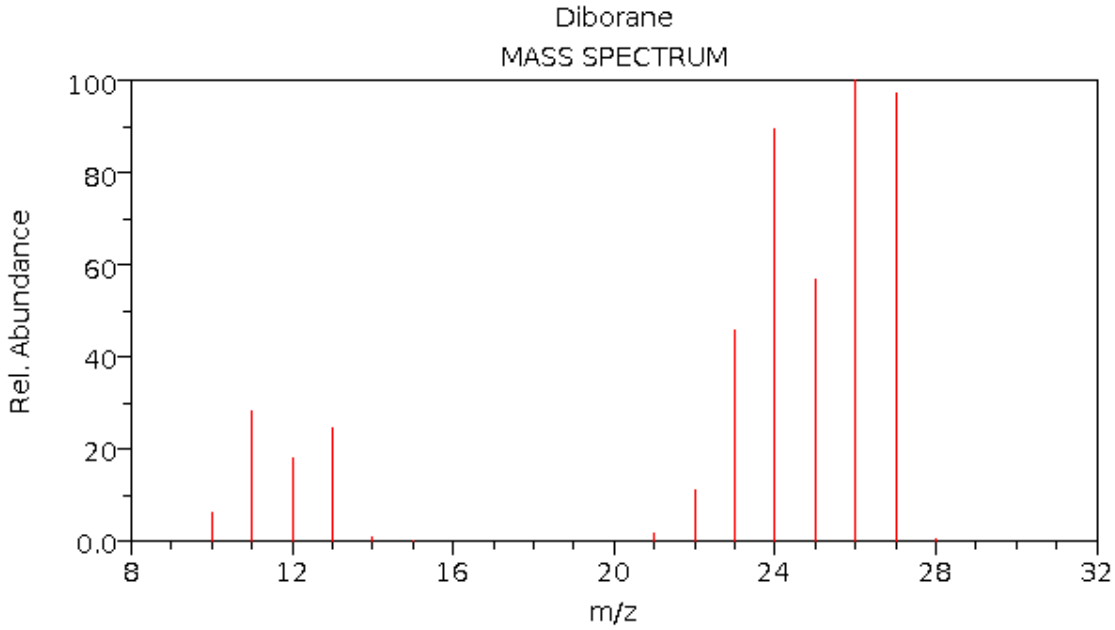

Figure 3.I.11 (below): Mass spectrum of diborane from NIST database [@17]

According to many authors [58][83][96][97], with hydrogen also other gases are detected from samples of $LiBH_4$ during the desorption: BH_3, H_2O and B_2H_6, respectively with M/Z ratios 11-13,18 and 26-27. From the work of Bardaji [76] it was found that also the fragments of diborane have to be controlled. The emission is said to decrease in the case of nano-confined composites [96].

In order to analyze the full range of masses which might be observed, it has first been measured the sample A011 in BAR (scanning) mode, figure 3.I.10.
In this configuration the MS is able to scan, at each step of the temperature during the heating treatment, all the spectra of M/Z from between two set ratios. It has been decided to study the range from 4 to 30, excluding the big signals of He (the carrier) and H_2 to better focus on the secondary masses.

It has been detected that the sample contained some water (M/Z 18) and, during the heating, some 27-28 masses have been released, that could correspond to B_2H_6. Another signal, 15-16 M/Z, has been detected but it could not be addressed with any possible compound. From that moment all the analyses have been carried on monitoring one of each group of these masses as well as M/Z 2, i.e. hydrogen. The results are comparable to the data that can be found in the NIST web site database [@17].

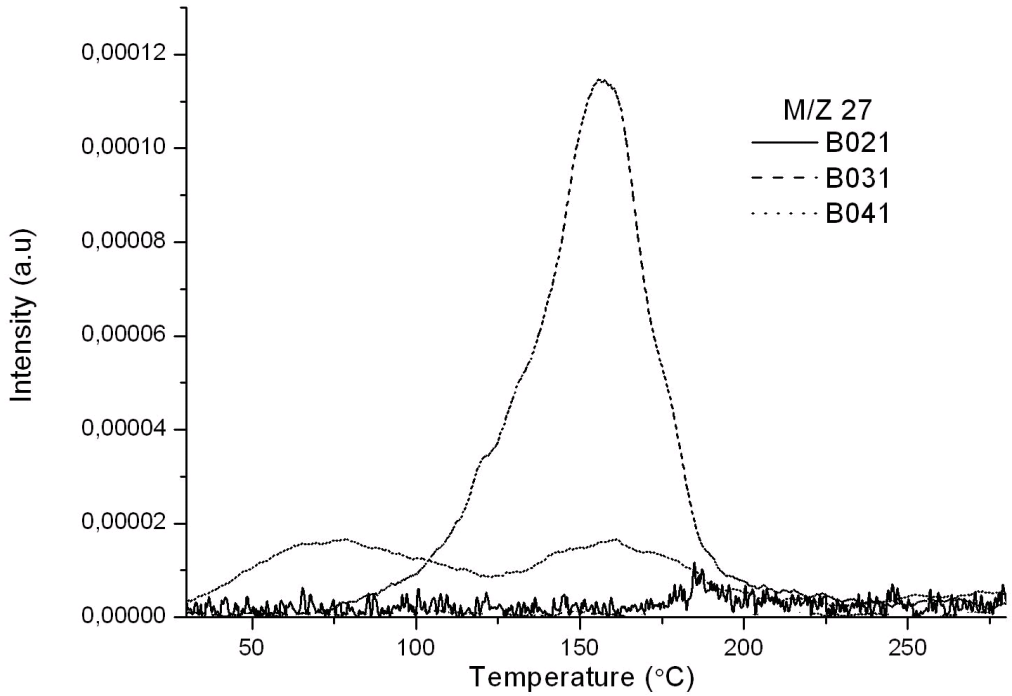

Figure 3.I.12: example of MS spectra of M/Z 27 (borane) for series of samples with composition B(1:2), from the top: ball milled, dried from solution and impregnated sample. The DFS shows the worse feature, with a high peak corresponding to the first desorption step

From the analyses carried on after, a different behaviour was discovered between dried from solution and ball milled samples. The BMs show a continuous release of borane that could be confused with the background while the DFS samples show defined peak around 150 ^{o}C, see figure 3.I.12.
This temperature corresponds to the first H_2 desorption as it can be seen in figure 3.I.13.

In the impregnated samples it was expected a decrease in borane emission [96] but the results show that there is still a release and in this case it takes place in two steps, one at low temperature and one corresponding to the hydrogen desorption temperature of the dried from solution samples. The amount of emitted borane of impregnated samples seems lower in comparison to the dried from solution samples but it is still higher or equal to the BM ones, even if the hydrogen desorbed is much less. This is just a qualitative analysis since it is not possible to derive quantitative data from the MS spectra.

The quantity of borane anyway, for all the samples, has to be considered as an impurity in comparison to the hydrogen released, as it can be appreciated in figure 3.I.13.

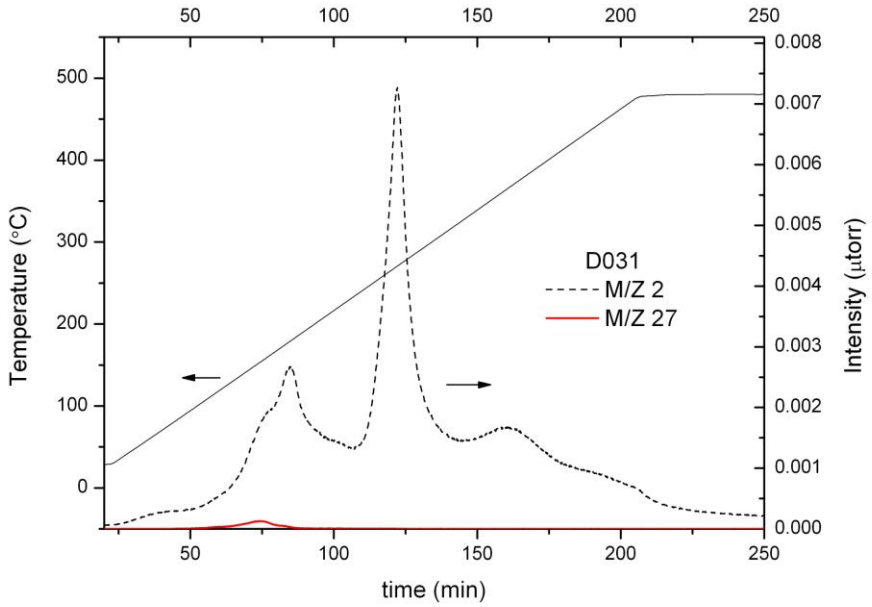

Figure 3.I.13: TDS spectra of DFS D031 sample (composition 1:2), M/Z 2 (hydrogen) and 27 (borane). The emission of borane is limited and almost negligible in comparison to the desorption of hydrogen, but it is present and might be a reason of the difficulties in cycling.

Comparison between preparation techniques

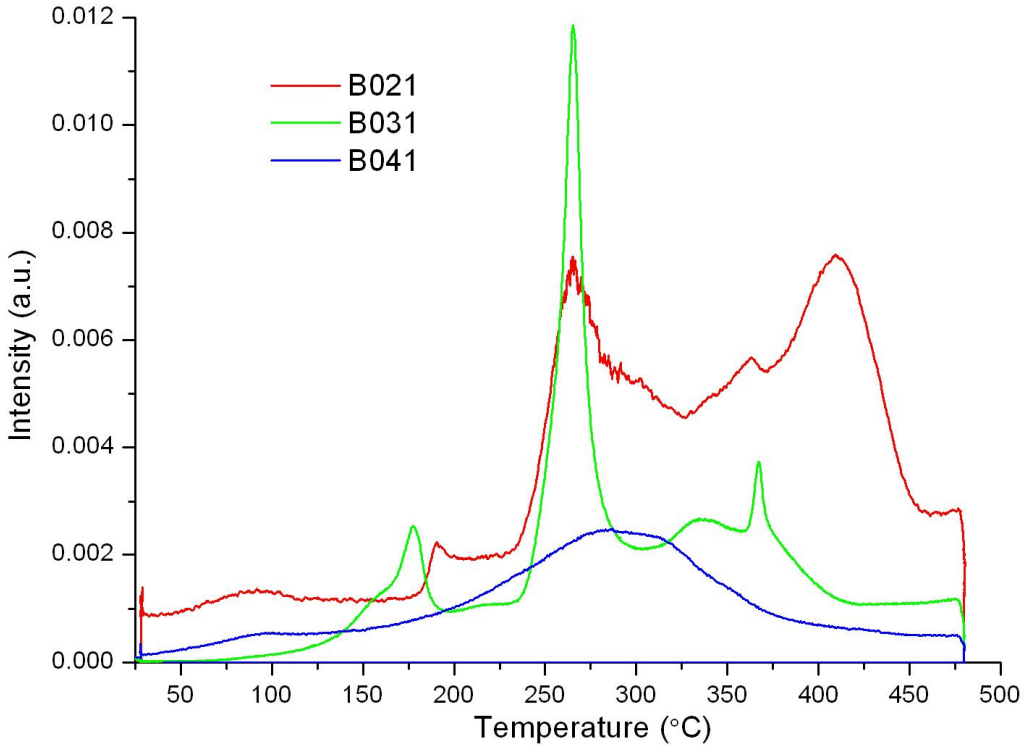

Figure 3.I.14: TDS spectra of BM, DFS and impregnated samples, composition B ($LiBH_4$-$Mg(BH_4)_2$ 2:1).

In figures 3.I.14, 3.I.15, 3.I.16 and 3.I.17 are reported the MS patterns of hydrogen taken during the TDS experiments grouped by composition.
It can be stated that the dried from solution samples show a promising behaviour in all the compositions but for pure Mg borohydride (for this composition a new sample DFS should be synthesized and analyzed).
The shapes are narrower and the desorption on-sets are at lower temperature in comparison to the BM samples and even in comparison to the impregnated ones.
Moreover almost all the hydrogen is desorbed at much lower temperature (~300°C depending on the composition) in comparison to the BM samples that keep desorbing till the temperature reaches 480°C; only impregnated samples do slightly better.

From these data it might be thought that only in the case of dried from solution samples nano-sizing has been achieved and that the ball milling was not as effective as the one of Bardaji's group [76]. The difference in dimensions and in the variance from the average might have explained why the desorption signal of the BM samples tested in Petten is broader and why the DFS ones are more well defined.
However from the SEM analysis, chapter I.3.5, it has been seen that it is the opposite: BM samples have smaller particles than DFSs, and are only partially aggregated in bigger clusters. Obviously the mismatch between the particles dimensions seen with SEM and XRD

patterns coupled with the behaviour in the TDS measurements might be explained considering the particles not mono-crystalline. Still this is an approximation that normally holds with micro- and nano- particles and the results of the TDS would remain unexplained.

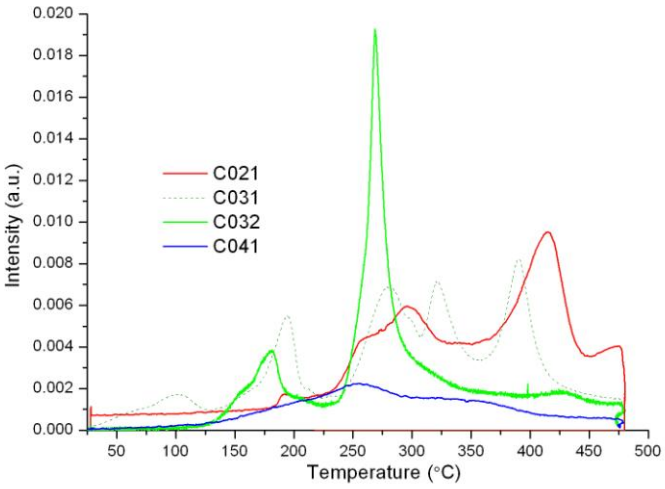

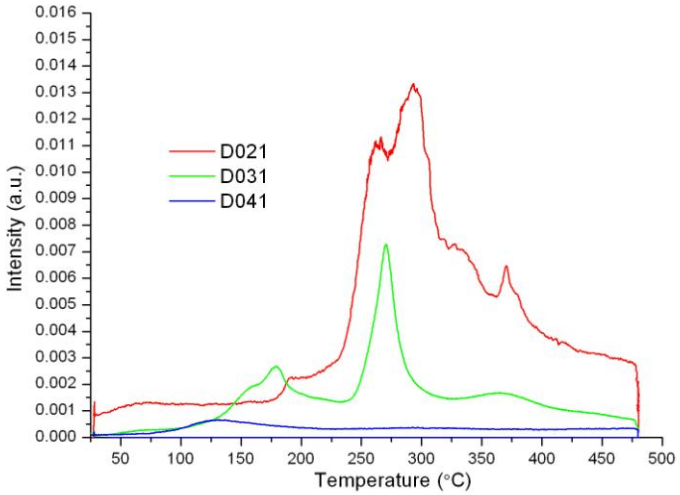

Figure 3.I.15 (left) and 3.I.16 (right): MS spectra of M/Z 2 of BM, DFS and impregnated samples, composition C (1:1) and D (1:2). For all the compositions the main desorption of hydrogen of DFS and Impregnated samples ends at lower temperature in comparison to the BMs. Moreover the desorption onset and, as it was expected by sample not mixed with inert material, the quantity of hydrogen desorbed are better in the case of DFS in comparison to the IMP.

Figure 3.I.17 (below): as synthesized (two samples received in Petten with two different expeditions), BM and DFS of composition E (pure $Mg(BH_4)_2$). The desorption temperature is lower in the case of the two treated samples and the results are similar comparing two samples from the same batch. E031 needs to be re-synthesized and tested to confirm the result.

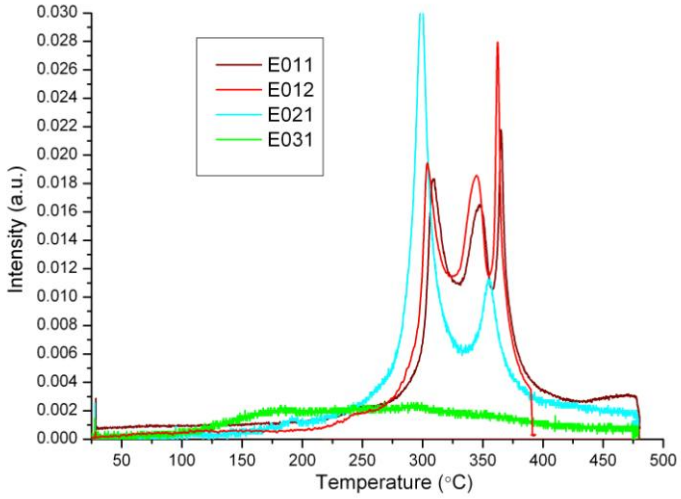

Quantitative Data

It is not possible to give completely reliable quantitative data with the instrument used for the TDS, due to a not constant calibration of the MS signal during the period when the data have been collected. For this reason gravimetric loss data can't be provided but it is possible to appreciate that the hydrogen partial pressure is higher in the case of ball milled samples in comparison to the dried from solution, while the quantity of material for all the tests was similar, around 20-30 mg.

Here below are reported the quantitative results from the spectra collected that show a reasonable calibration post-measurement.

Sample	H2 wt% TDS-Petten	H2 wt% AMC-PD
E012	8.99	12.23
E011	4.27	12.23
A021	10.28	-
B021	-	-
C021	-	8.65
D021	-	9.84
E021	5.45	-
A031	-	9.67
B031	6.97	-
C031	7.65	8.65
D031	4.97	6.19
E031	-	-
A041	-	5.41
B041	2.22	3.40
C041	1.75	3.76
D041	0.60	2.10
E041	-	3.41

Table 3.I.4: Comparison between the quantitative data collected in the two labs. The quantitative data acquired with the apparatus by Hiden are less reliable in comparison to the one taken with the Sivert's Volumetric apparatus, thus they have to be taken only as qualitative or semi-quantitative.

The quantity and quality of quantitative data collected is not enough to draw conclusions. Even samples that should give the same results, because they come from the same batch, is calculated that desorb very different quantity of gas, see E012 and E011.
A comparison with the data collected with the Sivert's apparatus in Padua leads to the same consideration.

I.3.2 Reversibility

To recharge the samples with H_2 it was decided a setting that is in line with the reported in literature, see table 3.I.2, and is feasible for the available machines. The pressure was set at 5 MPa and the temperature, after a ramp of 10 ^{o}C/min, was kept for more than 4 hours at 480ºC.

It seems that only a small part of the capacity can be recovered with the set conditions using IMP or DFS samples, less than 10%, see figure 3.I.18.
The signal of borane during the second desorption has been detected and the shape is similar to the ball milled samples, without defined peaks.

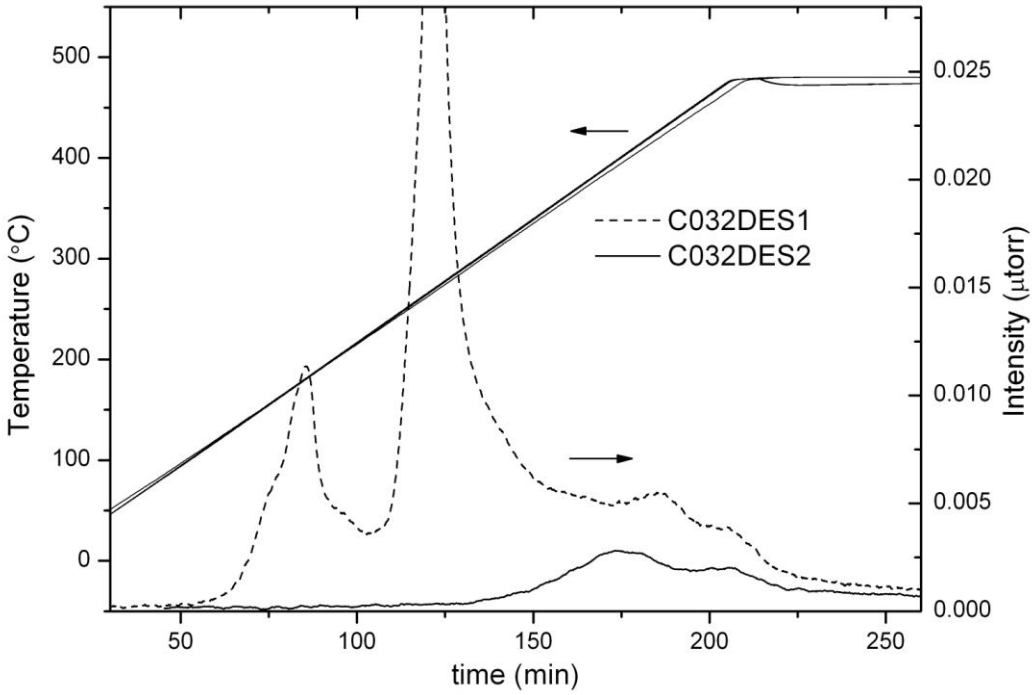

Figure 3.I.18: hydrogen MS spectra of first and second desorption of C032 sample. With the conditions used the samples are only partially cyclable.

I.3.3 XRD Analysis

First step of the work on the XRD has been the comparison between the patterns obtained in Padua and in Petten.
From figure 3.I.19 it is evident that the analyses from the two facilities are easy to compare and look very similar, and that the intensities are often almost the same.
The only differences are the peaks due to aluminum which can be attributed to the sample holder used in Petten (●) and, in some of them, some peaks due to $Mg(BH_4)_2$ (■) discussed later. The peaks of Al could have overlap with the LiH ones. Using a Plexiglas sample holder it has been demonstrated that this is not the case and LiH phase has not been detected in the dehydrogenated samples.
This polymer-based sample holder has not been used always because of the better resolution given by the aluminum one. Due to the little amount of powder and so the small layer thickness of sample used in the measurements, the amorphous phase of Plexiglas could be seen in the XRD patterns, worsening them, especially at low angles.

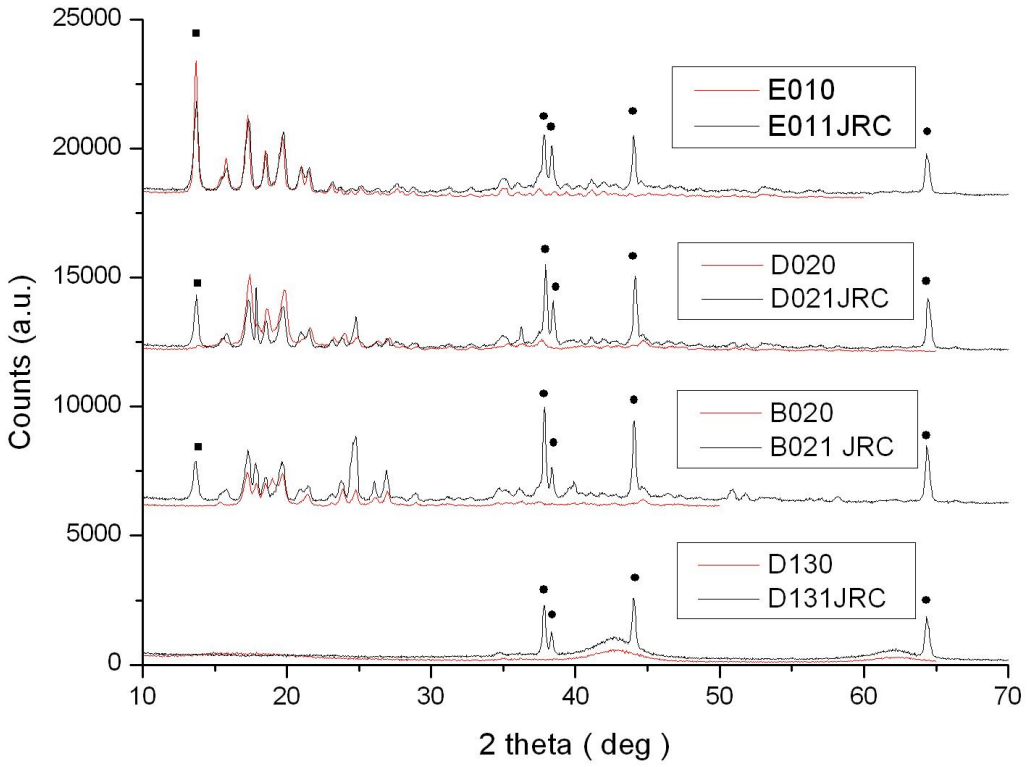

Figure 3.I.19: comparison between XRD patterns coming from Padua and Petten labs labelled JRC. From the bottom: D13, B02, D02 and E01 series. The patterns from the same samples are similar.

According to all the data available in literature only two phases of $Mg(BH_4)_2$, plus one at high pressure [103], have been discovered and solved, one orthorhombic (Fddd) at high and one hexagonal (P61 or P6122) at low temperature [104][105].
For $LiBH_4$ the situation is similar, even if 4 phases at different temperature and pressure are known [106], normally two are the most common and the transition from alpha to beta phase takes place around 110°C [55].

The situation is more complex when the two borohydrides are mixed together. According to the work of Fang [78] the two borohydrides react to form a new phase $Li_{1-x}Mg_{1-y}(BH_4)_{3-x-2y}$ like the one proposed for Li Ca system by the same scholar [77]; the single phase nature of the formed dual-cation borohydride is said to be supported by its well-characterized melting point.
In the study of Bardaji [76] on the other hand it is stated that no new phase has been seen in the system, even with different percentage of the two compounds and the only phases present are α and β $Mg(BH_4)_2$ and α $LiBH_4$.

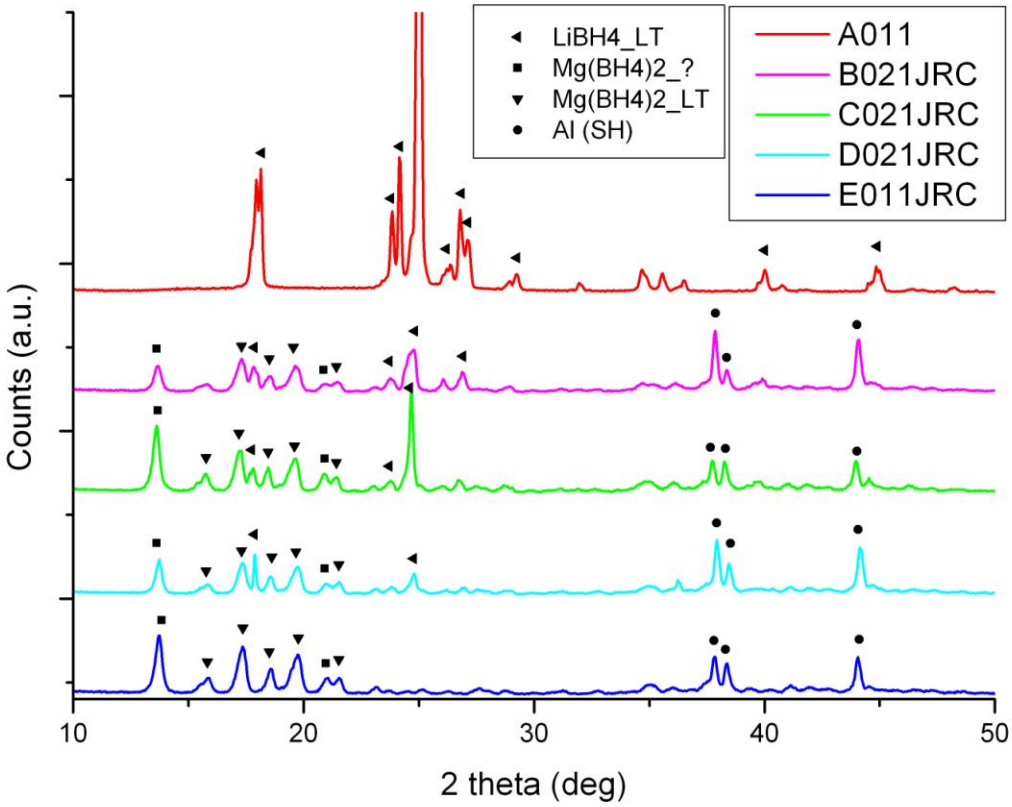

Figure 3.I.20: XRD Pattern of all the BM samples before dehydrogenation. From the top $LiBH_4$, composition 2:1,1:1,1:2 and $Mg(BH_4)_2$. All the peaks of the pure materials can be found in the mixed borohydrides.
No new phase as reported by Fang [78] has been detected.

From the XRD patterns, see figure 3.I.20, it is proved the theory of Bardaji: only the phases present in the two pure compounds are found in the milled samples. For the DFS samples, and even more for the impregnated, is much harder to say because of the lower quality of the patterns, see figure 3.I.21 and 3.I.22.
The absence of peaks in the XRD diagrams of Impregnated samples might be explained by the presence of a big amount of amorphous graphite in the powders. Still some small peaks should be visible. For the DFS samples this absence can't be explained and even from SEM analyses it is hard to explain this behavior: the particles are not small enough to think about a complete broadening due to nano-sizing effect. Thus the only possible conclusion is that the powders obtained with the two techniques are either amorphous or the dominions are nano-crystalline.

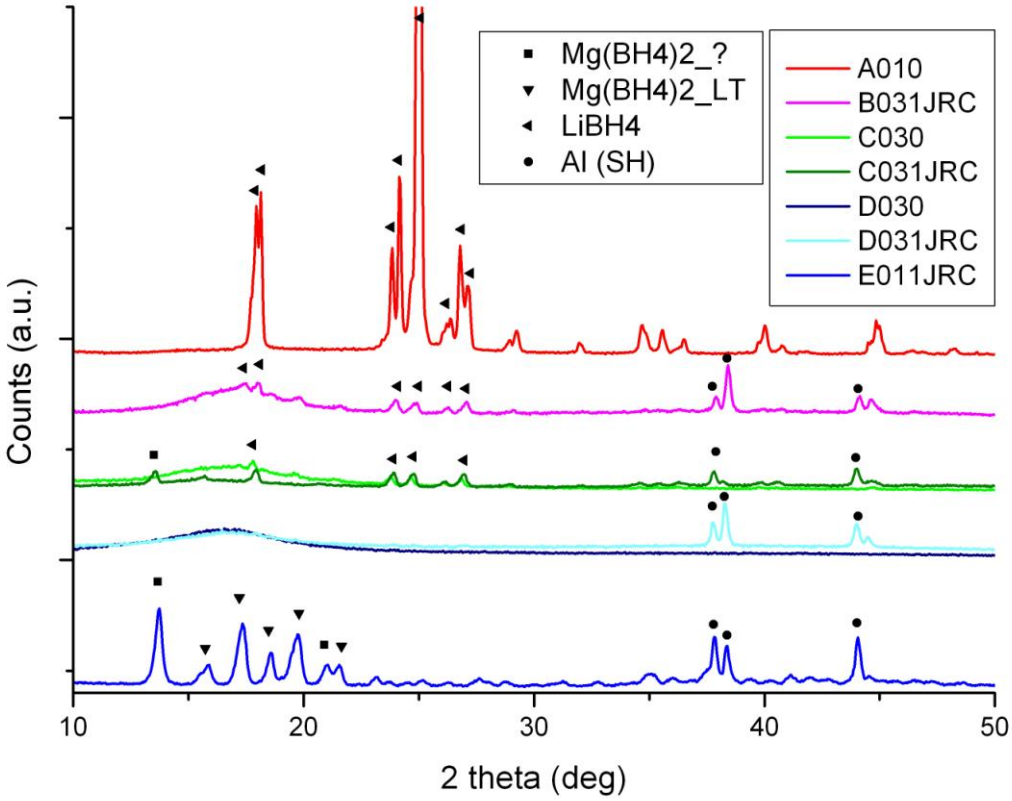

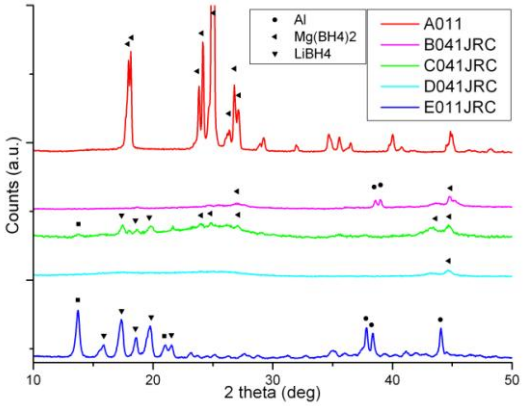

Figure 3.I.21 (top): XRD patterns of Dried From Solution samples. From the top $LiBH_4$, composition 2:1,1:1,1:2 and $Mg(BH_4)_2$. The patterns are harder to interpret in comparison to the BM ones, see figure 3.I.20. The same can be said for Impregnated samples, figure 3.I.22
Figure 3.I.22(side): XRD patterns of Impregnated samples.

XRD patterns of dehydrogenated $Mg(BH_4)_2$ and $LiBH_4$ can be easily found in literature. The first compound usually shows the peaks of Mg, MgH_2 and MgB_2 [64] while the second displays the peaks of LiH [52]. Boron is reported to be usually amorphous [95].

The only data available after dehydrogenation of the system under investigation are from Fang et al [78], and the only phases detected are MgO and an alloy of Mg and Li. The presence of oxygen is said to be a contamination during the handling from a machine to another. The products show not to be reversible to the borohydride stage but only to the MgH_2 phase.

The decomposition of the mixed borohydrides analyzed in Petten leads to the same phases in the case of dried from solution and ball milled series, see figure 3.I.23.
It is found that the decomposition products, Mg and MgO, do not correspond to the theoretical predictions found in literature. No trace of crystalline Boron, as reported also by other groups [52], or MgB_2 have been detected, which is, according to some authors, the key phase for reversible hydrogen storage in similar destabilized systems [58][88], even if other authors disagree [70]. No peaks of Li_4SiO_4 or Li_2SiO_3 [84] that would demonstrate the reaction with the quartz wool used as stopper for the powder in the sample holder of the TDS.
The patterns of the dehydrogenated samples, see figure 3.I.23, are very similar to the experimental one reported by Fang [78]. Further and deeper investigations are needed to demonstrate the presence of a Mg-Li alloy and the amorphous phase of B, as reported in previous works by Yu [70].

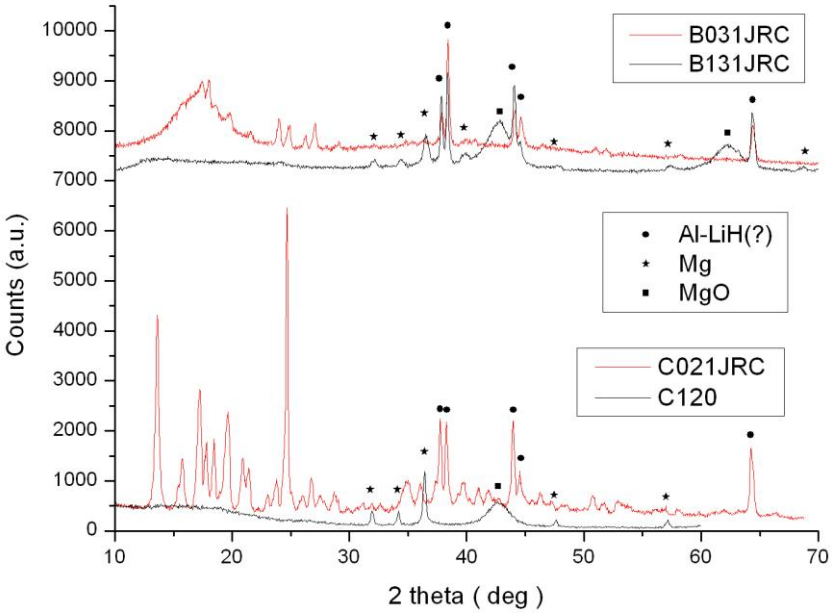

Figure 3.I.23: comparison between data collected before and after the dehydrogenation in Padua (C120) and in Petten (B131), with DFS (top) and BM (bottom) samples of composition 2:1 (B) and 1:1 (C). The labels refer to the desorbed samples. The dehydrogenated patterns show the same phases: Mg and MgO.

Thanks to the comparison with the patterns taken in Padua, without Al peaks due to the sample holder, it can be said with good certainty that no LiH (isomorph to Al) is present in the desorbed samples, see figure 3.I.23 pattern C120 and B131, and there is no overlapping with Al.

It was verified that the $Li_{0.3}Mg_{0.7}$ alloy Li-like phase is not present in the dehydrogenated samples while the $Li_{0.184}Mg_{0.814}$ (ICDS- 104740) Mg-like phase might be present. $Li_{0.184}Mg_{0.814}$ phase parameters were calculated modifying the Mg alpha to make it correspond to the d-spacings reported by Yu. The calculated lattice parameters are: 3.19 å (a), 3.19 å (b) and 5.13 å (c) instead of 3.2094 å, 3.2094 å and 5.2108 å.
It seems that no LiMg phase is formed but more analyses are needed to exclude completely this hypothesis.

I.3.4 FTIR analysis

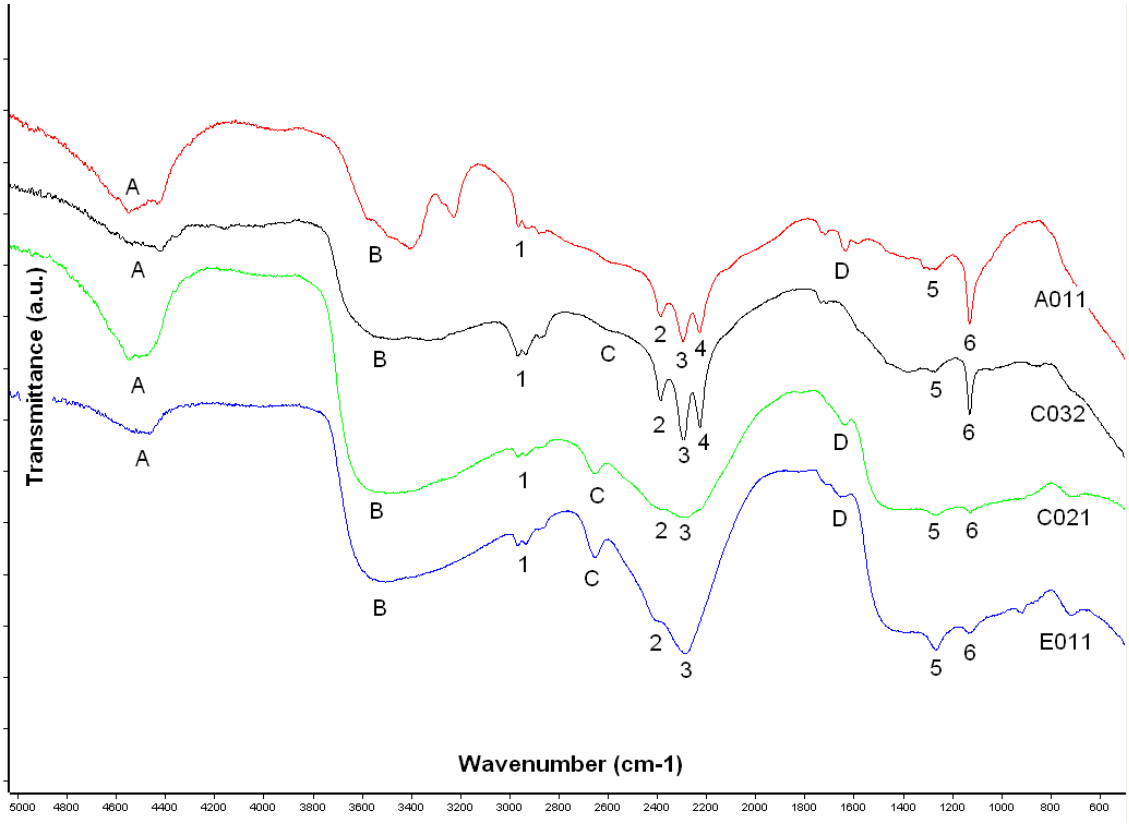

Figure 3.I.24: FTIR spectra, from the top: pure $LiBH_4$, DFS composition 1:1, BM 1:1 and $Mg(BH_4)_2$. Peaks 2 to 4 are characteristic of B-H stretching, 5 and 6 are B-H bending. 1 are the peaks characteristic of the dimethyl sulphide, see chapter 1.3.6.

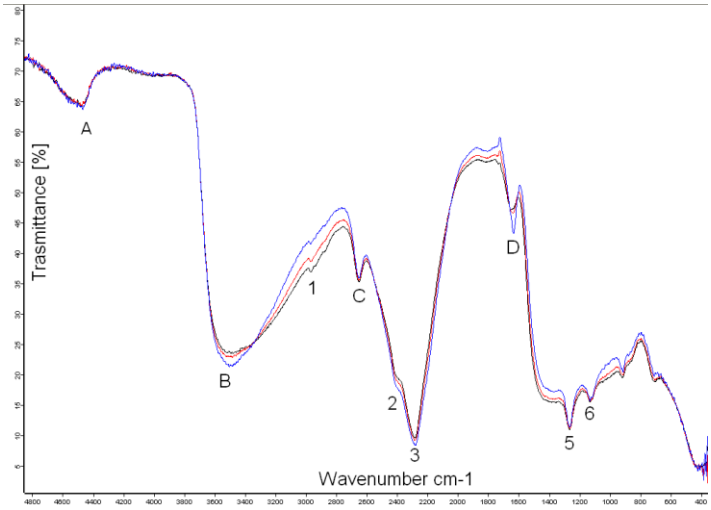

Figure 3.I.25 (bottom): FTIR spectrum of sample E012 (as received CNR $Mg(BH_4)_2$) after5 minutes in the vacuum chamber (darker), after 30 min and 90 min (lighter). B and D peaks vary with time and might be due to volatile compounds. A and C are stable.

Samples with composition C treated with wet chemistry and milling have been analysed with infra red technique.

To have a complete picture also the pure borohydrides have been scanned, $Mg(BH_4)_2$ from Padua's CNR and $LiBH_4$ from Sigma Aldrich.

In the spectra are visible the peaks of B-H stretching (2 to 4) and bending (4 and 5) that correspond to the data that can be found in literature [61][107].

Peak C can not be found in the work of some authors [61] while others have it well defined and addressed it as $\nu(B\text{-}H^t)$ peak [107].
According to Chlopek et al [61] the two borohydrides (Li and Mg) show the same peaks with a small shift in the wave number, especially in the bending mode around 1300 cm^{-1}.

If the spectra of the pure borohydrides, top and bottom in figure 3.I.24, are compared it is confirmed the result of Chlopek [61]: the main difference in the spectra is the shift of peak 5. Also peak 2,3 and 4 are less defined in the case of magnesium borohydride but it is not sure if this is due to the borohydride itself or to the presence of a different phase, see chapter 1.3.6. Peak C is present only where magnesium borohydride is present.

The spectra of mixed borohydrides, see figure 3.I.24, show feature similar to the pure borohydrides: the peaks of B-H vibration are visible (peaks 2 to 6) but surprisingly the spectrum of the DFS sample is very similar to the one of pure $LiBH_4$ while the BM one (third from the top) looks more like the pure $Mg(BH_4)_2$ from Padua's CNR. Peak 4 is barely visible and peak C is well defined.
The difference is not due to the composition, both are 1:1 mix, but to the synthesis.

When the pellet with the sample is left inside the chamber under vacuum for some minutes some peaks shift upward, see figure 3.I.25 peaks B and D. This might be due to volatile compounds present in the sample, such as water or solvents from the synthesis, or to reactions inside the pellet between active material and water still present in the KBr or with oxygen, still present in traces in the vacuum chamber.
Peak 1 can be addressed as dimethyl sulphide, coming from the synthesis of $Mg(BH_4)_2$ [102], but further analyses are needed even because, if this thesis is true, the atmosphere inside the glovebox might be polluted by the compound.

I.3.5 SEM analysis

Ball milled samples

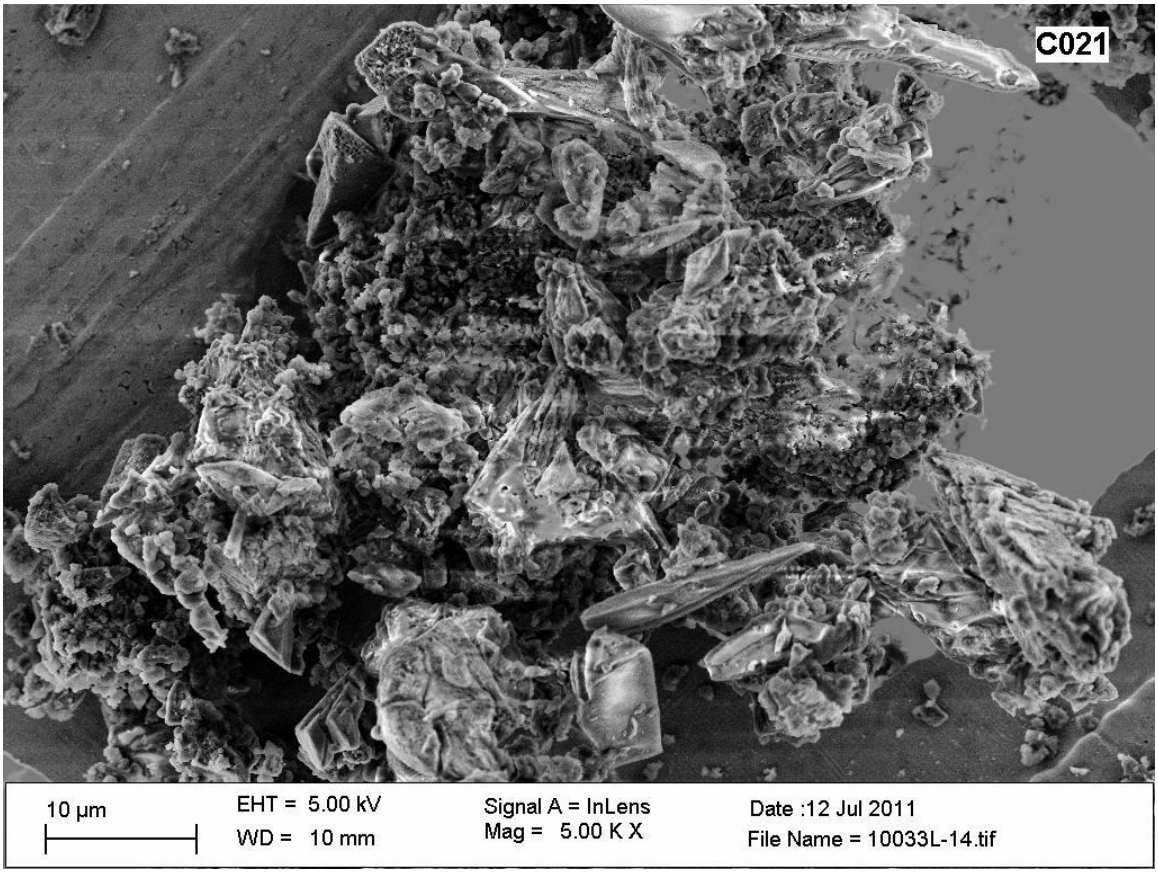

Figure 3.I.26 (top) and 3.I.27 (bottom): SEM picture of sample C021 (BM 1:1) at 5000x and 20000x. Sharp features can be seen due to the hard chemistry synthesis

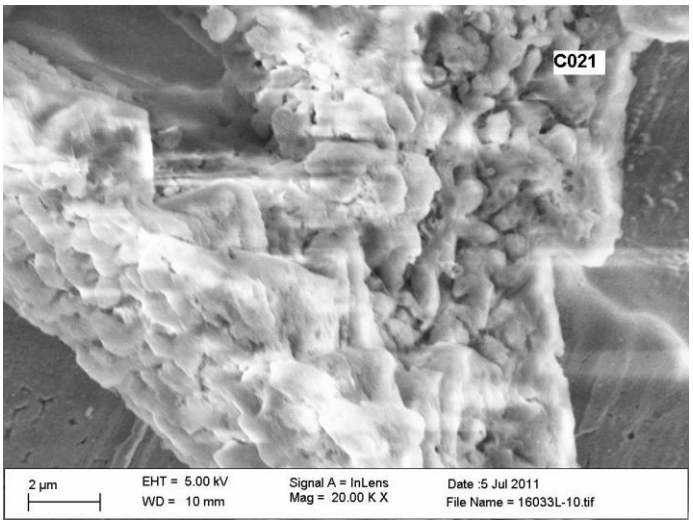

The samples treated with ball milling show the traces of the hard chemistry synthesis. Sharp features and edges are present and the crystals are aggregated in bigger clusters with complex shapes.
From a closer view it can be seen that the particle surface changes from place to place and in some zones the surface is not smooth but porous. See figure 3.I.26 and 3.I.27.

Dried From Solution Samples

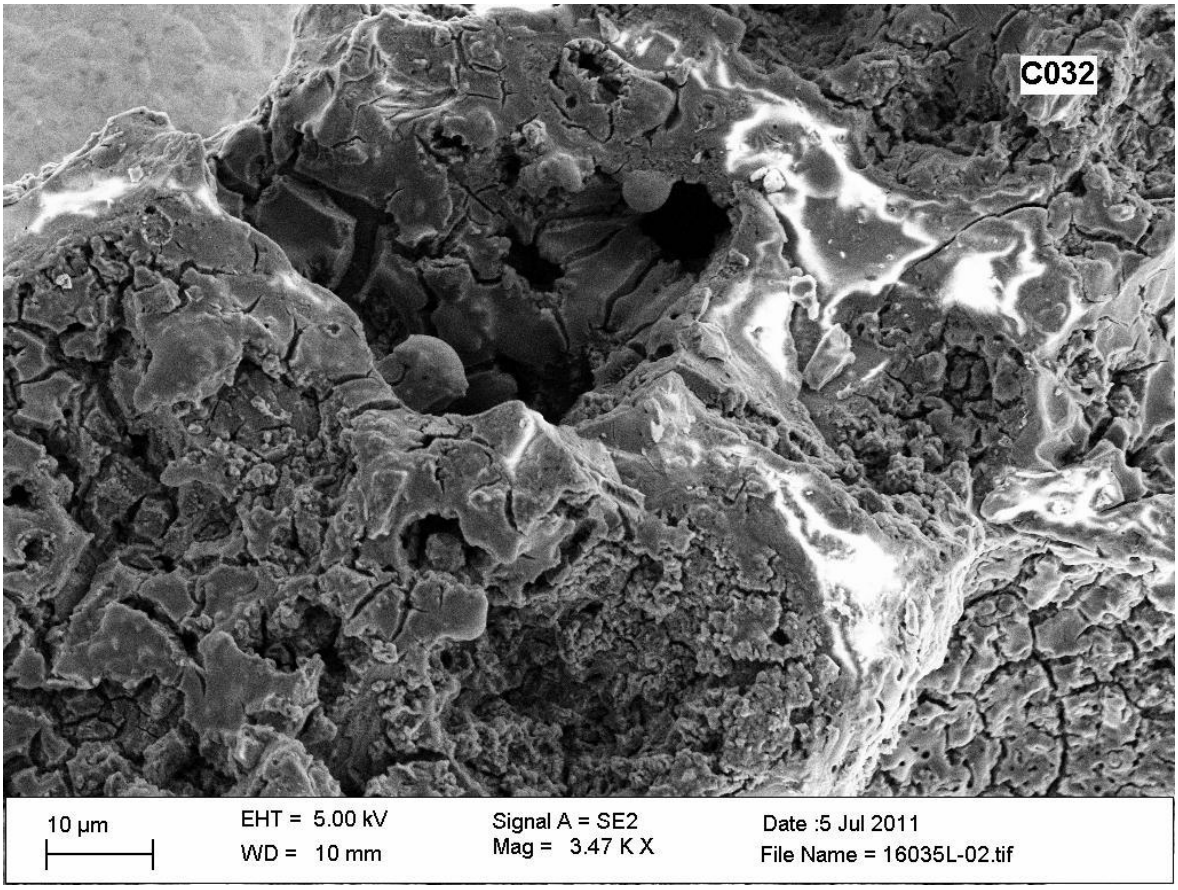

Fig. 3.I.28 (top) and 3.I.29 (bottom): SEM picture of sample C032 (DFS composition 1:1) at 3470x and 10000x. The cracks might be due to the drying process of the synthesis.

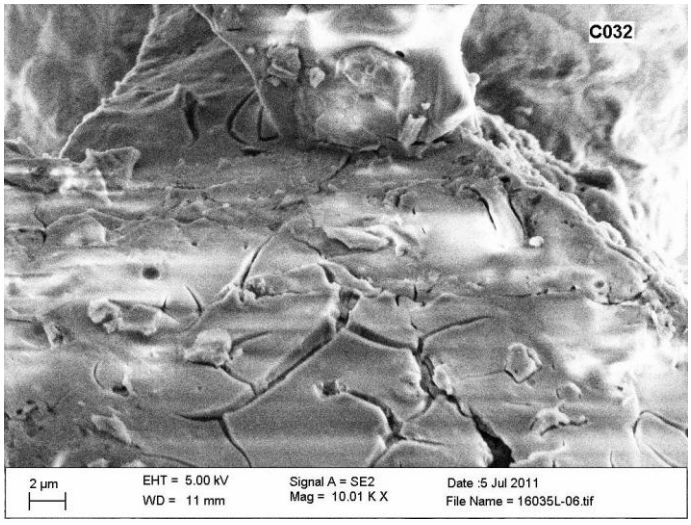

The samples dried from solution have a more porous surface and some characteristic well defined cracks. Those cracks can be found in all the samples synthesized with the soft chemistry method and might be due to the drying procedure.

From an analysis of sample C031, which showed a peculiar desorption behavior, see figure 3.I.7, it has been found out that the composition of the powder is not as homogeneous as in the case of sample C032. Some particles are smoother than others and show a different behavior when hit by the electronic beam, see figure 3.I.30. This might be one of the causes of the different desorption behavior of the sample.

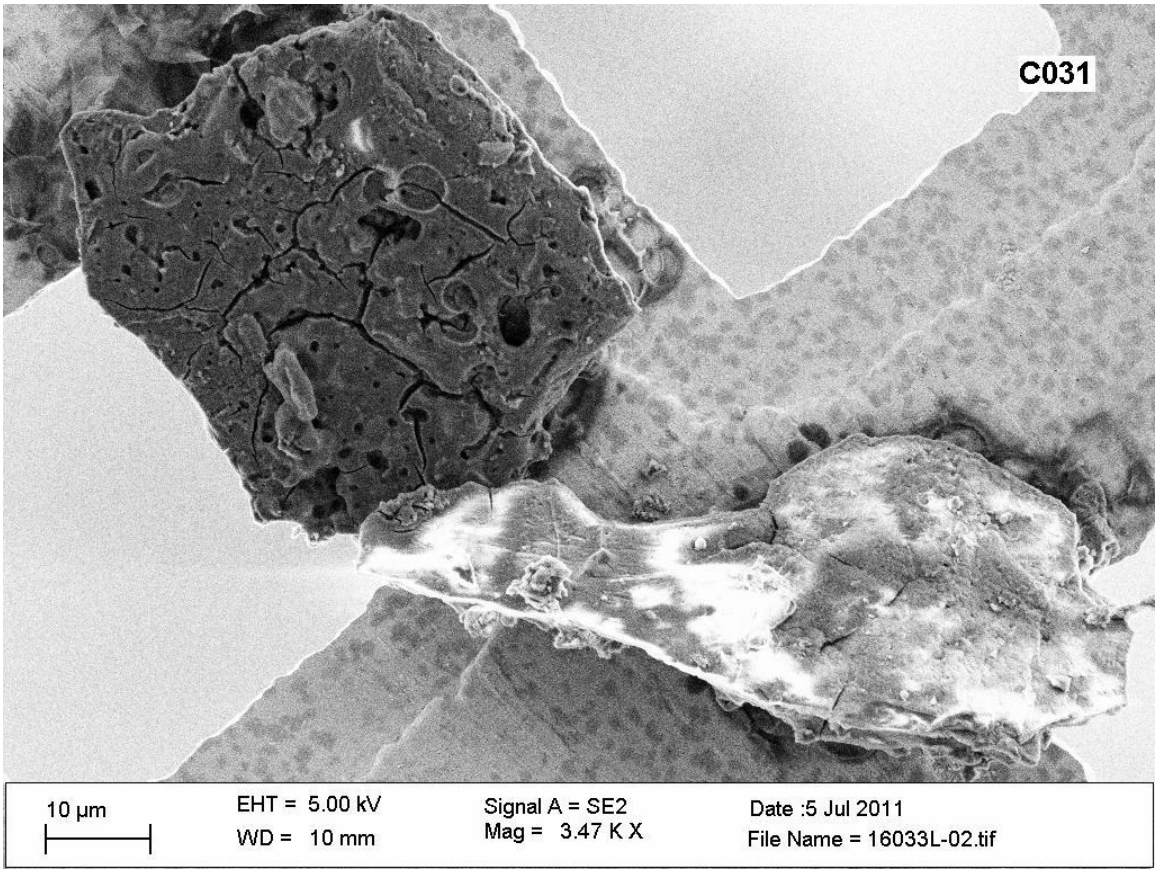

Figure 3.I.30: SEM picture of sample C031 at 3470x. It is evident that in this DFS sample the synthesis did not yield to a homogeneous material: shape and conductivity of those two particles are not the same.

Comparison between preparation techniques

Unfortunately is not possible to have a good elemental analysis of the samples, due to the impossibility to detect Li and lighter elements (among them hydrogen) with the EDS apparatus. Therefore it can't be stated if in one spot there are both Li and Mg or only one of the two. It is also hard to detect Boron and this make the analysis even more complicated due to the possible presence of MgH_2.
With a more qualitative approach anyway some information can be drew from the EDS spectra: the system is able to give an estimation of the distribution of the elements in the spot of interest, both in term of atomic % of the total and in terms of % of weight.
The ratio between the number of Mg atoms over B ones (always in terms of percentage) can give an idea of the composition of the sample in the spot.
From the mapping it can be seen that the Mg seems to be uniformly distributed in the particles, as is B. But, from the punctual analysis of atomic ratio B/Mg in various spots, see figure 3.I.31 and table 3.I.5, it has been observed that in some parts of the samples the ratio was around 7-8 while in others it was around 1-2 and in other around 3-4. The numbers are

not reliable because the uncertainty is high, but they give an idea on the mix of the two phases that might be not perfectly homogeneous in all the samples analyzed with the SEM.
Also from the backscattered electrons not much can be said. The difference in terms of composition seems to be so small that no bright spots can be seen with this detector, see figure 3.I.32.
Oxygen is present in all the powders analyzed but further investigation demonstrated that it comes only partially from the handling during the synthesis or during the loading for the SEM, see figure 3.I.33.

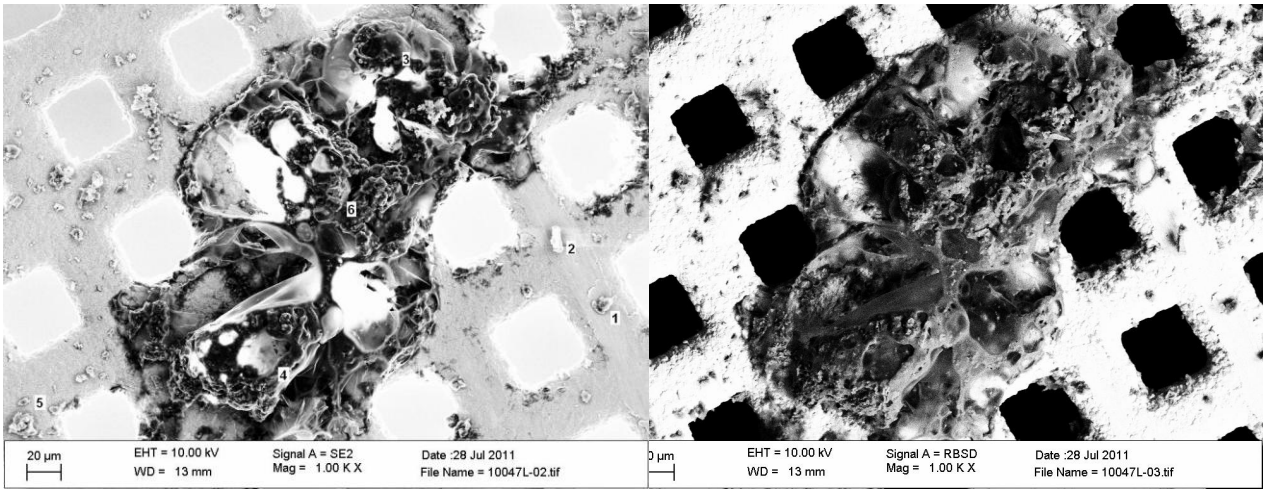

Figure 3.I.31 and 3.I.32 (top): Secondary Electrons and Back Scattered Electrons SEM images of in DFS sample D021 (composition 1:2) at 1000x.
Figure 3.I.33 (bottom): EDX general spectrum of figure 3.I.31. It is evident the presence of Mg and B, but also a big amount of oxygen that comes partially from the handling of the sample. Li unfortunately is too light to be detected.
Table 3.I.5: B/Mg atomic ratio in various points of figure 3.I.31.

Point	B/Mg
1	2.3
2	7.8
3	9.2
4	7.2
5	7.2
6	6.1

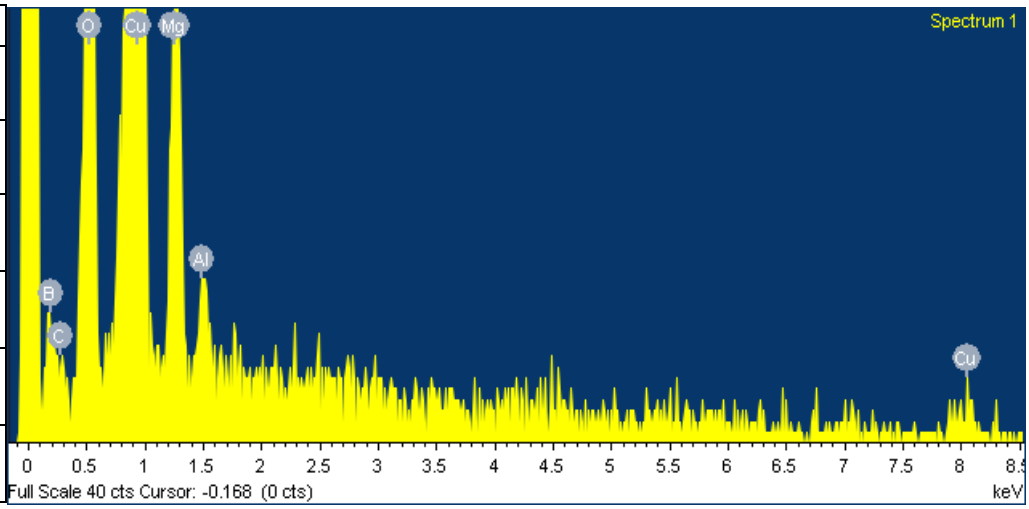

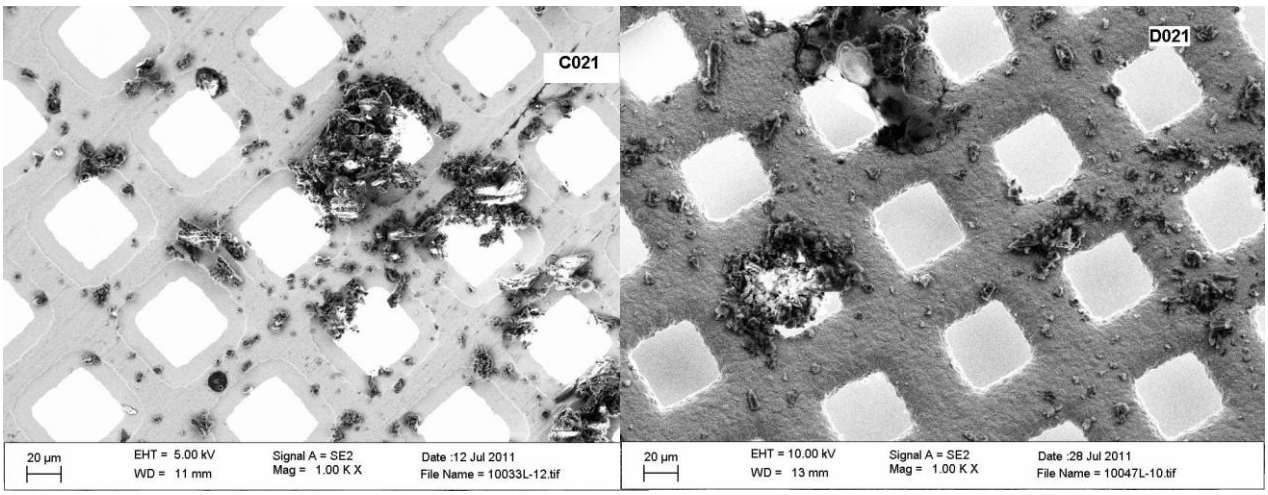

Figure 3.I.34 and 3.I.35 (top): SEM pictures of sample C021 (BM 1:1) and D021 (BM 1:2) at 1000x. The particles have a dimension of few µm but some of them are agglomerated in bigger clusters.
Figure 3.I.36 and 3.I.37 (bottom): SEM pictures of sample C032 (DFS 1:1) at 1000x. The particles have a big range of dimension: from few µm to tens of µm.

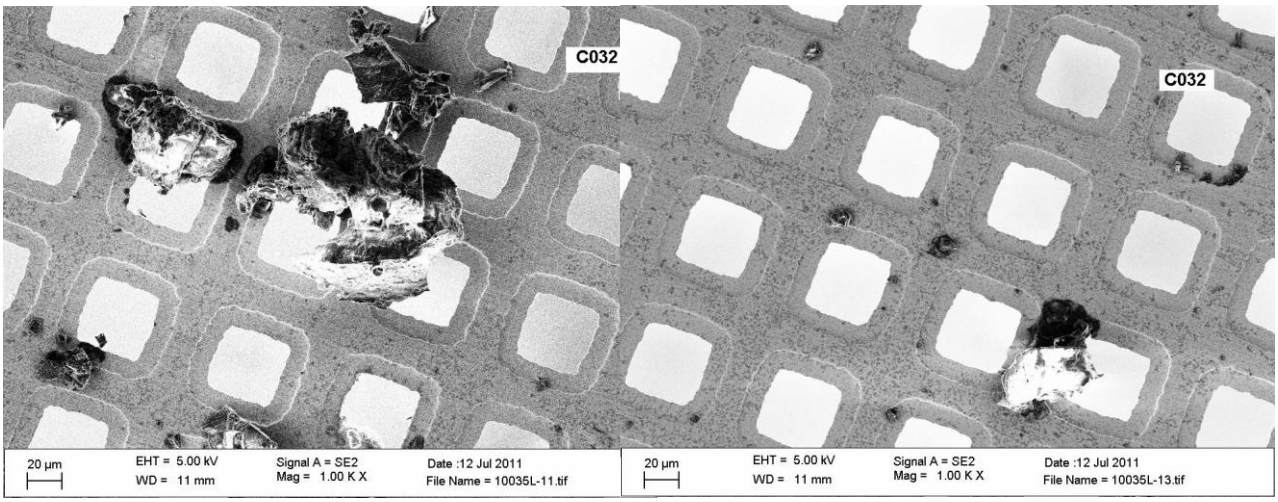

The clusters dimensions of the samples treated with DFS and BM techniques and analyzed with the SEM are comparable. The ball milled sample, see figures 3.I.34 and 3.I.35, is characterized by the presence of small particles (few µm) both free and agglomerated in bigger clusters of more than 20 µm.
Dried from solution samples, figure 3.I.36 and 3.I.37, have small particles too but the average dimension is tens of microns, like the clusters of the BMs.
It can be stated than that it is not the dimensions that lead to a better desorption of the DFS samples but probably the composition of the particles.

Impregnated Samples

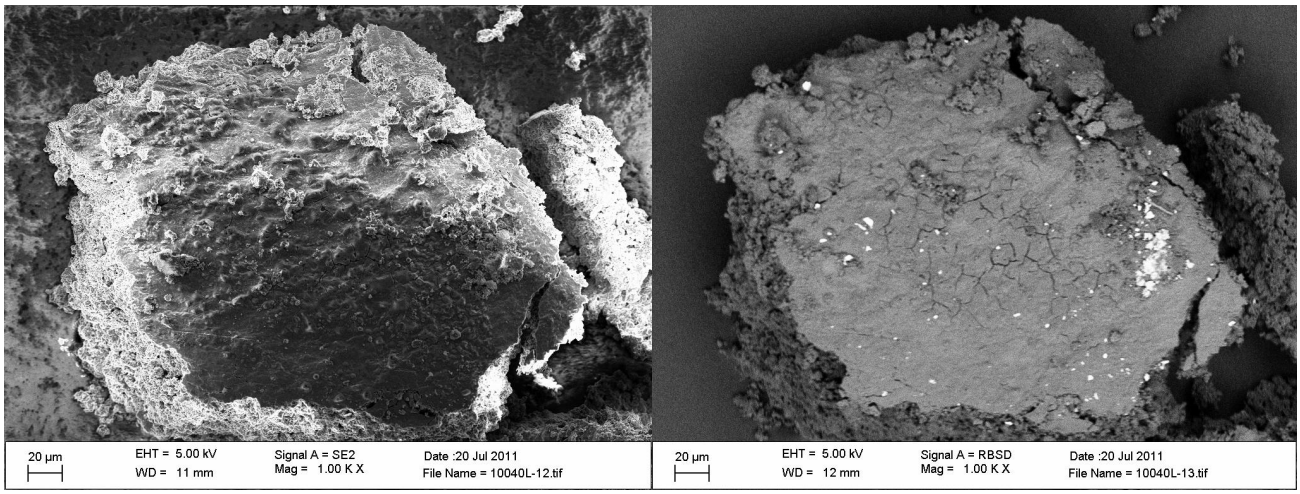

Figure 3.I.38 and 3.I.39 (top): SEM pictures of IMP sample C041 at 1000x taken with Secondary Electrons (left) and backscattered (right).
Figure 3.I.40 and 3.I.41 (side): Elemental maps of carbon (bottom) and Mg (top) of figure 3.I.38.

A different chapter is needed to discuss the impregnated samples. The information from SEM pictures of these samples are important but different from the ones coming from ball milled or dried from solution samples. The difference in atomic weight between the graphite and the borohydrides should be big enough to see brighter spots with the backscattered electrons.

Unfortunately this theory seems not to be supported by EDS data. From the elemental mapping Mg looks uniformly distributed on the surface of the particles, see figure 3.I.40, as are Boron and Carbon, see figure 3.I.41. Nevertheless from punctual analyses on different sites of interest it results that the ratio of C over Mg is not constant, and varies with the brightness of the site (in the SE image) and this can correspond to a different conductivity due to the different composition.

Surprisingly this difference in C/Mg ratio is not evident in brighter spots of backscattered images as it could be expected.

In conclusion the borohydrides are distributed more or less homogeneously on the carbon surfaces and clusters of borohydrides, if there are, are not detectable with an elemental analysis, probably because too small. This result is in line with the XRD patterns that do not show well defined peaks of the borohydrides, see figure 3.I.22.

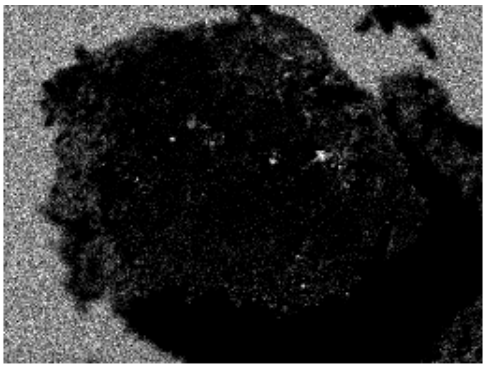

I.3.6 A new $Mg(BH_4)_2$ phase?

XRD, TDS-MS, IR and EDAX analysis

Since the first look at the XRD patterns it was observed that not all the peaks detected in the samples that have $Mg(BH_4)_2$ inside could be easily recognised with the databases of the JRC-IE or with the last reported in literature [104]. In particular the peak already mentioned and labelled with (■ and □) in figure 3.I.20 and 3.I.42, which is present in all the patterns collected in Petten and in some received from Padua.
The synthesis of the $Mg(BH_4)_2$ used for all the samples has been done following a US patent submitted by Zanella et al. [102][108] but the XRD pattern reported in the patent is different from the one that has been taken in Padua and in Petten which, as can be seen in figure 3.I.42, are almost the same.
The missing peaks do not correspond either to one of the known $Mg(BH_4)_2$ phase or to the high pressure phase indexed in the hexagonal P63 space group, found by George et al [103].
Some scholars predict a third phase for magnesium borohydride, basing on thermodynamics calculations. This is the case of Ozolins [109] and Zhou [110], who proposed other two more phases. From their calculations a lowest energy phase of the borohydride should exist with tetragonal I-4m2 symmetry. Other authors disagree with the previous two and propose other phases for low and high temperatures with symmetries: I41/amd and F222 [111].
From the theories reported above the patterns of all the predicted phases have been calculated and with a Rietveld analysis it has been discovered that it is possible that the I-4m2 phase exists and is mixed in the samples used in the experimental campaign with the well known hexagonal alpha phase, see figure 3.I.42. Still few minor peaks have to be assigned to known or predicted phases (□).

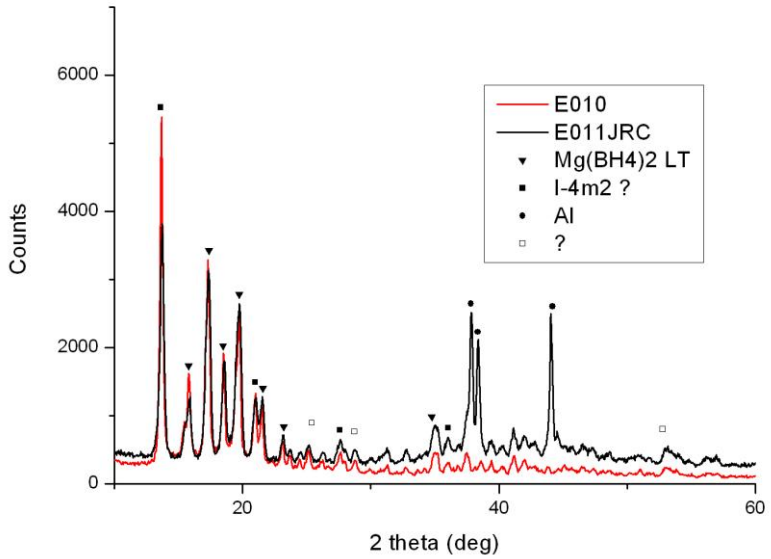

Figure 3.I.42: Pattern of E010 and E011 with the most evident picks detected.

The unassigned peaks in the XRD patterns fit with the ones already found by other authors that labeled them as a new γ phase [107] or $Mg(BH_4)_2 \cdot 2S(CH_3)_2$ [112] respectively. Both the groups used the same Zanella's recipe [108].
The work of Soloveichik et al [107] focuses on the differences between various methods to synthesize $Mg(BH_4)_2$ and the techniques to eliminate the residual solvents. In some of the syntheses they found the peaks of what they called a new γ phase mixed with the known phases of $Mg(BH_4)_2$.
One year later the group of Newhouse [112], in a study to improve the hydrogen release of magnesium borohydride, showed the pattern of the adduct $Mg(BH_4)_2 \cdot 2S(CH_3)_2$ and compares it to the pure $Mg(BH_4)_2$ obtained after leaving the sample in vacuum at 160°C overnight.

To further investigate this unknown phase present at least in all the ball milled samples, see figure 3.I.20, has been decided to compare the pure $Mg(BH_4)_2$ used for the synthesis of all the samples with a commercial magnesium borohydride bought from Aldrich.

It is calculated that from a TPD analysis the new predicted I-4m phase can not be detected because the difference between that and the low temperature P61 phase in the calculated dehydrogenation enthalpy is negligible, only 2 $kJ/molH_2$ [113]. But the presence of dimethyl-sulfide should give signal at 47 and 62 M/Z in the samples with the adduct [@17].
From the comparison between the hydrogen desorption of the bought and synthesized magnesium borohydride, see figure 3.I.44, nothing can be stated. The compound coming from Aldrich starts to desorb at 120 °C, a temperature that is far below that of sample E011 and even the ones reported in literature [64][99], but the hydrogen desorbed by the commercial material looks to be much less than the hydrogen desorbed by the sample synthesized in Padua.

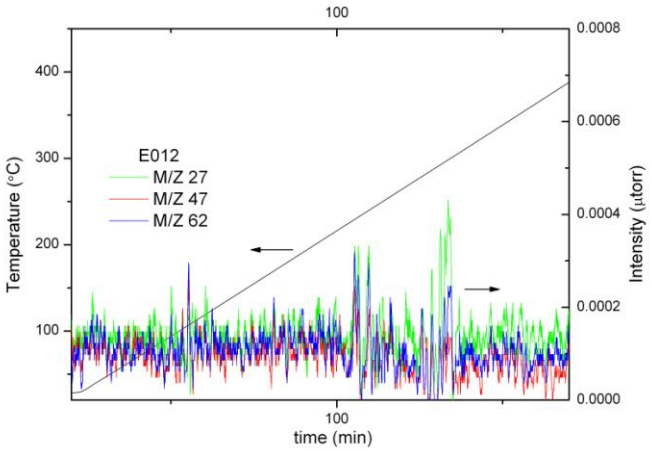

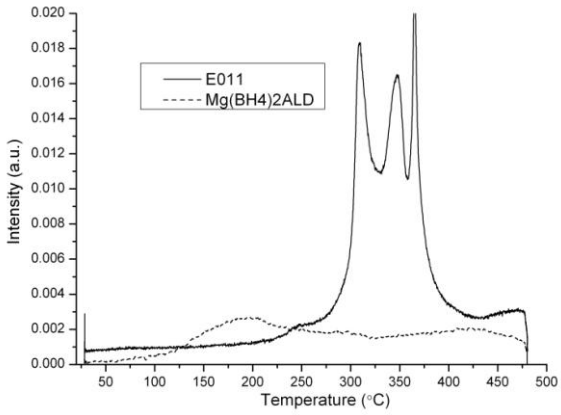

Figure 3.I.43 (left): MS spectrum of sample E012 (pure $Mg(BH_4)_2$ as received) of M/Z 27,47 and 62 (dimethyl-sulfide) during TDS.
Figure 3.I.44 (right) hydrogen desorption of commercial and CNR's $Mg(BH_4)_2$. The commercial material shows a much different behavior in comparison to the reported in literature [64][99].

From the mass spectrometer spectra of masses M/Z 47 and 62 the release of dimethyl-sulfide could not be detected. The signal is not present or it is confounded with the background as might be the case of borane reported for comparison, see figure 3.I.43.

Another approach to understand the nature of the different phase detected with the XRD has been the use of infrared. In figure 3.I.45 are reported the patterns of: the synthesized material, a sample from the same batch left for 19h under vacuum and the commercial one.

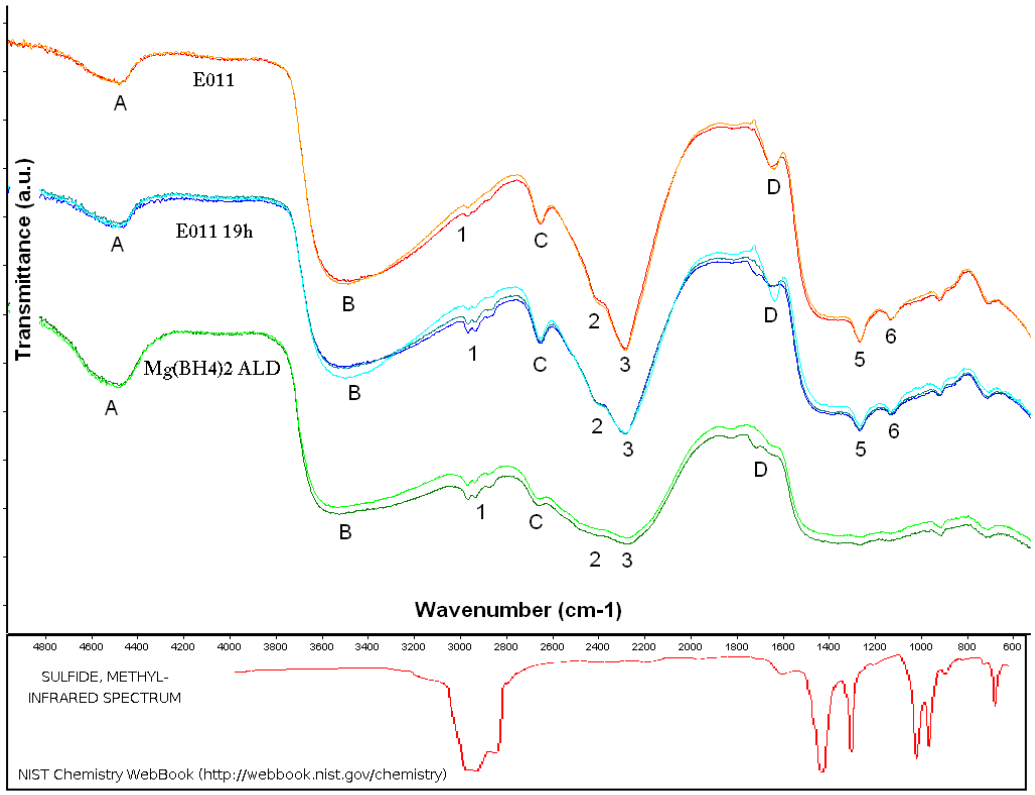

Figure 3.I.45: FTIR spectra of pure $Mg(BH_4)_2$ from CNR and from Aldrich. Between the two is the CNR compound left 19h under vacuum. All spectra seem to show the features of dimethyl-sulfide. For each experiment are drown the pattern after5 minutes under vacuum(darker), after 30 min and 90 min (lighter). Below is the dimethyl-sulfide spectrum from NIST database [@17]

Different authors have used the IR to analyze borohydrides. The typical features that can be seen in the spectra taken are the one of $[BH_4]$ groups: the bending modes at 1100-1300 cm^{-1} and the stretching ones at 2200-2300 cm^{-1}[61]. Another peak is at 2650 cm^{-1} is reported only by some authors [107] and labeled as a stretching of B-H group.
In the spectra recorded from sample E011 and Mg(BH4)2ALD, the home made by CNR and the one bought by Aldrich respectively, almost the same peaks can be detected. The bending and stretching mode are more or less visible (peaks 1 to 5), as well as the bump at 3600 cm^{-1} (B) and the peaks at 2900, 2600 and 1700 cm^{-1} (A and C).

Ratio	$Mg(BH_4)_2$	$2S(CH_3)_2$
E012/ ALD	↓	↑
E012/ E012_19h	↑	→
ALD/ E012_19h	↑	↓

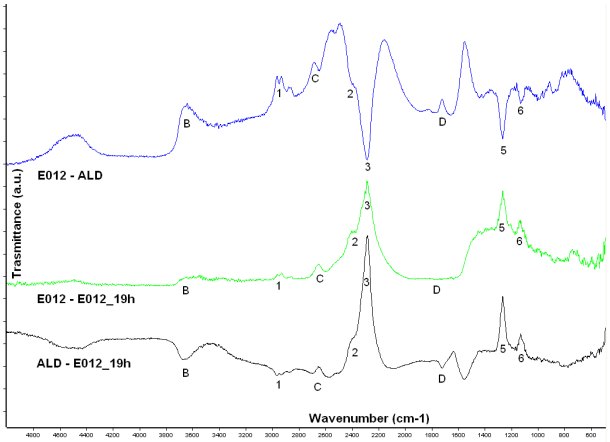

Figure 3.I.46 and table 3.I.6: Ratio between the patterns of the figure. The pellet with E012 has more sulfide and less borohydride because the characteristic peak of the first (1) goes up while the peaks of the second (2,3,5 and 6) go down.

Dimethyl-sulfide is reported to absorb in a large band from 2800 to 3000 cm^{-1}, the typical absorption of C-H compounds, and with four spikes at 1220, 1150, 1020 and 960 cm^{-1}. A representative pattern is reported under figure 3.I.45.
The low wavenumber peaks of the sulfide are covered by the typical features of B-H bonds, but, at a first sight, the band below 3000 cm^{-1} can be seen (1) in all the samples. Surprisingly the same peak is even more pronounced in the case of the material bought as a reference from Aldrich. Moreover the same peak can be detected and is more pronounced in a sample with the same composition of E012 but left 19h under vacuum.

To understand the unexpected and puzzling results a data elaboration is needed. In figure 3.I.46 are reported the ratio between: E012 and Mg(BH4)2ALD, E012 and E012 after 19h, Mg(BH4)2ALD and E012 after 19h.
Produce pellets with exactly the same amount of powder is impracticable since the amount of target powder in the KBr pellet is in near the limit resolution of the scale used to measure it. From the ratios anyway it can be understood which compound is more present in a pellet in comparison to another.
From the second line of figure 3.I.46, $Mg(BH_4)_2$ is more abundant in sample E012 than in the one left for 19h in vacuum (peaks 2,3,5 and 6 go up) but the peak of sulfide is barely visible, which means that the sulfide is partially gone in the sample used for the vacuum test. The same can be said for the sample made with the commercial powder in comparison to the synthesized one or the one left 19h in vacuum. In this case the borohydride signal is higher and the sulfide one is lower. The results are schematically summarized in table 3.I.6.

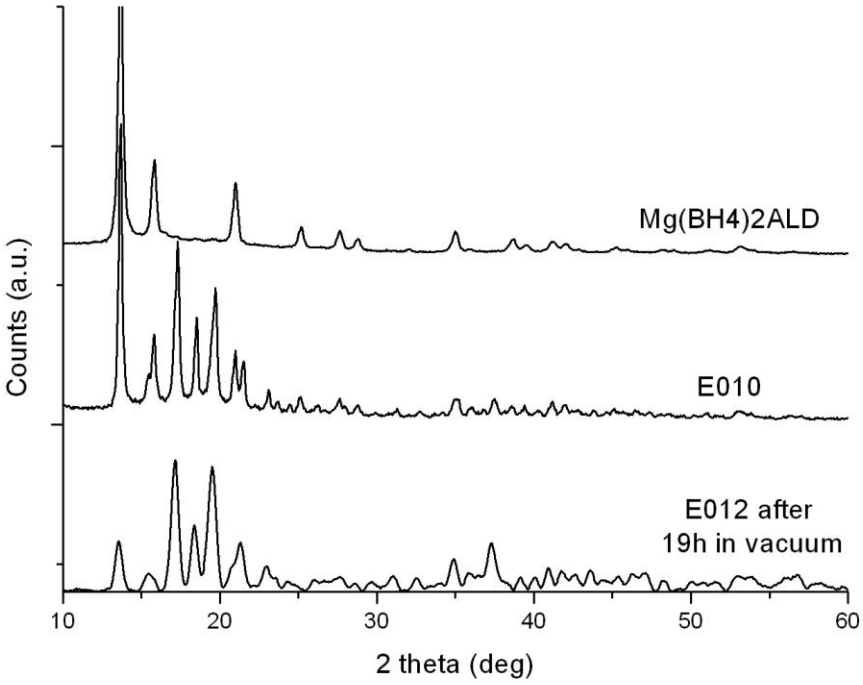

Figure 3.I.47: XRD patterns of sample Mg(BH4)2ALD (commercial material), samples synthesized in Padua E010 and E012 (same batch left 19h in vacuum)

The IR results are confirmed by XRD patterns. The sample coming from Aldrich, previously used as a reference and supposed pure, is in fact almost completely made by the unknown phase, see figure 3.I.47.
If a sample synthesized in Padua is left 19h in vacuum the XRD pattern change according to the results of the IR analyses. The peak of the unknown phase decrease considerably and the characteristic peaks of $Mg(BH_4)_2$ alpha phase are the most evident, see figure 3.I.47.

Last to be said is that some EDS spectra show the peaks of sulfur. The signal is low, even if S is a heavier element than magnesium or oxygen, but visible.

Conclusions

From the analyses on the unknown $Mg(BH_4)_2$ phase it can be stated that:
- There are strong evidences of the presence of the $Mg(BH_4)_2 \cdot 2S(CH_3)_2$ adduct or another sulfur compound in the samples.
- Evidences of a new phase are not as strong. For the purification procedure used in literature by some authors to remove the solvent, over 200°C in vacuum, is too harsh to be sure that no phase change takes place with the removal of the dimethyl-sulfide.

What is evident from this analysis is that the material synthesized by the CNR in Padua does not show properties that are too different from the data found in literature. The emission of sulfide, if there is, is so low that is even hard to be detected from the MS and the desorption of hydrogen is in agreement with the results of other groups.

It can be concluded than that it makes not much of a difference to use contaminated $Mg(BH_4)_2$ from CNR and not a perfectly pure compound in order to produce reliable results.

From the comparison with the commercial magnesium borohydride another important conclusion can be drawn: the $Mg(BH_4)_2$ supplied by Sigma Aldrich is not a pure compound and might have affected the results of other groups working on borohydrides.

I.4 Conclusions

From the data collected it can be conclude that:

- The main result is the already proved lower desorption temperature for the mixed borohydrides in comparison to the main desorption of the bulk pure ones, and this seems independent from the treatment.
- A different behavior has been detected for BM and DFS samples. The firsts disagree with the literature showing a higher decomposition temperature.
- The amount of borane and diborane has been successfully detected and shows that, with the experimental conditions used, the worst technique is the dried from solution synthesis. Still, also the compounds made with the other two techniques release the unwilled compounds.
- The cyclability of the samples has been demonstrated to be not possible with the available setting.
- The XRD patterns taken in the two facilities seem to be easily comparable.
- No new mixed borohydride phase, like the one claimed by Fang, appears after the ball milling.
- The two different preparations of the samples non impregnated (BM and DFS) lead to the same phases after dehydrogenation.
- Independently from the synthesis technique, no trace of crystalline Boron, LiH or MgB_2 have been detected in dehydrogenated samples. A different path may be followed by the reaction that can be recollected to the work of Yu with LiMg alloys. Further investigations are needed to confirm the results.
- From IR spectra taken, Li and Mg borohydrides look similar except for a shift in one peak and for the presence of another is not always found in literature.
- Even if the composition used was the same, the wet chemistry synthesis gives an IR spectrum similar to $LiBH_4$, while ball milling lead to one more similar to $Mg(BH_4)_2$.
- From SEM pictures it has been observed that the dimensions of the clusters of the BM and DFS samples are similar but the firsts are made by smaller particles aggregated while the seconds are made by bigger particles.
- It is not possible to distinguish Li and Mg borohydride phases from the pictures, not even with the EDS apparatus.
- Impregnated samples look uniformly covered by borohydrides, and no cluster of these compounds could be detected.
- Samples containing $Mg(BH_4)_2$ might all be polluted with a sulphur compound or with a new phase, even if this possibility is less probable.
- The results obtained, even if the samples were polluted, should still be reliable since the amount of pollutant is barely detectable.

Future work on the presented materials might follow four main directions:

The studies on sample C031 show that the presence of impurities can modify and even lower the desorption temperature of the borohydrides mix. This suggests that the use of catalysts might decrease the desorption temperature without compromising too much the gravimetric capacity of the compound.
A first choice would surely fall upon Ti halides, especially TiF_3, because other Ti compounds show to be ineffective with $Mg(BH_4)_2$. MgB_2 or materials with the same lattice structure are another option to act as nucleating agents during desorption.

Infiltrated samples might be improved using multiple impregnations to increase the load of active material. Another possibility to improve the technique can be the use of a different scaffold, for instance activated carbon or carbon aerogel, that have larger surface area than graphite.

It would be interesting also to investigate on the re-loading of the compounds. A possibility could be doing the desorption under a back pressure, as it has been demonstrated to be effective with another destabilized system: $LiBH_4/MgH_2$. But unfortunately this setting is not possible with the used TPD apparatus

D04 sample might be re-synthesized to have more reliable data, more similar to the other two impregnated samples.

Additionally the analyses on the unknown phase in the $Mg(BH_4)_2$ should be concluded with the help of Padua's CNR where the material have been synthesized.

II MgH_2 and magnesium based electrodes

II.1 Introduction on the materials

Catalyzed MgH_2

MgH_2 is one of the first and most studied materials for hydrogen storage because of its low cost, abundance, light weight and high theoretical storage capacity of 7.6 Hwt%. However, concerning possible practical applications, it has limitations due to its high thermodynamic stability and slow hydrogen absorption/desorption kinetics.
Many efforts, similar to the ones described previously for borohydrides, have been made to come out of these practical shortcomings [89]: nanosizing the hydride by high energy ball milling, nano-confining in a polymer-based matrix [93], and adding destabilizes [114] or catalysts to improve the hydrogen a/d kinetics with little reduction in the gravimetric capacity [115].
Up to date the most interesting results have been achieved by adding TiF_3 or embedding nano-particles in PMMA matrices.

For hydrogen storage Ti has been seen as a better catalyst for Mg based materials in comparison to V, Ni, Mn and Fe [116]. After the first cycle Ti assumes the hydride state and, since the plateau pressure is much higher than the one of Mg, it will not go back to the metal phase [116].
Halides have shown a good catalytic effect on hydrogen storage materials. Studies on FeF_3 show how this is a better catalyst than metallic Fe and niobium oxide (Nb_2O_5) which was previously seen as the best catalyst on the market for Mg alloys [23][117][118].
As a source of both the species, TiF_3, attracted a great interest as a catalyst and demonstrated to have better characteristics in comparison to $TiCl_3$ and FeF_3 [119][120]. Peng et al.[120] did not found big differences between magnesium hydride catalyzed with Fe and Ti fluorides, only in the kinetics and in the different composition of the active dispersed particles: made of Fe in the first case, and of TiH_2 in the second. It is reported in all the literature on the subject that, at the dehydrogenated stage, the $TiFe_3$ or FeF_3 phases disappear completely. The reaction can be summarized as follow:

$$MgH_2 + \tfrac{2}{3}TiF_3 \leftrightarrow \tfrac{2}{3}TiH_2 + MgF_2 + \tfrac{1}{3}H_2 \quad (3.10)$$

The role of fluorine anion has been studied by Ma et al. [121]. On the basis of X-ray Photoelectron Spectroscopy (XPS) studies they claim that F^- differs significantly from its analogous Cl^- in terms of bonding state. In samples with $TiCl_3$ only one stable bonding state of Cl is present in the form of $MgCl_2$. In contrast, F anion in samples with TiF_3 is partially stabilized as MgF_2. it is claimed that a considerable amount of F participates in the generation of metastable active Ti–F–Mg species.
These findings suggest that the advantage of TiF_3 over $TiCl_3$ as catalytic additive is closely related to the generation of F-containing active species.
Evidences show that Ti based particles are well dispersed in the sample when halides are present, but this cannot be the only reason for the better kinetics of MgH_2 catalyzed with TiF_3

since the particle distribution due to Cl^- or F^- anions is the same but the resulting desorption temperatures are different [119].
Ma et al. [119], after a preliminary investigation on the system done varying the composition atmosphere and comparing with $TiCl_3$, concluded that the catalytic enhancement of the hydrogenation and dehydrogenation properties observed in the MgH_2–TiF_3 system can not be readily attributed to the individual or synergetic function of the TiH_2 and MgF_2 phases detected in the XRD examination. They propose the presence of a ternary phase with Mg, Ti and F which catalytic effect depends on the interaction with the surrounding chemical environment.
Thanks to in situ neutron diffraction Mulder et al. [122] proposed the seeding effect of MgF_2, iso-structural to MgH_2, as the reason of the compound's catalytic properties. Ti acts both as a reservoir for F while Mg is in the hydride phase and as a thin layer on the particles, see figure 3.II.1. The number of vacancies in the Mg-β phase and the interaction between β and α phase, rich of hydrogen, is argued to play an important role in the solubility limits. It has been found a much different behavior in the Van't Hoff plot in comparison to the bulk material and absorption at low temperature and pressure (-10°C, 10 bar).

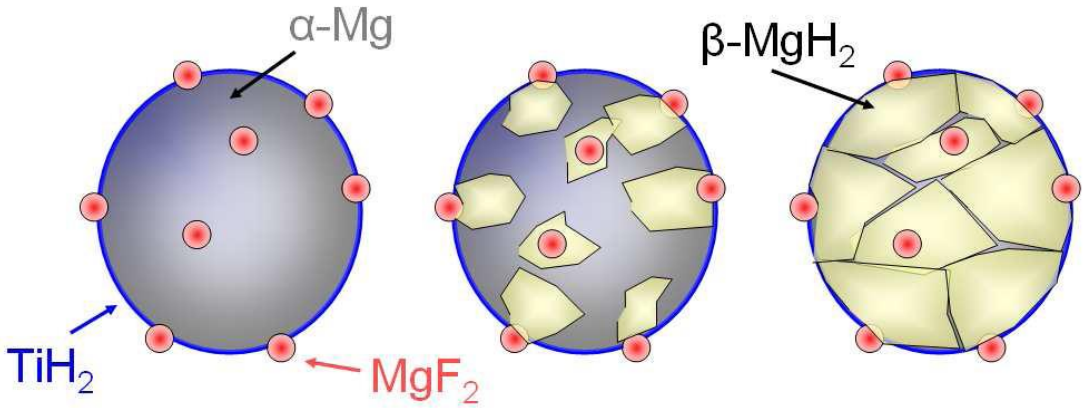

Figure 3.II.1: Role of TiH_2 and MgF_2 in the absorption of hydrogen in the MgH_2-TiF_3 composite, from [122]

Mg based electrodes

According to the knowledge of the author nobody has studied a pure Mg electrode yet having appreciable results. The thermodynamic stability is not the only issue to overcome: in basic aqueous solutions Mg gets covered by an insulator layer of $Mg(OH)_2$ that makes the surface of the material no more active [123].
This is a common problem for Ni-MH anodic materials mainly caused by the harsh conditions imposed by the electrolyte [33].

To overcome the problems of high stability and enhance the corrosion resistance, different methods have been attempted, with pure Mg and with alloys:

- modify the surface composition, even with electroless deposition of chromate or mechanical coating with TiO_2 [124],
- mix the Mg based material with AB_5 alloys [124][125]
- modify the bulk composition with: Ti [41][126][127], Ni [60][126], Sc [41][128], V [41], Cr[41], Ti-Ni [127], NI-Al [129], Ni-Ti-Al [127].

$Mg_{80}Sc_{20}$ thin films showed capacities of 1790 mAh/g, corresponding to 6.7 Hwt%, around six times the capacity of a common Ni-MH electrode. Ti alloyed films showed similar properties (~1700 mAh/g) and the cost is much lower since nowadays the price of Scandium is several hundreds of euro per gram [@19][@20].

In many of the works reported in literature the films were capped with a Pd layer both to enhance the absorption/desorption properties and to protect the thin film from the electrolyte solution avoiding the passivation [41][130].
This method has been already proposed in the 90s to overcome the degradation of the $MmNi_5$ electrode showing good results when Pd was applied via electroless deposition on the powder surface before pressing the pellet [131][132].
Films of pure Mg, covered with a thin Pd layer, have been studied for non electrochemical hydrogen storage since the late eighties [133] showing better properties than bulk material and thin films without the Pd protection. Pd cap layers were observed to play a key role as catalysts in enhancing the rate-limiting dissociation of hydrogen molecules at the sample surface, as well as in lowering the hydrogen loading and desorption temperatures significantly. However it is reported that the high temperatures used favored the formation of Mg-Si and Mg-Pd alloys at the interfaces [134].
Important for the electrode protection is the synthesis of a pinhole and defect free Pd layer, which is not an easy procedure. In the FC field many studies have been done to reduce the amount of precious metal in the electrodes, and thin films are one of the options. In the last years the use of Pd-Cu and Pd-Ag alloys has given better results also on porous substrate, working both as protective layer and as gas selective membrane [135].

A recent work on 200 nm thick Mg thin films capped with 20 nm of Pd [50] describes the mechanism of nucleation and growth of the system. Hydrogenation and dehydrogenation start at the interface with Pd, as shown in figure 3.II.2.

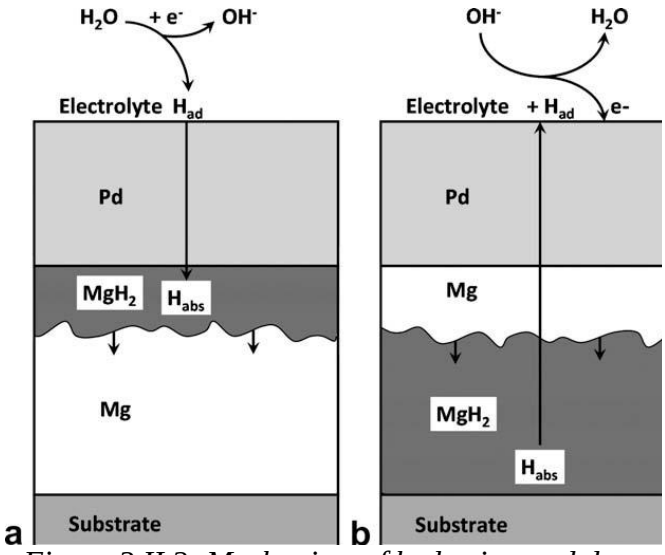

Figure 3.II.2: Mechanism of hydration and de-hydration of Mg films capped with Pd layers

The film could be charged and discharged but the currents have to be very low (0,012 mA over a 20 mm electrode, corresponding to ~0,038 µA/mm^2) otherwise, even if the film is 200 nm thin, the total capacity resulted in only 0.18 Hwt% with 0.12 mA discharge current.

In a work of 2005 Kalisvaart et al. [130] compared the electrochemical hydrogen storage properties of bulk and thin film of a MgSc alloy. While the thin films were capped with Pd layers, the powders were just made by melting the components (Mg, Sc and Pd) in the appropriate amount. The pressed powders showed similar electrochemical properties but a minor capacity (1495 instead of 1740 mAh/g), even if a lower current was used.
Works on MgTi powders from the same authors [126] with similar settings have been carried on but with not as good results as with MgSc alloy. The pressed powder electrodes showed one third of the capacity of the thin films with the same composition. It is reported that the main problem of the MgTi system lays on the stability and corrosion resistance which is very poor: the electrodes degrade in less than 10 cycles.
Different approaches have been applied to overcome the degradation of Mg based powder electrodes [124] but none of them seems to be satisfactory.
A possibility for MgTi alloys might be the addition of another element: Ni. The capacity of the system is reduced to 400-500 mAh/g (less than 2 Hwt%) but can be kept for 15 cycles [127]. This resistance is higher than the pure material but not yet enough for commercial applications.

II.2 Experiments

The active powder was synthesised at the Reactor Institute of the Delft Institute of Technology, as reported in literature [122]: MgH_2 (98% purity, from ABCR GmbH & Co. KG) and 5 mol% TiF_3 (purity >99.9%, Alfa Aesar) were milled under Ar atmosphere in a Fritsch Pulverisette 6 planetary monomill with a ball to powder ratio close to 50:1 (32×4 g balls: 2.67 g of initial weight of total powder) for a period of 60 minutes with a rotational speed of 400 rpm. A pause of 15 minutes was taken after every 15 min rotation interval.
In order to study the electrochemical hydrogen storage properties of the new MgH_2-TiF_3 system, also an electrode layout and composition had to be chosen.
Before being pressed into pellets, the sample powder was mixed with Ag or C to enhance the electric conductivity and also with Poly Tetra Fluor Ethylene (PTFE) to improve the mechanical strength of the pellets. The binder is not necessary with all materials [137] but it is with the MgH_2 and the proper amount has been found only after several trials.
At the TU Eindhoven the testing procedure consists in mixing the active material with 10 wt% Pd during ball milling and afterwards hand mix the obtained powder with Ag in 5:1 ratio. A second procedure make use of 1% carbon and 2% PTFE hand mixed with the active material before pressing the pellet. For the tests run in Delft only the second procedure was adopted in order to get rid of the precious materials and keep the composition as Pd and Ag free as possible.
A protective layer of Ni or Pd was chosen to keep the active powder away from the basic solution which, as said before, is aggressive for Mg based materials and passivate them.
Two different coating techniques have been tested: a magnetron sputtered film and a bulk thin foil applied over the pellet surface. The first method produces thin layers with good adhesion, the second is easier to apply but uses thicker layers with lower adhesion to the sample.
The thin foils with thickness 120μm have been applied over pressed pellets and glued together in the glovebox with a silver paint.
The sputtered layers have been analyzed with SEM and AFM as reported in chapter I.2 of the Experimental introductory chapter. In order to handle the pellets before and after sputtering them, Teflon rings have been set around them.
The experiments done in Eindhoven and in Delft are listed below.

<u>Three Electrodes Setup (TU Eindhoven)</u>

Sample Name	Composition and Synthesis	Current [mA/g]	Capacity [mAh/g]
Ein1	(MgH_2-TiF_3 + 10 wt% Pd) + 5:1 Ag	50	<200 mAh/g
Ein2	MgH_2-TiF_3 + 1%C + 2% PTFE + 0,5h Pd sputtered layer	50	Failed due to bubbles when in contact with the solution.
Ein3	Mg-5mol%TiF_3 + 5:1 Ag 2h Pd sputtered layer	50	Failed due to bad contact with the Ag holder
Ein4	Mg-5mol%TiF_3 + 1%C + 2% PTFE 2h Pd sputtered layer	50	

Table 3.II.1: Experiments ran in Eindhoven: Name of the sample, composition and synthesis, current density and calculated capacity.

Swagelok Setup (TU Delft)

Sample Name	Composition and Synthesis	Current [mA/g]	1st and 10th cycle Disch. Capacity [mAh/g]
GP1_1	Sealed battery from GP batteries	~57	88,67 – 42,84
Gamma_3	Comm. Anode from Gamma battery	50	115,50 – 58,84
Gamma_4	Pellet made of commercial $MmNi_5$ + 0.5%C + 0.5% PTFE	50	1,99 – 2,05
Gamma_4.1	Pellet made of commercial $MmNi_5$ + 0.5%C + 0.5% PTFE	20	151,82* - 48,32
Gamma_5	Commercial anode ($MmNi_5$ alloy on Ni grid) from Gamma battery	50	125,92 – 195,34
MgTiF3_2	Mg-5mol%TiF_3 + 1%C + 2% PTFE	50	0 - 0
MgTiF3_3	Mg-5mol%TiF_3 + 1%C + 2% PTFE	20	0 - 0
MgTiF3_4	Mg-5mol%TiF_3 + 1%C + 2% PTFE 2h Pd sputtering, Ag paint on the back	50	0 – n.d.
MgTiF3_5	Mg-5mol%TiF_3 + 1%C + 2% PTFE Ni foil on top, Ag paint on the back	1	1,68* - <0,82
MgTiF3_5.1	Mg-5mol%TiF_3 + 1%C + 2% PTFE Ni foil on top, Ag paint on the back	0.5	1,89 – 0
MgTiF3_6	Mg-5mol%TiF_3 + 1%C + 2% PTFE Ni foil on top, Ag paint on the back	1	0 – n.d
MgTiF3_7	Mg-5mol%TiF_3 + 1%C + 2% PTFE Pd foil on top, Ag paint on the back	1	0,63 – 1,63
Ni_1	99,99% pure Ni foil, same setting of sample MgTiF3_5.	< 1	0 – n.d.
Pd_1	99% pure Pd foil	50	29,92 – n.d.
Pd_2	99% pure Pd foil	20	16,91 – 12,84
Pd_3	99% pure Pd foil, same setting of sample MgTiF3_7	< 1	7,27* - 9,30

*Table 3.II.2: Experiments ran with the Swagelok cells and the Maccor battery tester setup : Name of the sample, composition and synthesis, current and calculated capacity at first and 10th cycle. Experiments with the symbol * needed some activation before reaching a good capacity value and the second cycle capacity instead of the first is reported.*

II.3 Results and Discussion

Characterization of the material

MgH_2-5mol%TiF_3 powder was synthesized different times during the research period, always with the same recipe (described before) starting materials and equipment.
For each synthesis the powders have been checked with XRD technique. To obtain desorbed material the ball milled powders have been either desorbed in a volumetric Sivert's apparatus or with a hot plate at 300°C in the glovebox for several hours. After each desorption the material has been checked again with XRD.
In figure 3.II.3 are reported as examples the XRD spectra of two samples prepared during the research period. The ball milled sample (hydride stage) mainly shows the peaks of MgH_2 and smaller features due to TiF_3.
After desorption all the hydride phase disappears and a well defined pattern due to the hexagonal phase is detected. In agreement with literature [120][136] and equation 3.1, also the peaks of MgF_3 and TiH_2 are visible.

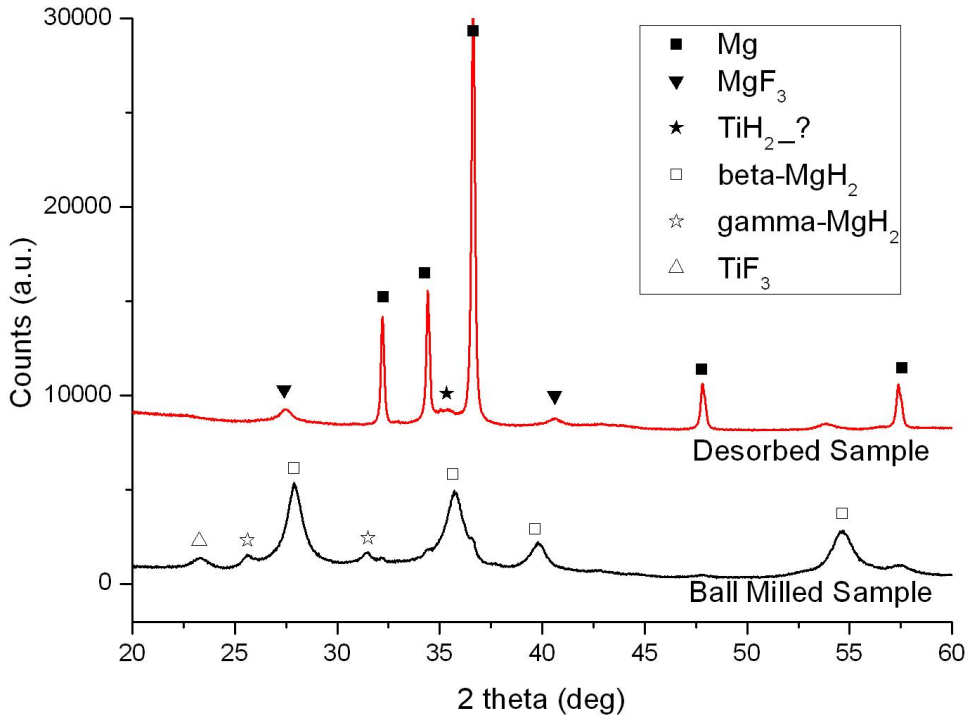

Figure 3.II.3: XRD Pattern of all the samples before (bottom) and after (top) dehydrogenation. All the peaks of the pure materials can be found after ball milling and the phases are transformed during dehydrogenation in agreement with reaction 3.10

Characterization of sputtered layers

The samples, made by pressed ball milled powder and sputtered with Pd have been observed with SEM and the thickness of the layer estimated with AFM.

Unfortunately all SEM pictures have been taken with secondary electrons and not with backscattered. Therefore only the surface morphology can be investigated but not the composition of the samples. Due to the lack of compositional contrast, it is not possible to verify if the sputtered layer is homogeneous, if it covers the entire surface and how thick it is.

As can be seen in picture 3.II.4, the Pd layer cannot be detected and distinguished from the pressed powder with this technique. It is evident how the upper face of the sample is covered not only with Palladium but also with Teflon fibers residuals.
These residuals, see picture 3.II.4 and 3.II.5, are due to the press machine used. In particular they are due to Teflon spacer discs placed above and under the powder during the pressing.

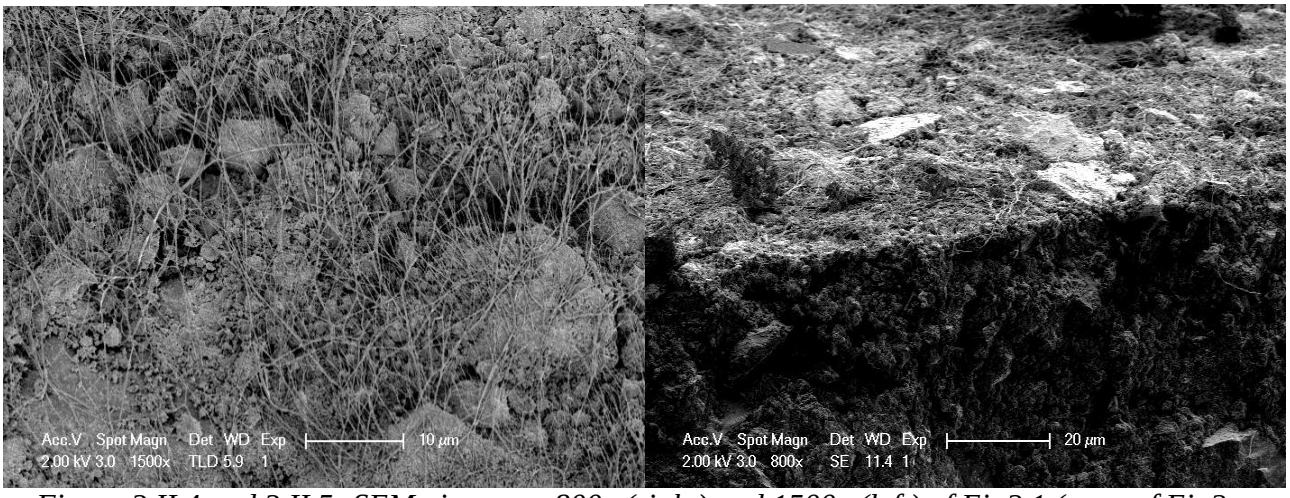

Figure 3.II.4 and 3.II.5: SEM picture at 800x (right) and 1500x (left) of Ein2.1 (copy of Ein2: MgH_2-5mol%TiF_3 sputtered for 0,5h with Pd). The particles are not well aggregated and Teflon fibers are detected on one of the faces of the pellet.

For this reason, and for the difficulties connected with the use of that press, another one has been used afterwards. The new press, even if less powerful, can be used in the glovebox and does not require the use of any Teflon liner or separating disc to operate.
The pellets obtained with the new press have been sputtered, tested and observed with SEM, see figure 3.II.8, 3.II.9, 3.II.10 and 3.II.11.
After the bad results of the test Ein2, see table 3.II.1, the deposition time has been increased to two hours.
To have a more precise idea of the deposition rate and the thickness of the produced layer, a different setup has been applied for the magnetron sputtering: during the sputtering procedure, a quartz plate has been attached on the sample holder, partially covered with adhesive tape which held it to the piece.

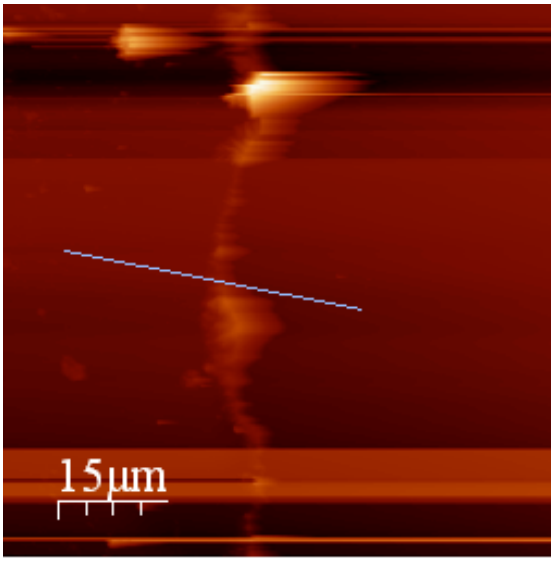

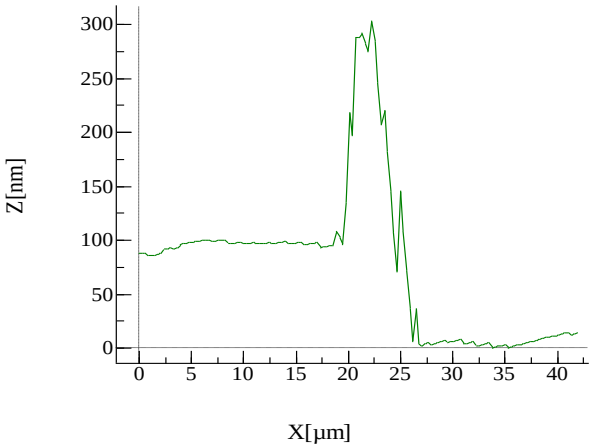

Figure 3.II.6: Map of a half sputtered quartz plate.
Figure 3.II.7: Profile along the bright line. The deposition after 2h is of ~100nm.

After the sputtering the tape has been removed and the step left between the sputtered Pd layer and the uncoated surface has been checked and mapped with AFM, see figure 3.II.6 and 3.II.7.

It can be observed that the layer, at least over the quartz piece, is uniform and after two hour of sputtering it is around 100 nm thick, resulting in a deposition rate of 50 nm/h.

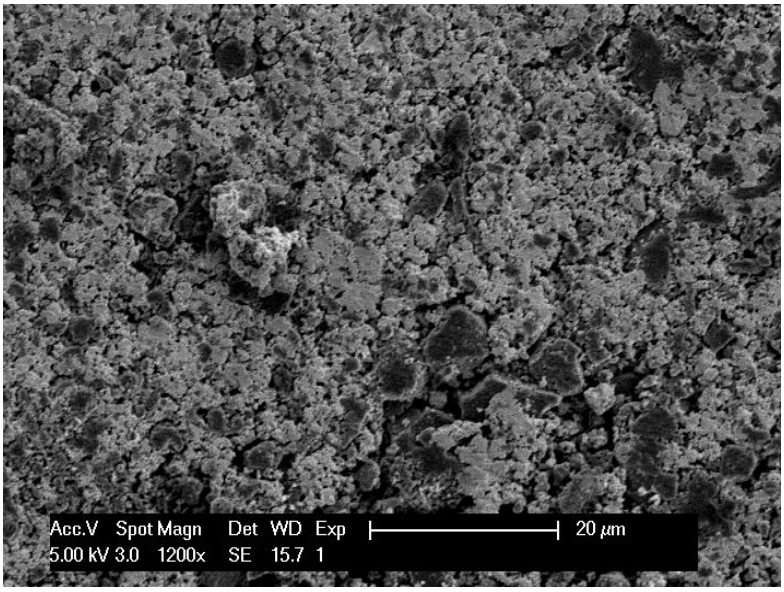

Figure 3.II.8: SEM picture at 1200x of Ein3.1 (copy of Ein3: Mg-5mol%TiF3 + 5:1 Ag, sputtered for 2h with Pd). The pellet looks homogeneous (no fibers and no segregations) and more compact than sample Ein2.1.

Also the composition of the pellets has been changed after the results of Ein2: the active material used was desorbed MgH_2-5mol%TiF_3, hereafter abbreviated with Mg-TiF_3.
Samples Ein3 and Ein4 have been sputtered with the same conditions and procedures. Together with the sample for the tests in Eindhoven, other two copies for each composition have been sputtered. The copies have been used either for Swagelok tests (MgTiF3_4) or for SEM analysis: Ein3.1 and 4.1.

From SEM pictures, but also with naked eye, it can be observed that the surface on both sides of both samples produced with the second press, is much smoother in comparison to the samples produced with the previous one.

Sample Ein3.1 (copy made for SEM of Ein3) has been made by mixing Mg-TiF_3 with silver and, even if the particles can still be distinguished one from another, the surface is flatter and PTFE residuals free, see figure 3.II.8. A thin layer of palladium is present but, as reported previously, can't be distinguished from the rest of the sample.

Sample Ein4.1 (copy made for SEM of Ein4) was analyzed in more details: the sample was observed on both faces and was broken, as has been done for Ein2.1, to have a look to the inner morphology of the pellet and to the surface from a transversal point of view.
The powders are compact also inside the pellet but domains of carbon can be seen also with necked eye on the surface, see figure 3.II.10. These spots are due to a not excellent hand mix and segregation during pressing.

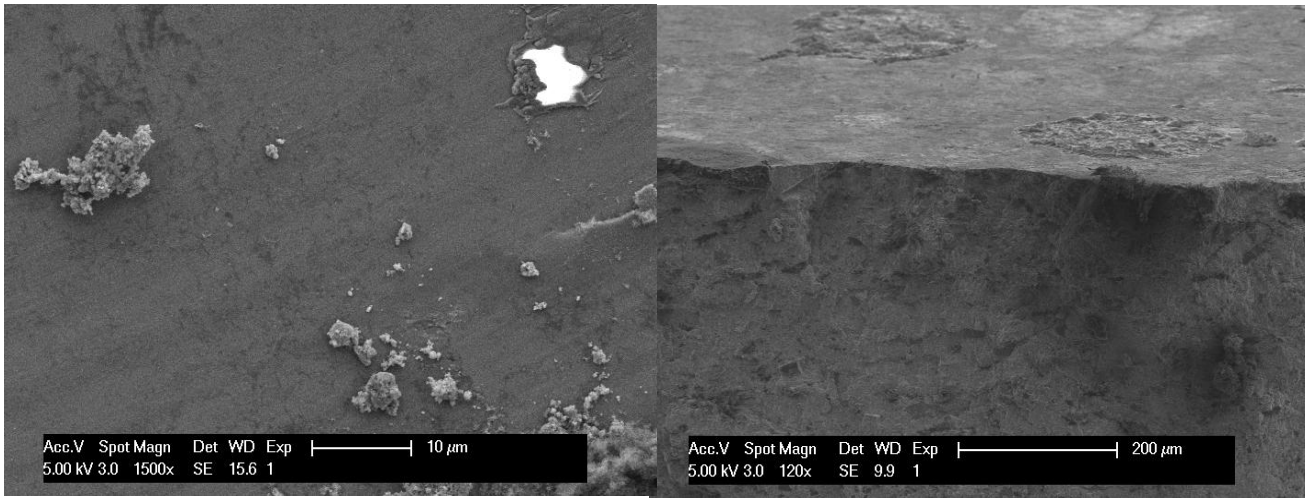

Figure 3.II.9 and 3.II.10: SEM picture at 1500x (left) and 250x (right) of Ein4.1 (copy of Ein4: Mg-5mol%TiF3 + 1%C and 2% PTFE, sputtered for 2h with Pd). The pellets are more compact and the surface flatter in comparison to Ein2, but some segregated domains of carbon can be detected on the surface even at low magnification.

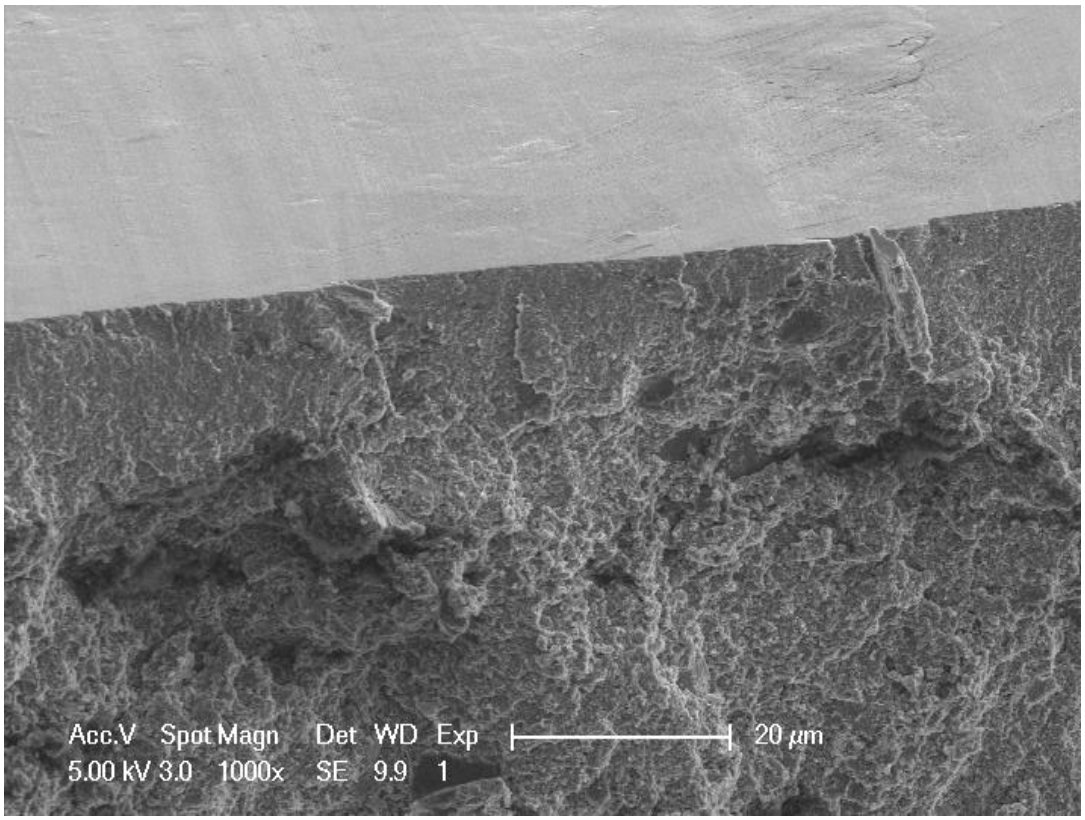

Figure 3.II.11: SEM picture at 1000x of sample Ein4.1 showing the sputtered surface and part of the inside of the pellet.

Hydrogen desorption properties - DSC

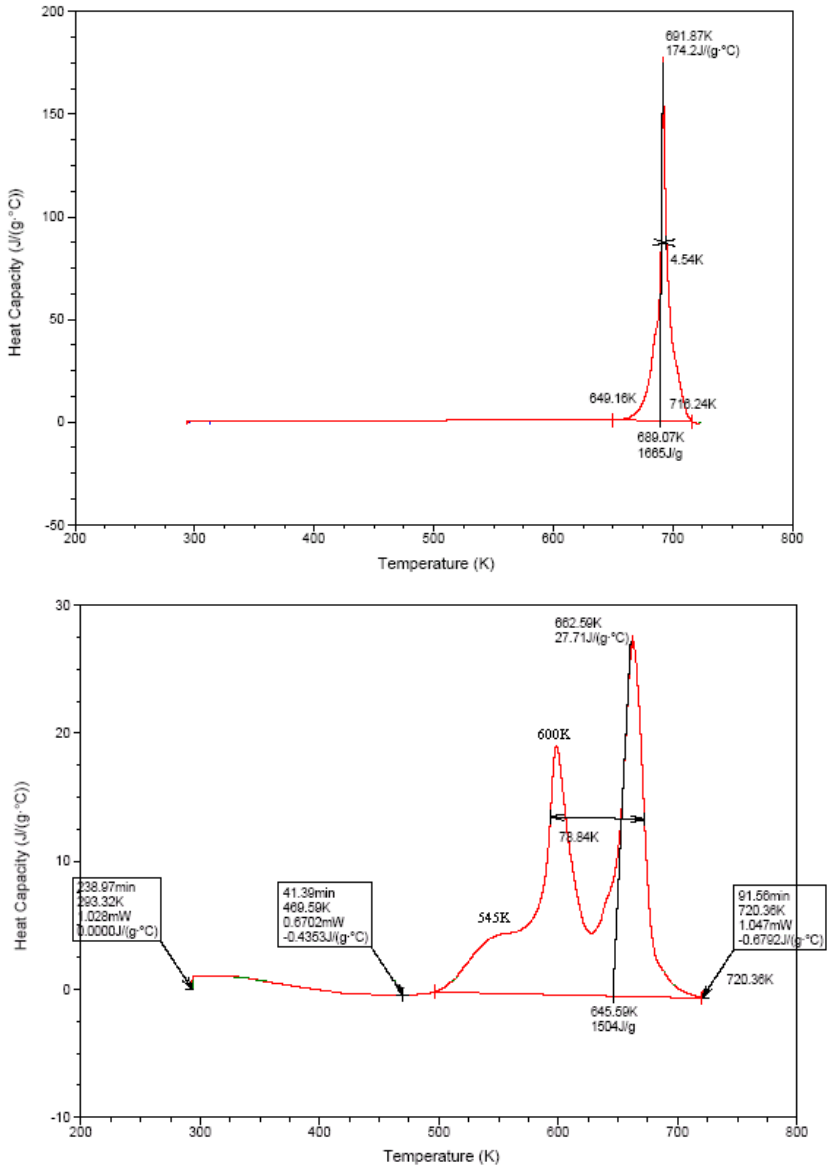

Figure 3.II.12 (top) and 3.II.13 (bottom): DSC spectra or pure MgH_2 and ball milled MgH_2-5mol%TiF_3. In the first case the decomposition takes place in one step (one peak) while if the catalyst is present a multiple step reaction is observed and, as reported in literature [136], the desorption temperature is lowered.

With Differential Scanning Calorimetriy (DSC) experiments it has been verified the improvement in hydrogen desorption properties given by the catalyst to MgH_2.
The desorption in the case of the pure magnesium hydride takes place at ~420°C, see figure 3.II.12, while, if TiF_3 is mixed during the ball milling, three peaks are present, see figure 3.II.13. From the comparison between the two graphs it can be observed that the temperature is lowered of 30°C in the case of the main peak and 90°C and 140°C if the lower peak or the low temperature bump is considered.

Three electrodes setup tests at TU Eindhoven

Thanks to the already ongoing collaboration with the University of Eindhoven (TU Eindhoven), it was possible to run some tests with a three electrodes setup of Professor Notten research group.
Unfortunately only four samples have been tested due to the lack of time and organizational problems.

The first sample, Ein1, has been synthesized according to the procedure normally used at the TU Eindhoven: mixing the material with 10 wt% of Pd and then the resulting powder with Ag in 5:1 ratio.
The cycling of the pellet brought to results very similar to the ones seen with the Swagelok tests, see figure 3.II.14 and 3.II.18. With a 250 mA/g current the curve in the V vs t plot is just a floating value that testify the impossibility to load and discharge the electrode.

While the results of cycling have been unsatisfactory, the ones coming with small (according to the group and setup standards) current (50 and 10 mA/g) are more interesting.
The sample has been charged for five hours with a time limited charging procedure. In the case of a three electrodes setup the decomposition of the electrolyte, which takes place after the first plateau, see figure 3.II.15, is not a problematic issue as it is with Swagelok testers as will be explained afterwards.
The pellet could be charged for nominally 2,78 Hwt% but discharged of only part of this capacity: 252,5 mAh that correspond to 0,96 Hwt%. Moreover part of this capacity is probably coming from the Pd mixed with the Mg based material, for at least an amount of approximately 0,1 Hwt%, reducing this way the capacity to ~0,86 Hwt%.

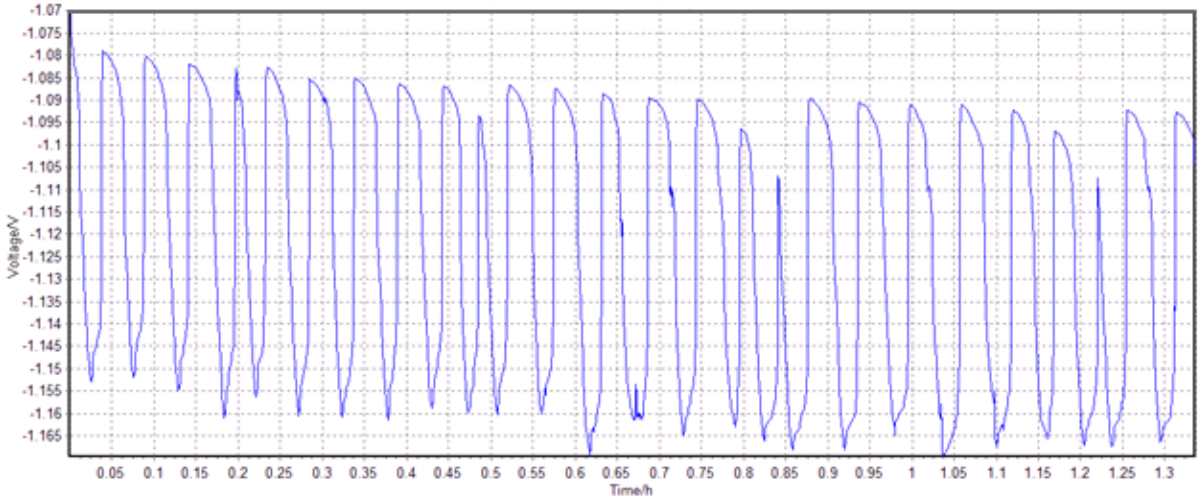

Figure 3.II.14: Charge-discharge curve with constant current of sample Ein1 taken with the three electrodes setup in at the TU Eindhoven

As already explained, after the preliminary test a sandwich-like pellet, Ein2, has been synthesized and sent to Eindhoven to be tested. The pellet has been prepared according to a more precious materials free procedure, avoiding the mix with Ag in 5:1 ratio and limiting the Pd to only a thin sputtered layer over one of the faces.
Unfortunately the pellet made with this procedure was impossible to test because it reacted instantaneously with the solution producing bubbles.

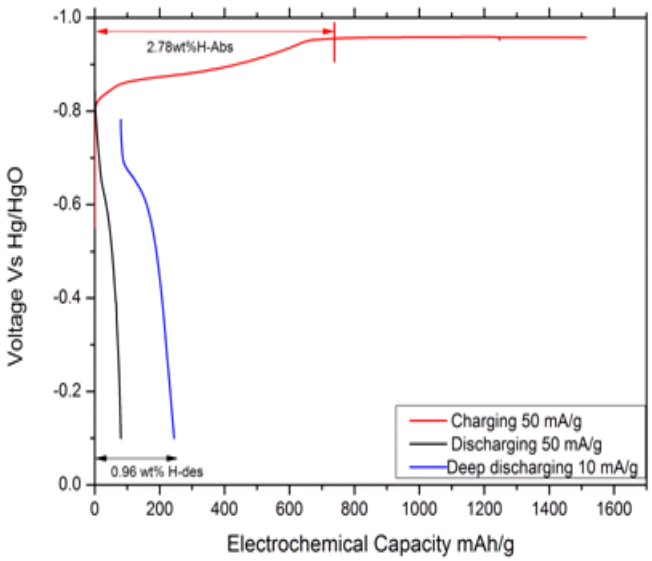

Figure 3.II.15: Charge, discharge and deep discharge curves of sample Ein1.

It was decided then to increase the deposition time with the sputtering to two hours, sample Ein4 and to try a composition similar to the one used for Ein1, with 5:1 ratio of Ag, sample Ein3.
This time a connection problem with the silver rod current collector ruined the experiments.

Swagelok tests- The New Procedure Setup

In order to test the new anodic material with the Maccor apparatus, a new procedure had to be implemented. Before this experimental campaign started the FAME research group had focus only on "direct" hydrogen storage and Li-ion batteries, therefore the knowhow and a valid procedure to test electrochemical hydrogen storage were missing.
As shown in the introduction, figure 1.II.2, several commercial batteries have been disassembled both inside and outside the glovebox. Thanks to this not only a better understand of the state of art has been achieved, but also the commercial materials have been spared to be used for testing.
From the experience gained studying and disassembling commercial batteries it can be said that the average AA anode is a 115 cm^2 area (considering one face only) Ni grid pasted with $MmNi_5$ with a capacity of ~310 mAh/g. A safe charge of 16h requires ~1.7 mA/cm^2 (data from GP Recyko Ni-MH batteries), considering the calculations of Notten [138]. This corresponds to ~23 mA/g.
Experimental tests with Ni-MH batteries materials normally make use of higher currents, in the order of 50-100 mA/g or more, especially if three electrodes layouts are used [130]. Still it was observed that, with only ~57 mA/g current and a safety cut off voltage at 1,45V for charge and 0,6V for discharge, the capacity of a commercial battery, see experiment GP1, decreases cycle after cycle, and after 10 cycles only half of it is left. See figure 3.II.17.
A Ni-MH battery has been disassembled and the cathodic and anodic materials have been reassembled in a Swagelok battery setup using a quartz wool separator imbibed with 6M KOH aqueous solution as electrolyte, experiment Gamma3.
With the same experimental program (current density and voltage cut offs) the results obtained are comparable both in terms of potentials and in terms of capacity. See figure 3.II.17 and 3.II.18.

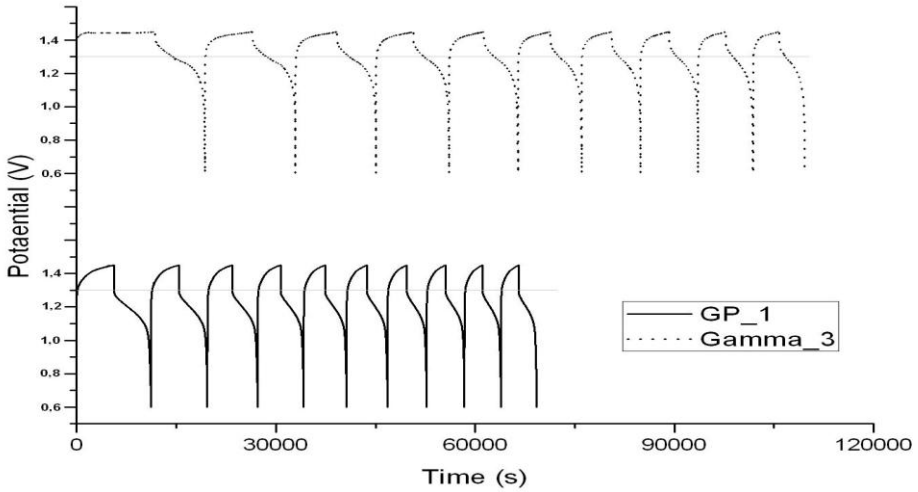

Figure 3.II.16: Charge-Discharge at constant current of a sealed commercial battery (GP1) and a Swagelok cell assembled with the commercial materials (Gamma3). The lower plateau, highlighted with a grey line at 1,3V, and the shorter cycles testify that the current used for the sealed battery (~57 mA/g) is far too high, as can also be seen in the cycling, figure 3.II.17.

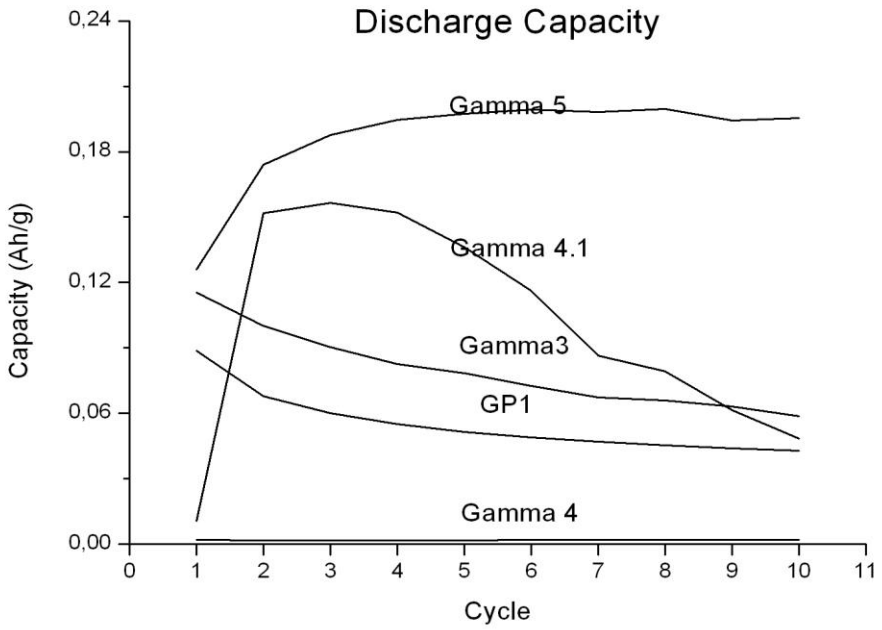

Figure 3.II.17: discharge capacities of GP1, sealed battery; Gamma3, commercial materials reassembled in a Swagelok cell; Gamma 4, pellet of MmNi5 + 2% carbon; Gamma 4.1, same pellet of the previous experiment but current lowered from 50 to 20 mA/g; Gamma 5, commercial materials and same current of Gamma3 (50mA/g) but time limited charge instead of voltage cut off.

Second step in the implementation of the new procedure has been the production of pellets based on the commercial anodic material ($MmNi_5$) mixed with carbon and PTFE and the testing of different current densities (Gamma_4 and Gamma_4.1).
After this change a different experimental program has been tested: charge limited by time and not by a voltage cut off (Gamma_5).

It is interesting to observe that, figure 3.II.17, the use of high current (50 mA/g) on a pellet mainly made of active material brings to unsatisfying results, while the imposition of lower currents (20 mA/g) leads to good experimental results, see Gamma4 and Gamma4.1.
Experiments with time limited charge have shown good results on the "activation" of the batteries: some of the assembled Swagelok cells needed one or two cycles before reaching the real value of capacity, see MgTiF_5 (figure 3.II.23), Gamma_5 (figure 3.II.17) or Pd_3 (3.II.22). Still, this technique has a drawback: during charge the potential raise and the electrolyte decomposes leading to a decrease of the capacity with cycling, see MgTiF_5 and MgTiF_7 (figure 3.II.22).

After few preliminary experiments, the assembling procedure has been set, and consists in the following steps:

- The central body of the Swagelok and one of the pistons (see figure 2.IV.5*)* are brought inside the glovebox.
- The anode, which for the tests described in this thesis is always the sample to investigate, and two dried quartz wool separators are put in position inside the chamber of the Swagelok.
- The first assembled part is then brought outside from the glovebox and directly to the fume hood. There the separator is wetted with three drops of alkaline solution using a pipette.
- After the solution has been poured in the chamber of the central body, a piece of commercial cathodic material is placed in contact with the separators and the Swagelok is closed with the second piston and sealed with the last nut.
- The sealed Swagelok is then wrapped with a Parafilm layer to prevent the possibility of leaking of the basic solution and to avoid further contamination with open air.
- The Swagelok is then ready for the experiment and can be connected with the Maccor apparatus

The described results gave confidence to start experiments on MgH_2-5mol%TiF_3 and to test, in parallel, other materials like the Ni and Pd foils after used as protective layers for the pellets. In all the cases the method showed to be reliable as will be explained in the following paragraph.

Also a three electrodes setup has been implemented during the researching period trying to emulate the setup used in Eindhoven, see figure 2.IV.4. Unfortunately the lack of time and of know how stopped the project at the preliminary tests.

Swagelok tests-Results with Mg based electrodes

Pellets made of desorbed MgH_2-TiF_3 +1%C +2%PTFE coupled with commercial cathodes have been tested with different current densities and the hydroxidation (oxidation to the hydroxide stage), according to the Pourbaix diagram [123], lead to the impossibility of draining any capacity out of the samples. The capacity registered during the charge is nothing but the decomposition of the electrolyte and the discharge curves are sharp vertical lines, see MgTiF3_3 figure 3.II.18.

Palladium foils can be cycled for more than 20 cycles with different current densities, obtaining plateaus both during charge and during discharge. Even for a good conductor and a well known hydrogen storage material as palladium, the capacities obtained with high current densities are not the ones predicted in literature. Moreover only with very low currents, Pd_3, the charge and discharge capacities are similar.
Surprisingly the ΔV between the charge and discharge plateaus is very broad, ~1,1 V and 0,8 V with 50 and 20 mA/g respectively (Pd_1 and Pd_2), but decreases with the current density to ~0,2V with 1mA/g, Pd_3. See figure 3.II.19, 3.II.20 and 3.II.22

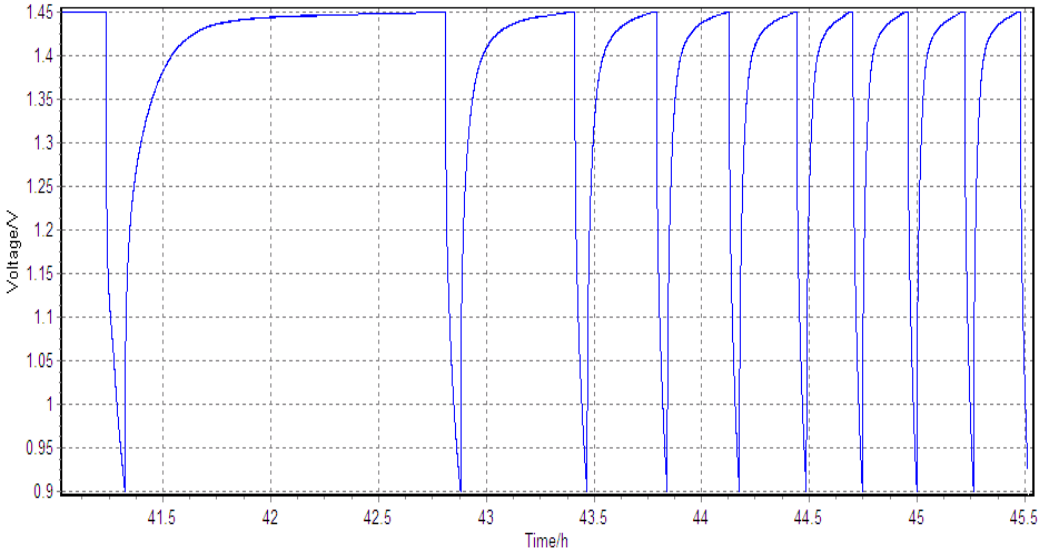

Figure 3.II.18: Charge-discharge curve at constant current of sample MgTiF3_3 (MgH_2-TiF_3 +1%C +2%PTFE). The discharge voltage is an almost vertical line and the discharge capacity is zero.

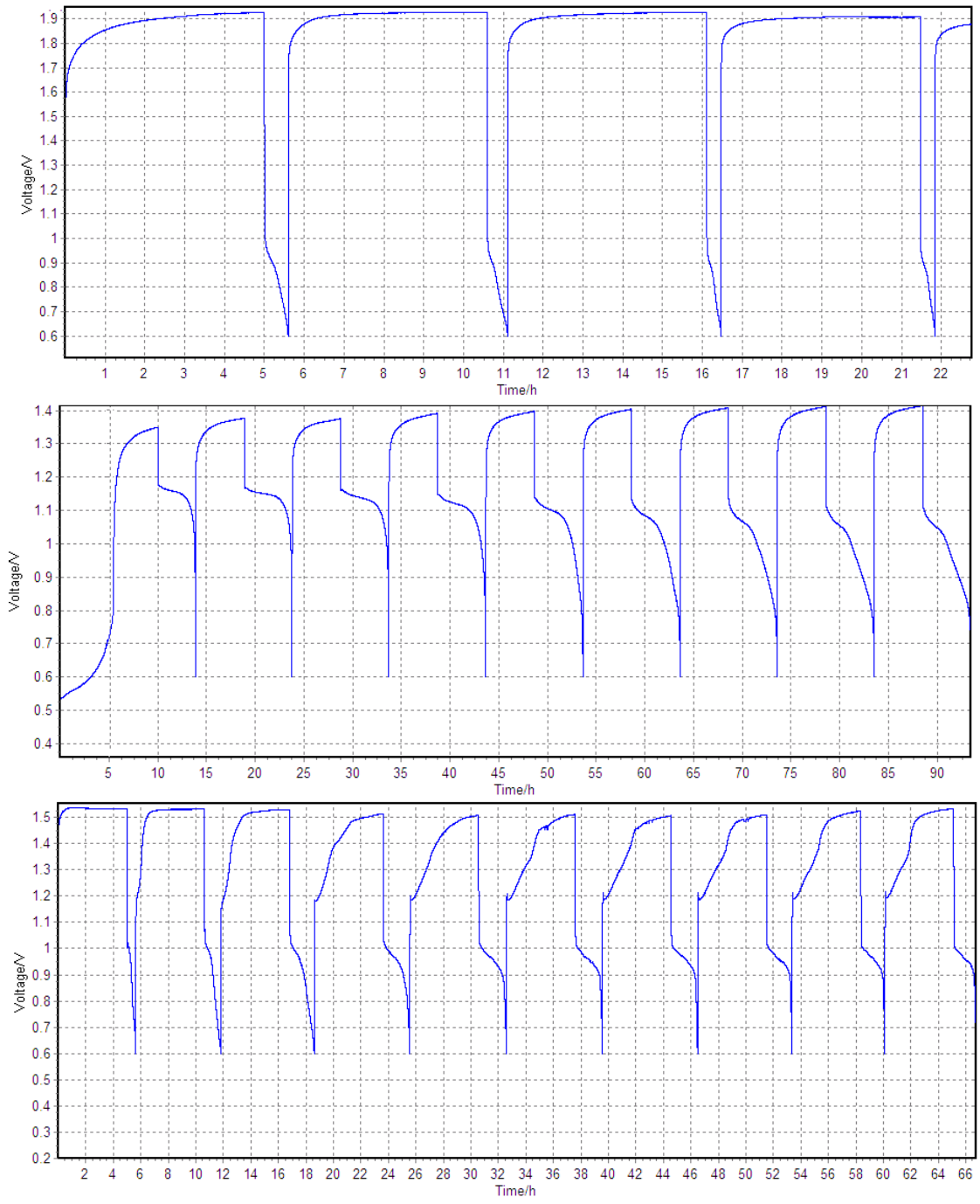

Figure 3.II.19 (top): Charge-Discharge at constant current of a Pd foil, using high current density (20mA/g), experiment Pd_2.
Figure 3.II.20 (centre): Charge-Discharge at constant current of a Pd foil with low current density (<1mA/g), experiment Pd_3.
Figure 3.II.21 (bottom): Charge-Discharge at constant current of MgTiF3_7. It's evident an activation process during the first cycles and then three peculiar features: an early bump, a first steep plateau and last the sharper plateau already seen for the Pd alone, figures above.

When the same Pd foil used for the previous experiments is used as layer over a Mg-TiF_3 pellet the capacity drops to one third, see figure 3.II.22, but the shape of the V vs t (potential versus time) plot, figure 3.II.20 and 3.II.21, varies as well. It shows, after two cycles of activation, three regions: an early bump, a first steep plateau and last the sharper plateau already seen for the Pd alone.
The capacity drop is probably linked to the not yet optimized sandwich structure since it is not possible to have lost the capacity of the palladium foil just by placing the pellet next to it.
Another possibility can be a variation in performance linked to the also not yet perfect Ni-MH testing procedure.
Nevertheless the difference in shapes of the voltage curves leads to assume that the pellet was charged and discharged and therefore that the protection given by the Pd layer was effective.

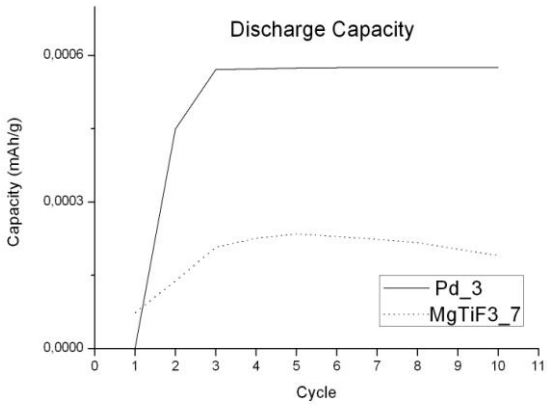

Figure 3.II.22: Capacities of samples Pd_3 and MgTiF3_7. The presence of the pellet decreases the capacity taken with the same current of the Pd foil alone.

Nickel foils show a different behavior in comparison to palladium foils: Ni is not a good hydrogen storage material, therefore the plots V vs t are very similar to the ones of uncoated Mg-TiF_3, see figure 3.II.24. The charge curve is a plateau at high voltages, corresponding to the decomposition of the electrolyte, and the discharge curve is just a vertical line corresponding to no capacity drainable from the sample, very similar to the one already reported for sample MgTiF3_3 in figure 3.II.18.

When a pellet of active material is covered with a Ni foil and protected with silver paint, similarly to how was done with Pd, the V vs t curves vary drastically both from the one of pure Mg-TiF_3 and from the one of the Ni foil alone. See figure 3.II.24 and 3.II.25.
The sandwich-like composite created put together the corrosion resistance nickel with the hydrogen desorption properties of Mg-TiF_3. Unfortunately the capacity obtainable with the sample was not the full capacity expected from literature, but it is stable after 10 cycles and decreases, if the current density is changed, till the complete annihilation after 20 cycles.
It's interesting to notice how the presence of the Mg-TiF_3 pellet somehow decreases the capacity of the Pd foil alone while in the case of Ni the capacity is increased both in comparison to unprotected Mg and to the Ni foil alone.
Similarly to what has been observed in the V vs t of sample MgTiF3_7, three regions can be observed: bump, first plateau (more horizontal in this case) and second plateau at high voltage, see figure3.II.21 and 3.II.25.

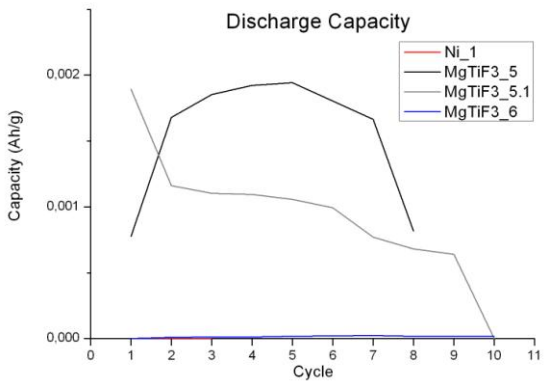

Figure 3.II.23: Capacities of samples Ni_1, MgTiF3_5,5.1 and 6. The Ni layer protects the pellet allowing to measure a discharge capacity for more than 10 cycles.

The limited capacity is probably due to the assembly of the composite: the contact between Ni layer and pellet is not optimized and the silver paint used as glue on the sides and back face, could have cracks and discontinuities that made the insulation from the solution not perfect. In fact the very same procedure has been repeated to prepare experiment MgTiF3_6 with all the materials coming from the same batches and suppliers of experiment MgTiF_5.
The pellet obtained in this case however was impossible to charge and discharge demonstrating that the material itself, if the Ni layer does not work, even under low current density (1mA/g of active material), cannot be cycled.

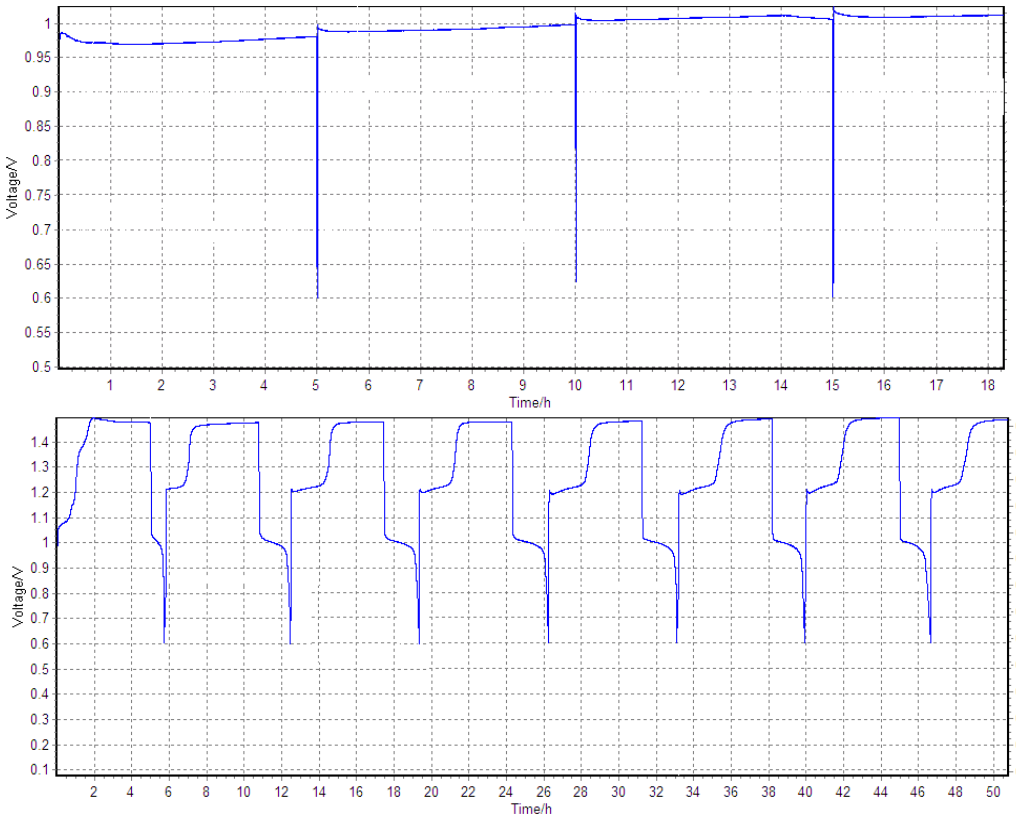

Figure 3.II.24 (top): Charge-Discharge at constant current of a Ni foil. The curves are similar to the ones observed with pure Mg-TiF_3, figure 3.II.18.
Figure 3.II.25 (bottom): Charge-Discharge at constant current of MgTiF3_5. It's evident an activation process during the first cycles and then three peculiar features: an early bump, a first steep plateau and last the sharper plateau already seen for the Pd alone.

II.4 Conclusions

In conclusion a new procedure based on the already implemented one for Li-ion batteries has been defined in order to test Ni-MH batteries with the Maccor apparatus. The technique has still to be further optimized but gives already good and reliable results both with commercial and classic materials, as $MmNi_5$ Ni and Pd, and with innovative materials like Mg-TiF_3.

MgH_2 with 5 mol% of TiF_3 was synthesized and checked with XRD and DSC and compared with pure MgH_2. It is evident how the addition of the fluoride decreases the desorption temperature of 30°C in the case of the main peak, and of 90°C and 140°C if the lower peak or the low temperature bump are considered.

A new sandwich-like composite electrode has been designed and prepared. The layer has been applied over the pressed powder pellet with two techniques: sputtering and "gluing" a metal foil with silver paint.

Samples sputtered with Pd have been checked with SEM microscopy and the layer measured with AFM. The sputtering was done for 30 minutes or for 2 hours resulting in a deposition rate of 50 nm/h.

Tests in Eindhoven with 3 electrodes setup were mainly unsuccessful. The main reason is that a more intense experimental campaign was needed but the short period didn't allow to do it. Nevertheless it was demonstrated that the addition of Pd, even if only mixed with the powder and not used as a barrier, allow to gain some capacity out of the MgH_2-TiF_3 compound while without Pd the sample behaves like it was reported with other techniques.

The tests ran with the Maccor apparatus and the new ad-hoc procedure show that:

- The material alone does not resist the corrosive environment.
- The same material protected with Pd or Ni could resist the contact with the alkaline solution.
- The electrode can be cycled different times maintaining a stable capacity either using Pd or Ni as protection.

Still the capacity is much lower than expected, about 0,1%. In the sample with Pd the presence of the pellet actually decreases the capacity previously measured with the Pd layer alone.
Moreover sometimes the sandwich pellet is not assembled properly and the electrode cannot be charged or discharge.

Meanwhile this thesis has been written, in Delft and Eindhoven several tests have be ran.

For the experiments in Eindhoven the idea is to achieve the deposition of a Pd layer thick enough to prevent the solution to get in contact with the active material, as happened with sample Ein2. Therefore pellet with 4h deposition treatment has been done.
To overcome the connection problem with the silver rod a thinner Teflon ring has been used covered with conductive silver paint.

In order to exploit further the shielding technique with Ni demonstrated and reported in this thesis, a new thin Ni foil has been bought. The Ni foil has been wrapped and sealed around a pellet made by MgH_2-5mol%TiF_3 and the pocket sandwich has been tested with a Swagelok cell.
Further developments of the experimental program will focus on the improvement of the Ni protection especially focusing on the repeatability of the results.
Afterwards a quantitative characterization will be indispensable in order to exploit the discovery and the results for a publication or a patent.

Some chosen parameters, like the Swagelok cell assembling procedure, are far from being perfect but were chosen and kept constant during the experimental campaign just to have the most reliable results possible with the smaller number of variables. The choice of three drops of solution and two separators showed not to be the best already during the work reported in this thesis and has now being corrected and improved by the colleagues of TU Delft.

Conclusions

In conclusion, thanks to the work reported in this thesis, two different aspects of an answer to energy storage can appreciated: hydrogen and hydrides in particular.

Treated mixed borohydrides have shown to be an improvement in comparison to the pure borohydrides but the temperature of desorption is still too high for applications. Moreover, with the available machines, the decomposed compounds could not be reloaded after having released the hydrogen. The emission of borane must be eliminated since the compound is poisonous both for man and for fuel cells.
Nevertheless before put these materials aside some techniques have still to be tested and some ideas might come out in the meanwhile with possible solutions.

Ni and Pd layers over MgH_2 based electrodes have shown to be effective in allowing the material to be electrochemically cycled. The detected capacity anyway is still far from the capacity of a commercial electrode and even further from the predicted capacity of the compound.
So far only technical issues seem to limit the results; therefore improvements in the assembling and testing technique are expected and should lead to interesting results if not from an industrial point of view, at least for a scientific one.

After the joined experiences in the two main aspects of hydrogen storage with hydrides, the author feels the necessity to draw a more general conclusion on this technology:

Since almost all the electrochemical hydrogen storage materials can be used as “direct” solid hydrogen storage (only few exceptions exist but this is not the place where to discuss them), and since the other way round might be true after the scientific evidences described in this work; a material that satisfy the DOE target for hydrogen storage will be the answer not only for the solid hydrogen storage itself but also for NiMH batteries.

A cyclable 6 Hwt% material will fulfill the 2015 DOE target but would also lead to at least 1,5 time (the anodic material account for the 30% of the total weight in commercial batteries) more capacity density batteries. With a similar value of capacity density NiMH batteries would gain back a big amount of market lost with Li-ion batteries.
Thus, for example: Ni-MH batteries hybrid cars ran with hydrogen as fuel stored in small MH tanks would probably be the cars of the future.

On the other hand, if this new hydride is not found, Li-ion’s, or a new technology like Na-S, batteries are going to rule the majority of the battery market. The hydrogen storage for fuel cells, if necessary, will probably be addressed mainly with compressed tanks similarly to how it is done now.

Acknowledgements

It is hard to summarize in few lines all the acknowledgements and the thanks I should give for this year of work around Europe.

My first thanks go to my formal and my informal promoters: Professor Amedeo Maddalena and Professor Giovanni Principi who started the whole mechanism that brought me first in Petten, then in Delft and finally here writing this thesis. I have to thank also Giovanni Capurso who prepared the samples for the analyses, gave me suggestions and help from Padua when I was abroad and is now writing an article on the results obtained.

A special thank goes to my action leader at the European Commission, Pietro Moretto who first gave me the enormous chance to come in Petten and then the guidance during the months of research, finding the time for me among the many commitments he has.
I would like to thank also my supervisors: Marek Bielewski, Renato Campesi and Francesco Dolci who gave me all the support I could need and were always available to answer my questions, explain how the machines work and discuss with me the results.
I would like to thank all the technicians or people responsible for the equipments who helped me trough the many problems connected with the machines during experimental works: Frederik (Frijk), Jacob (Jaap), Laars, Philippe and Ricardo.

From Delft I want to thank first Professor Ekkes Bruck who gave me the possibility of presenting my work at the Reactor Institute when I was still working for the JRC, and introduced me to professor Mulder. A special thank goes exactly to him, Professor Fokko Mulder, who was my promoter at the TU Delft and who always supported and encouraged me.
I cannot miss to express my gratitude to Anna Grzech who was always at my side and has been a wonderful team mate and a good friend during my stay in Delft. I would like to thank also all the colleagues and technicians who helped me and suggested me when I needed, among them: Anca, Gijs, Jacob Jan, Marnix, Stephan, Swapna, Walter, Xiaoyu.

Last but not least, I'd like also to thank all my family and my friends for the support they gave me and the efforts to understand what I was doing giving also their personal contributions. Not everybody can count on a family like mine and I am very proud of it. It is not easy to bear a person under thesis and it is even harder if it goes around Europe instead of staying with you, for this reason my last acknowledgment goes to Giulia who was an inestimable companion during this year of work.

References

[1] "World Population to 2300" report of the United Nations, New York 2004.
[2] "Which way to energy utopia?", Mark Schrope *Nature 414, 682-684(Dec. 2001)*
[3] "Peak oil production may already be here" Richard A. Kerr, *Nature 331, 2011*
[4] "Is 'Peak Oil' Behind Us?" J.C. Rudolf , The New York's Time, *Nov 14, 2010.*
[5] "BP statistical review of World Energy, June 2009" BP publication.
[6] "Acceleration of global warming due to carbon-cycle feedbacks in a coupled climate model" P. M. Cox, R. Betts, C. Jones, S. Spall & IJ. Totterdell, *Nature 408, 184-187 (9 Nov 2000)*
[7] "EU promises 20% reduction in carbon emissions by 2020" Ian Traynor and David Gow *The Guardian, 21 Feb 2007*
[8] "US oil spill: 'Bad management' led to BP disaster" Mark Mardell et al. *BBC 6 Jan 2011*
[9] "Ammonia and related chemicals as potential indirect hydrogen storage materials" Rong Lan , John T.S. Irvine, Shanwen Tao, *Int. Jour.Hydrogen Energy 37 (2012) 1482–1494*
[10] "Conversion materials for hydrogen storage and electrochemical applications—Concepts and similarities" Maximilian Fichtner, *Journal of Alloys and Compounds Vol 509, Supplement 2, Sep 2011, S529–S534*
[11] "Hydrogen production comes naturally to ocean microbe" K.Sanderson *Nature News Dec 2010*
[12] "A metal-free polymeric photocatalyst for hydrogen production from water under visible light" X.Wang et al. *Nature Materials Vol 8 Jan 2009.*
[13] "Photocatalyst releasing hydrogen from water" Lu et al. *Nature, brief communications, vol 440 March 2006*
[14] "A realizable Renewable Energy Future" J.Turner *Science Vol 285 Jul 1999*
[15] "World History of the Automobile" E. Eckermann, 2001 Warrendale, PA: Society of Automotive Engineers.
[16] "The wind/hydrogen demonstration system at Utsira in Norway: Evaluation of system performance using operational data and updated hydrogen energy system modeling tools" Øystein Ulleberg, Torgeir Nakken, Arnaud Ete, *Int. Jour. of Hydrogen Energy35 (2010) 1841-1852*
[17] "Fuel cell vehicles: Status 2007" Rittmar von Helmolt and Ulrich Eberle, *Journal of Power Sources Vol 165, Issue 2, 2007, 833–843*
[18] "Hydrogen vehicles: Fuel of the future?" Jeff Tollefson, *Nature 464, 1262-1264 (2010)*
[19] "Is the Hydrogen Car of the Future Running on Empty?" Steven Ashley, *Scientific American, Oct. 2008*
[20] "The hydrogen blacklash" Robert F. Service, *Science Vol 304 Aug 2004*.
[21] "Hydrogen –fuelled vehicles" L. Schlapbach, *Nature Vol 460 Aug 2009*
[22] "Hydrogen-storage materials for mobile applications" Louis Schlapbach & Andreas Züttel, *Nature 414, 353-358 (2001)*
[23] "The problem of solid state hydrogen storage" G. Principi, F. Agresti, A. Maddalena, S. Lo Russo Energy 34 (2009) 2087-91.
[24] " The U.S. Department of Energy's National Hydrogen Storage Project: Progress towards meeting hydrogen-powered vehicle requirements" Sunita Satyapal et al., *Catalysis Today 120 (2007) 246–256*
[25] "Onboard storage of hydrogen" P. Mazabraud and I. Moysan, *The hydrogen pathway CLEFS no 50/51 Winter 2004-2005.*
[26] "Solid-state hydrogen storage for mobile applications: Quo vadis?" C. Weidenthaler and M. Felderhoff *Energy Environ. Sci., 2011, 4, 2495-2502*
[27] "Hydrogen storage methods" Andreas Z ttel, *Naturwissenschaften (2004) 91:157–172*
[28] "A 70 MPa hydrogen compression system using metal hydrides" X.Wang, H. Liu, H.Li Int. Jour. Of Hydrogen Energy 36 (2011) 9079-9085
[29] "Recent challenges of hydrogen storage technologies for fuel cell vehicles" D. Mori, K. Hirose, *International Journal of Hydrogen Energy 34-10 (2009) Pages 4569-4574*
[30] "On-board and Off-board performance of hydrogen storage options for light-duty vehicles" R.K. Ahluwalia, T.Q. Hua, J.K. Peng, *Int. Jour. of Hydrogen Energy 37 (2012) 2891-2910*
[31] "Metal hydride materials for solid hydrogen storage: Areview" B. Sakintuna, F. Darkrimb, M. Hirscher, Int. *Jour. of Hydrogen Energy 32 (2007) 1121 – 1140*
[32] "Hydrogen Storage Materials" Shashikala, *Functional Materials 2012, 607-637.*

[33] "Performance of an AB_2 alloy in sealed Ni–MH batteries for electric vehicles: quantification of corrosion rate and consequences on the battery performance" B Knosp, L Vallet, Ph Blanchard, *Journal of Alloys and Compounds 293–295 (1999) 770–774*
[34] "Boron- and nitrogen-based chemical hydrogen storage Materials", Tetsuo Umegaki et al, International Journal of Hydrogen Energy 34 (2009) 2303–2311
[35] "Automotive storage of hydrogen in alane" R.K. Ahluwalia, T.Q. Hua and J.K. Peng, *Int.Jour.Hydrogen Energy 34 (2009) 7731-7740*
[36] "Experimental results of an air-cooled lab-scale H_2 storage tank" I. Utz, N. Schmidt, A. Worner, J.J. Hu, O. Zabara, M. Fichtner, *Int. Jour. of Hydrogen Energy 36 2011, 3556-3565*
[37] "Thermal coupling of a high temperature PEM fuel cell with a complex hydride tank" P. Pfeifer et al., *Int. Jour. Hydrogen Energy Vol 34, 8 (2009) 3457–3466*
[38] Stetson, DoE, *Annual Merit Review 2010*
[39] "Building better batteries" M. Armand & J.-M. Tarascon, *Nature 451, 652-657 (2008)*
[40] "Development of Mg-containing MmNi5-based alloys for low-cost and high-power Ni–MH battery" Tetsuya Ozaki et al, *Journal of Alloys and Compounds 408–412 (2006) 294–300*
[41] "Electrochemical Hydrogen Storage Characteristics of Thin Film MgX (X=Sc, Ti, V, Cr) Compounds", R. A. H. Niessen and P. H. L. Notten, Electrochem. *Solid-State Lett., Vol 8, Issue 10, A534-A538 (2005)*
[42] "Recent advances in rechargeable battery materials: a chemist's perspective" M. Rosa Palacín, *Chem. Soc. Rev., 2009, 38, 2565-2575*
[43] "Fundamentals of Analitical Chemistry" D. A. Skoog et al., VIII ed, Brooks Cole 2004
[44] "Hydrogen Sorption Measurements on potential storage materials" D. P. Broom. Experimental Methods and Measurement Accuracy, *JRC Scientific and Technical Reports EUR 23242 EN – 2008*
[45] "Variation of peak temperature with heating rate in differential thermal analysis" H.Kissinger, *Anal. Chem., 29, 1702 (1957).*
[46] "Determination of Activation Energies of Chemical Reactions by Differential Thermal Analysis" G. O. Piloyan, I. D. Ryabchikov & O. S. Novikaova *Nature 212, 1229 (Dec 1966)*
[47] "Low-temperature hydrogen desorption and the structural properties of spark discharge generated Mg nanoparticles" V.A. Vons et al., *Acta Materialia Volume 59, Issue 8, May 2011, Pages 3070-3080*
[48] "Techniques for characterization of hydrogen absorption/desorption in metal hydride alloys", S.Bliznakov et al. *Int. workshop "Advanced Techniques for Energy Sources Investigation and Testing" Sept 2004, Sofia (Bulgaria)*
[49] "Relationship Between Equilibrium Hydrogen Pressure and Exchange Current for the Hydrogen Electrode-Reaction at Mmni(3.9-X)Mn(0.4)A1(X)Co(0.7) Alloy Electrodes" H. Senoh, K. Morimoto, H. Inoue, C. Iwakura and P.H.L. Notten, *Journal of the Electrochemical Society, Vol. 147(2000), No. 7, 2451-2455*
[50] "Thermodynamics and kinetics of the thin film magnesium–hydrogen system", P. Vermeulen, A. Ledovskikh, D. Danilov, P.H.L. Notten, *Acta Materialia 57 (2009) 4967–4973*.
[51] "Oxygen Evolution and Recombination Kinetics Inside Sealed Rechargeable, Ni-Based Batteries" P. H. L. Notten, E. Verbitskiy, W. S. Kruijt and H. J. Bergveld , *Journal of the Electrochemical Society, Vol 152, Issue 7, A1423-A1433 (2005)*
[52] "Dehydriding and rehydriding reactions of LiBH4"; S. Orimoa, Y. Nakamoria, G. Kitaharaa, K. Miwab, N. Ohbab, S. Towatab, A. Zuttel, *Journal of Alloys and Compounds Volumes 404-406, (2005) , Pages 427-43*
[53] "Metallo Borohydrides. Lithium Borohydride**"** H.J. Schlesinger and H.C. Brown. *J. Am. Chem. Soc. 62 (1940), 3429–3435*
[54] E.M. Fedneva, V.L. Alpatova and V.I. Mikheeva, *Russ. J. Inorg. Chem.* 9 (1964), p. 826.
[55] "Hydrogen storage properties of $LiBH_4$", A. Zuttel, et al, *Journal of Alloys and Compounds Vol. 356-357, (2003), 515-520.*
[56] "Production of hydrogen" Muller, A.; Havre, L.; Mathey, F.; Petit, V. I.; Bensoam, J. *U.S.Patent 4,193,978, 1980*
[57] "Reversibility of the hydrogen desorption from $LiBH_4$: a synergetic effect of nanoconfinement and Ni addition" Peter Ngene, M. (Rien) van Zwienen and Petra E. de Jongh, *Chem. Commun, 2010, 46, 8201-8203*
[58] "Reversible Storage of Hydrogen in Destabilized LiBH" John J. Vajo et al *J. Phys. Chem. B, 2005, 109 (9), 3719–3722*
[59] "Enhanced hydrogen sorption properties in the $LiBH_4$–MgH_2 system catalysed by Ru nanoparticles supported on multiwalled carbon nanotubes" Jianfeng Maoa, Zaiping Guoa, Xuebin Yuc, Huakun Liu, *Journal of Alloys and Compounds 509 (2011) 5012–5016.*

[60] "Nanocrystalline materials for Ni–MH batteries" M Jurczyk L Smardz, A Szajek**,** *Materials Science and Engineering B108 (2004) 67–75*
[61] "Synthesis and properties of magnesium tetrahydroborate, $Mg(BH_4)_2$", Krzysztof Chłopek, Christoph Frommen, Aline Le´on, Oleg Zabara and Maximilian Fichtner, *J. Mater. Chem., 2007, 17, 3496–3503*
[62] "Some properties of magnesium borohydride" Konoplev and Bakulina, *Izvestiya akademii nauk SSSR, 1 1971 pp 159-161.*
[63] "Hydrogen storage properties of Mg[BH4]2" T. Matsunaga et al, *Journal of Alloys and Compounds 459 (2008) 583–588*
[64] "Thermal decomposition of $Mg(BH_4)_2$ under He flow and H2 pressure" Nobuko Hanada et al., *J. Mater. Chem., 2008, 18, 2611-2614*
[65] "Development of group II borohydrides as hydrogen storage materials" Ewa Rönnebro, *Current Opinion in Solid State and Materials Science 15 (2011) 44–51*
[66] "Dehydriding and rehydriding processes of well-crystallized $Mg(BH_4)_2$ accompanying with formation of intermediate compounds" H.-W. Li a, K. Kikuchi, Y. Nakamori, N. Ohba, K. Miwa, S. Towata, S. Orimo, *Acta Materialia 56 (2008) 1342–1347*
[67] "Direct hydrogenation of magnesium boride to magnesium borohydride: demonstration of >11 weight percent reversible hydrogen storage" Godwin Severa, Ewa Ronnebrow and Craig M. Jensen, *Chem. Commun., 2010, 46, 421–423 421*
[68] "Reaction of hydrogen with alloys of magnesium and nickel and the formation of Mg2NiH4" Reilly Wiswall, *Inorganic Chemistry, 6, 1967, pg. 2220*
[69] "Hydrogen storage in destabilized chemical systems", John J.Vajo and Gregory L.Olson, *Scripta Materialia 56 (2007) 829–834*
[70] "A new dehydrogenation mechanism for reversible multicomponent borohydride systems—The role of Li–Mg alloys" X.B. Yu, D.M. Grant, G.S. Walker, *Chem. Commun. (2006) 3906–3908.*
[71] "Phase Boundaries and Reversibility of LiBH4 MgH2 Hydrogen Storage Material" *J. Phys. Chem. C 111 (2007), 12881–12885.*
[72] "A Reversible Nanoconfined Chemical Reaction" Thomas K. Nielsenet al. *ACS Nano, 2010, 4 (7), 3903–3908*
[73] "Hydrogen storage performance of $LiBH_4$-1/2MgH_2 composites improved by Ce-based additives" Bin Hong Liu, Bang Jie Zhang, Ying Jiang. *Int. Jour. of Hydrogen Energy 36 (2011), 5418-5424*
[74] "Correlation between thermodynamical stabilities of metal borohydrides and cation electronegativites: First-principles calculations and experiments" Yuko Nakamori et al, *Physical Review B 74, 045126 (2006)*
[75] "Materials designing of metal borohydrides: Viewpoints from thermodynamical stabilities" H.-W. Li, S. Orimo, Y. Nakamori, K. Miwa, N. Ohba, S. Towata, A. Zuttel, *Journal of Alloys and Compounds 446–447 (2007) 315–318*
[76] "LiBH4 Mg(BH4)2 A Physical Mixture of Metal Borohydrides as hydrogen storage material" Elisa Gil Bardaji` *J. Phys. Chem. C*, 2011, *115 (13), 6095–6101*
[77] "Formation and Hydrogen Storage Properties of Dual-Cation (Li, Ca) Borohydride" Zhan-Zhao Fang, Xiang-Dong Kang, Jun-Hong Luo, Ping Wang, Hai-Wen Li and Shin-ichi Orimo *J. Phys. Chem. C 2010, 114, 22736–22741*
[78] "Unexpected dehydrogenation behavior of LiBH4/Mg(BH4)2 mixture associated with with the in situ formation of dual-cation borohydride"; Z.-Z. Fang et al. *Journal of Alloys and Compounds 491 (2010) L1–L4*
[79] "A Series of Mixed-Metal Borohydrides" Dorthe Ravnsbæk, Yaroslav Filinchuk,* Yngve Cerenius, Hans J. Jakobsen, Flemming Besenbacher, Jørgen Skibsted, and Torben R. Jensen, *Angew. Chem. Int. Ed. 2009, 48, 6659 –6663*
[80] "Nanoconfined mixed Li and Mg borohydrides as materials for solid state hydrogen storage**"** Giovanni Capurso et al, *4th World Hydrogen Technologies Convention,* 2011, Glasgow, U.K.
[81] "Hydrogen Storage Materials: Present Scenarios and Future Directions". Tapas K. Mandal, *Ann. Rep. Prog. Chem., Sect. A: Inorg. Chem. 2009, 105, 21-54*
[82] "Dehydrogenation of LiBH4 Destabilized with Various Oxides", X. B. Yu, D. M. Grant, and G. S. Walker *J. Phys. Chem. C 2009, 113, 17945–17949*
[83] "Modified Lithium Borohydrides for Reversible Hydrogen Storage", Ming Au and Arthur Jurgensen, *J. Phys. Chem. B, 2006, 110 (13), 7062–7067 (20)*
[84] "Reactivity of LiBH4: In Situ Synchrotron Radiation Powder X-ray Diffraction Study" C Mosegaard et al., *J. Phys. Chem. C*, 2008, *112 (4), 1299–1303*

[85] "Effects of ball milling and additives on dehydriding behaviors of well-crystallized $Mg(BH_4)_2$**"** H.-W. Li, K. Kikuchi, Y. Nakamori, K. Miwa, S. Towata and S. Orimo**,** *Scripta Materialia, 57, (2007) 679-682.*
[86] *"*Combined Effects of Functional Cation and Anion on the Reversible Dehydrogenation of $LiBH_4$" Zhan-Zhao Fang, Xiang-Dong Kang, Zhu-Xian Yang, Gavin S. Walker and Ping Wang *J. Phys. Chem. C, 2011, 115 (23), pp 11839–11845*
[87] "Catalyzed $LiBH_4$ and MgH_2 mixture for hydrogen storage" P. Sridechprasat et al. *Int. Jour. of Hydrogen Energy 36 (2011) 1200-1205*
[88] "A comparative study of the role of additive in the MgH_2 vs. the $LiBH_4$–MgH_2 hydrogen storage system**"** A. Fernández, E. Deprez and O. Friedrichs, . *Int. Jour. of Hydrogen Energy 36, 6, 2011*
[89] "Nanosizing and nanoconfinement: new strategies towards meeting hydrogen storage goals". de Jongh PE, Adelhelm P., *ChemSusChem. 2010 Dec 17;3(12):1332-48.*
[90] "Room-temperature hydrogen storage characteristics of ZnO nanowires" Q. Wan, C. L. Lin, X. B. Yu, and T. H. Wang, *Appl. Phys. Lett. 84, 124 (2004)*
[91] "Nanoscaffold Mediates hydrogen release and reactivity of ammonia borane" Anna Gutowska, Liyu Li, Yongsoon , Chongmin M. Wang, *Angew. Chem. Int. Ed. 2005, 44*.
[92] "Keeping out the oxygen" Petra E. de Jongh, *Nature Materials10 265–266 (2011)*
[93] "Air-stable magnesium nanocomposites provide rapid and high-capacity hydrogen storage without using heavy-metal catalysts" Ki-Joon Jeon, Hoi Ri Moon, Anne M. Ruminski, Bin Jiang, Christian Kisielowski, Rizia Bardhan and Jeffrey J. Urban, *Nature Materials 2011*.
[94] "Improvement of dehydrogenation kinetics of LiBH4 dispersed on modified multi-walled carbon nanotubes" F. Agresti,A. Khandelwal, G. Capurso, S. Lo Russo, A. Maddalena, G. Principi, *Nanotechnology 21 (2010) 065707*.
[95] "Enhanced Hydrogen Storage Kinetics of LiBH4 in Nanoporous Carbon Scaffolds" A. F. Gross, J. J. Vajo, S. L. Van Atta, G. L. Olson, *J. Phys. Chem. C 2008,112, 5651 – 5657*.
[96] "Systematic Pore size effects of nanoconfinement of $LiBH_4$" X.Liu et al. *Chem. Mater., 2011, 23 (5), pp 1331–1336*
[97] "Controlling the Decomposition Pathway of LiBH4 via Confinement in Highly Ordered Nanoporous Carbon". Xiangfeng Liu, David Peaslee, C. Z. Jost and E. H. Majzoub, *J Phys Chem C 114 2010 14036*
[98] "Improved hydrogen storage properties of LiBH4 by mechanical milling with various carbon additives" Zhan-Zhao Fang, Xiang-Dong Kang, Ping Wang, *Int. Jour. of Hydrogen Energy 35 (2010) 8247 – 8252*
[99] "The kinetic properties of Mg(BH4)2 infiltrated in activated carbon" Maximilian Fichtner et al. *Nanotechnology 20 204029 (2009)*
[100] "Small-angle scattering investigations of Mg-borohydride infiltrated in activated carbon" Sabrina Sartori, Kenneth D Knudsen, Zhirong Zhao-Karger, Eisa Gil Bardaij, Maximilian Fichtner and Bjørn C Hauback. *Nanotechnology 20 505702 (2009)*
[101] "Confinement of $NaAlH_4$ in Nanoporous Carbon: Impact on H_2 Release, Reversibility, and Thermodynamics" Jinbao Gao et al. *J. Phys. Chem. C, 2010, 114 (10), 4675–4682*
[102] "Facile High-Yield Synthesis of Pure, Crystalline Mg(BH4)2" Pierino Zanella, Laura Crociani, Norberto Masciocchi, and Giovanni Giunchi *Inorg. Chem., 2007, 46 (22), 9039-9041*
[103] "Structural phase transitions of Mg(BH4)2 under pressure", George L., Bardaji E.G., *J.Phys.Chem. C 2009,113, 486-492*
[104] "Magnesium Borohydride: Synthesis and Crystal Structure" Radovan Cerny, Yaroslav Filinchuk, Hans Hagemann, and Klaus Yvon, Angew. *Chem. Int. Ed. 2007, 46, 5765 –5767*
[105] "Synthetic approaches to inorganic borohydrides" Hans Hagemann and Radovan Cerny, *Dalton Trans., 2010, 39, 6006–6012*
[106] "Pressure-temperature phase diagram of LiBH4: Synchrotron x-ray diffraction experiments and theoretical analysis" V. Dmitriev et al. *Physical Review B 77, 174112 (2008)*
[107] Magnesium borohydride as a hydrogen storage material: Synthesis of unsolvated $Mg(BH_4)_2$, Grigorii L. Soloveichik et al, . *Int. Jour. of Hydrogen Energy, 34, 5, 2009, Pages 2144-2152*.
[108] "Process for the preparation of crystalline magnesium borohydride", P. Zanella, L. Crociani, G. Giunchi, *U.S. patent 2007/0286787*.
[109] "First-Principles Prediction of a Ground State Crystal Structure of Magnesium Borohydride". Ozolins et al., *Phys. Rev. Lett. 100, 135501 (2008)*
[110] "Crystal structure and stability of magnesium borohydride from first principles" Xiang-Feng Zhou, *Physical Review B 79, 212102 _2009*

[111] "Structural stability and decomposition of $Mg(BH_4)_2$ isomorphs—an ab initio free energy study" J Voss1, J S Hummelshøj, Z Łodziana and T Vegge; *J. Phys. Condens. Matter 21 (2009) 012203*
[112] "Reversibility and Improved Hydrogen Release of Magnesium Borohydride" Rebecca J. Newhouse et al., *J. Phys. Chem. C 2010, 114, 5224–5232*
[113] "First-principles prediction of thermodynamically reversible hydrogen storage reactions in the Li-Mg-Ca-B-H system", V. Ozolins, *J. Am. Chem. Soc., 2009, 131 (1), pp 230–237.*
[114] "Destabilisation of magnesium hydride by germanium as a new potential multicomponent hydrogen storage system" Gavin S. Walker, Marwa Abbas, David M. Grant and Chima Udeh *Chem. Commun., 2011*
[115] "Pellets of MgH2-based composites as practical material for solid state hydrogen storage" Khandelwal, F. Agresti, G. Capurso, S. Lo Russo, A. Maddalena, S. Gialanella, G. Principi, *Int. J. Hydrogen Energy 35 (2010) 3565*.
[116] "Catalytic effect of transition metals on hydrogen sorption in nanocrystalline ball milled MgH_2–Tm (Tm=Ti, V, Mn, Fe and Ni) systems" G. Liang, J. Huot, S. Boily, A. Van Neste, R. Schulz, *Journal of Alloys and Compounds 292 (1999) 247–252*
[117] "Improvement in H-sorption kinetics of MgH_2 powders by using Fe nanoparticles generated by reactive FeF_3 addition", A.R. Yavari et al., *Scripta Materialia 52 (2005) 719–724*
[118] "Study of Mg-based materials to be used in a functional solid state hydrogen reservoir for vehicular applications" A. Maddalena et al. *Int. J. Hydrogen Energy 31 (2006) 2097 – 2103*
[119] "Preliminary investigation on the catalytic mechanism of TiF3 additive in MgH2–TiF3 H-storage system" Lai-Peng Ma, Ping Wang, Xiang-Dong Kang, Hui-Ming Cheng, *Journal of Materials Research (2007), 22: 1779-1786.*
[120] "Hydrogen storage behaviors and microstructure of MF3 (M=Ti, Fe)-doped magnesium hydride" Peng Shu-ke et al., *Transactions of Nonferrous Metals Society of China Vol 20, 10, October 2010, 1879-1884*
[121] "Superior catalytic effect of TiF3 over TiCl3 in improving the hydrogen sorption kinetics of MgH2: Catalytic role of fluorine anion" L.-P. Ma, X.-D. Kang, H.-B. Dai, Y. Liang, Z.-Z. Fang, P.-J. Wang, P. Wang, H.-M. Cheng, *Acta Materialia 57 (2009) 2250–2258*
[122] Extended Solubility Limits, and Nano Grain Refinement In Ti/Zr Fluoride Catalyzed MgH2" Mulder Fokko, Singh Sarita, Bolhuis Sabine; Eijt Stephan W. H., *The Journal of Physical Chemistry*, in press.
[123] "Atlas of Electrochemical Equilibria in Aqueous Solutions", M. Pourbaix, 2nd English edition, p. 141, NACE International 1974 and CEBELCOR.
[124] "Evaluation of different approaches for improving the cycle life of MgNi-based electrodes for Ni-MH batteries", C. Rongeat et al. *Journal of Power Sources 158 (2006) 747–753*
[125] "Development of Mg-containing $MmNi_5$-based alloys for low-cost and high-power Ni–MH battery" Tetsuya Ozaki et al, *Journal of Alloys and Compounds 408–412 (2006) 294–300*
[126] "Mg–Ti based materials for electrochemical hydrogen storage" W.P. Kalisvaart, H.J. Wondergem, F. Bakker and P.H.L. Notten. *Journal of Materials Research (2007), 22: 1640-1649*
[127] "Comparative study on the structure and electrochemical hydriding properties of MgTi, Mg0.5Ni0.5Ti and MgTi0.5Ni0.5 alloys prepared by high energy ball milling" Steeve Rousselot, Daniel Guay, Lionel Roué *Journal of Power Sources 196 (2011) 1561–1568*
[128] "Hydrogen storage in thin film magnesium–scandium alloys" R.A.H. Niessen, P.H.L. Notten, *Journal of Alloys and Compounds 404–406 (2005) 457–460*
[129] "Electrochemical characteristics of Al-substituted Mg Ni As negative electrode" Xue Jianshe, Li Guoxun, Hu Yaoqin, Du Jun, Wang Chaoqun, Hu Guangyong, *Journal of Alloys and Compounds 307 (2000) 240–244*
[130] "Electrochemical hydrogen storage in MgSc alloys: A comparative study between thin films and bulk materials" W.P. Kalisvaart, R.A.H. Niessen, P.H.L. Notten, *Journal of Alloys and Compounds 417 (2006) 280–291*
[131] "Electrochemical characterization of $MmNi_5$-based alloy powder coated with palladium and nickel-palladium" Mingming Geng *Journal of Alloys and Compounds, 215* (1994) 151-153
[132] "Electrochemical characteristics of Ni-Pd-coated MmNis-based alloy powder for nickel-metal hydride batteries" Mingming Geng et al, *Journal of Alloys and Compounds 217 (1995) 90-93*
[133] "Hydrogen uptake by Pd-coated Mg: absorption-decomposition isotherms and uptake kinetics", Anatol Krozer and Bengt Kasemo**,** *J Less-common Met. 160 (1990), p. 323*.
[134] "Nanoscale structure and the hydrogenation of Pd-capped magnesium thin films prepared by plasma sputter and pulsed laser deposition" S. Singh, S.W.H. Eijt, M.W. Zandbergen, W.J. Legerstee, V.L. Svetchnikov, *Journal of Alloys and Compounds 441 (2007) 344–351*

[135] "Characterization of Pd–Cu–Ni ternary alloy membrane prepared by magnetron sputtering and Cu-reflow on porous nickel support for hydrogen separation" Shin-Kun Ryi, et al., *Separation and Purification Technology 50 (2006) 82–91*
[136] "Improving hydrogen sorption kinetics of MgH_2 by mechanical milling with TiF_3" Lai-Peng Ma, Ping Wang, Hui-Ming Cheng, *Journal of Alloys and Compounds 432 (2007) L1–L4*
[137] "Preparation and properties of no-binder electrode Ni/MH battery" Deyi Yan and Weiguo Cui, *Journal of Alloys and Compounds 293–295 (1999) 780–783*
[138] "High energy density strategies: from hydride-forming materials research to battery integration" P.H.L. Notten et al. *Journal of Power Sources 129 (2004) 45–54*

Web

[@1] http://www.columbia.edu/~mhs119/Emissions/Emis_moreFigs/
[@2] http://www.bp.com/sectiongenericarticle800.do?categoryId=9037716&contentId=7069274
[@3] http://www.youtube.com/watch?v=ow1w33VAPII&feature=fvw
[@4] http://www.nature.com/news/specials/japanquake/index.html
[@5] http://ec.europa.eu/europe2020/priorities/sustainable-growth/index_it.htm
[@6] http://www.chimica.unipd.it/lab_DiNoto/
[@7] http://www.hydrogencarsnow.com/hydrogencars1807-1986.htm
[@8] www.wikipedia.com
[@9] http://www.global-hydrogen-bus-platform.com/
[@10] http://www.hydrogenhighway.ca.gov/
[@11] http://www.mantruckandbus.de/de/media/show_press.jsp?id=86774
[@12] http://www.egmcartech.com/2010/04/13/bmw-working-on-hydrogen-fuel-cell-hybrid-drivetrain-for-2014/
[@13] http://www.autocar.co.uk/News/NewsArticle.aspx?AR=248670
[@14] http://www.altenergystocks.com/archives/2010/09/rareearths1.html
[@15] http://www2.chemistry.msu.edu/faculty/reusch/VirtTxtJml/Spectrpy/InfraRed/infrared.htm
[@16] University of Michigan website http://instructor.physics.lsa.umich.edu/adv-labs/Mass_Spectrometer/MassSpecQMS.pdf
[@17] http://webbook.nist.gov/chemistry/form-ser.html
[@18] http://www.scribd.com/doc/57509934/Manual-Vertex-70vs
[@19] http://www.alfa.com/it/gp140w.pgm
[@20] http://www.goodfellow.com